Distribution Agreement

In presenting this thesis as a partial fulfillment of the requirements for a degree from Emory University, I hereby grant to Emory University and its agents the non-exclusive license to archive, make accessible, and display my thesis in whole or in part in all forms of media, now or hereafter now, including display on the World Wide Web. I understand that I may select some access restrictions as part of the online submission of this thesis. I retain all ownership rights to the copyright of the thesis. I also retain the right to use in future works (such as articles or books) all or part of this thesis.

Yulin Gong April 9, 2020

Variability Classification of Disk Detective Candidates

by

Yulin Gong

Alissa Bans
Adviser

Physics Department

Alissa Bans

Adviser

Stefan Boettcher

Committee Member

Yuanzhe Xi

Committee Member

2020

Variability Classification of Disk Detective Candidates

By

Yulin Gong

Alissa Bans

Adviser

An abstract of
a thesis submitted to the Faculty of Emory College of Arts and Sciences
of Emory University in partial fulfillment
of the requirements of the degree of
Bachelor of Science with Honors

Physics Department

2020

Abstract

Variability Classification of Disk Detective Candidates
By Yulin Gong

Disk Detective is one of the NASA led and funded collaboration projects with Zooniverse. The project aims at searching for stars that are surrounded by dust-rich circumstellar disks. This paper mainly focuses on the detection and classification of variability among a subset circumstellar disk candidates from Disk Detective. We performed two different procedures for searching for variability. We used archival WISE data with periodogram analysis to find candidates' potential variabilities, and we also observed some of the candidates with Emory's 24 inch telescope in order to look for long-term variability as well as to validate and compare the periods we found with the archival data. We found 340 variabilities among the 467 objects with the archival search, and 28 of those were clear periodic variables. While preliminary, our observations identified 7 variables with confidence, including AWI0005w5z, AWI0002d9y, AWI0005yjf, etc. We conclude that a large number of variables may exist among the Disk Detective candidates and that variability could be an important tool used for categorizing the types of objects the project identifies.

Variability Classification of Disk Detective Candidates

By

Yulin Gong

Alissa Bans

Adviser

A thesis submitted to the Faculty of Emory College of Arts and Sciences
of Emory University in partial fulfillment
of the requirements of the degree of
Bachelor of Science with Honors

Physics Department

2020

Table of Contents

Chapter I. Introduction

The Disk Detective citizen science project is one of the NASA led and funded project that collaborates with Zooniverse. The project aims at finding stars that are surrounded by dust-rich circumstellar disks (Kuchner et al. 2016). Since dust absorbs starlight and reemits light in the infrared, dusty circumstellar disks can be identified by looking for objects emitting more infrared radiation than a dust-less star should have.

All-sky mid-infrared surveys, by discovering young stars and main-sequence stars with excess infrared radiation, have made a new mark stone for the science of planet formation (Kenyon & Bromley 2002). These disks include protoplanetary disks (which are dust and gas rich) around young stars and debris disks (dust rich but gas poor) around older main-sequence stars. Useful information such as the timescales and the environment that planets are formed in, as well as planets' current locations and dynamics can be learned from these disks (Kuchner et al. 2016).

The Disk Detective Project used data from NASA's Wide Field Infrared Telescope (WISE) to select stars with infrared excess. WISE scanned the sky at 3.4 μm, 4.6 μm, 12 μm, and 22 μm bands (W1, W2, W3, and W4 respectively) (Wright et al. 2010).

To select sources with Infrared excess, the Disk Detective team removed all sources with [w4] > [w1] - 0.25 (where [W1] and [W4] is the magnitude in WISE's 3.4 μm and 22 μm band), a more detailed selection process is discussed in (Kuchner et al. 2016). As a citizen science project, volunteers viewed images for each object online in 10 different bands to identify false positives from dusty sources that are not stars (galaxies, nebula, interstellar matter, image artifacts, etc.). However, among those stellar objects with signs of infrared excess, there are still a lot of candidates that are not just debris disks (the nominal goal of the Disk Detective project). Those objects could include: Herbig Ae/Be stars, Classical Be stars which have decretion disks, later type young stellar objects, and giant stars which produce their own dust, etc. (we describe the definitions of these objects in Chapter 2).

Spectral follow-up was necessary to help further classify all the various stellar objects that might have infrared excess. The Disk Detective team also did spectral follow-up to better understand the nature of candidates with infrared excess. They obtained optical spectra for objects of interest using the FAST spectrograph for objects in the northern hemisphere, and the REOSC spectrograph at the CASLEO observatory for objects in the southern hemisphere (Bans et al. 2020). The original spectral follow-up all happened before the data release from GAIA (Gaia Collaboration et al. 2018b), a space observatory that measured stellar parallax data, which is used to find distances. Hence the Disk Detective team didn't have distance data on a lot of the objects when obtaining the spectra. Since distance is an important variable

needed to understand the nature of a stellar object, the set of objects the Disk Detective team obtained spectra for included many objects with similar features to debris disks and young stellar objects, that were not actually these objects. Thus, the full set of things the Disk Detective team got spectra for is diverse (Bans et al. 2020).

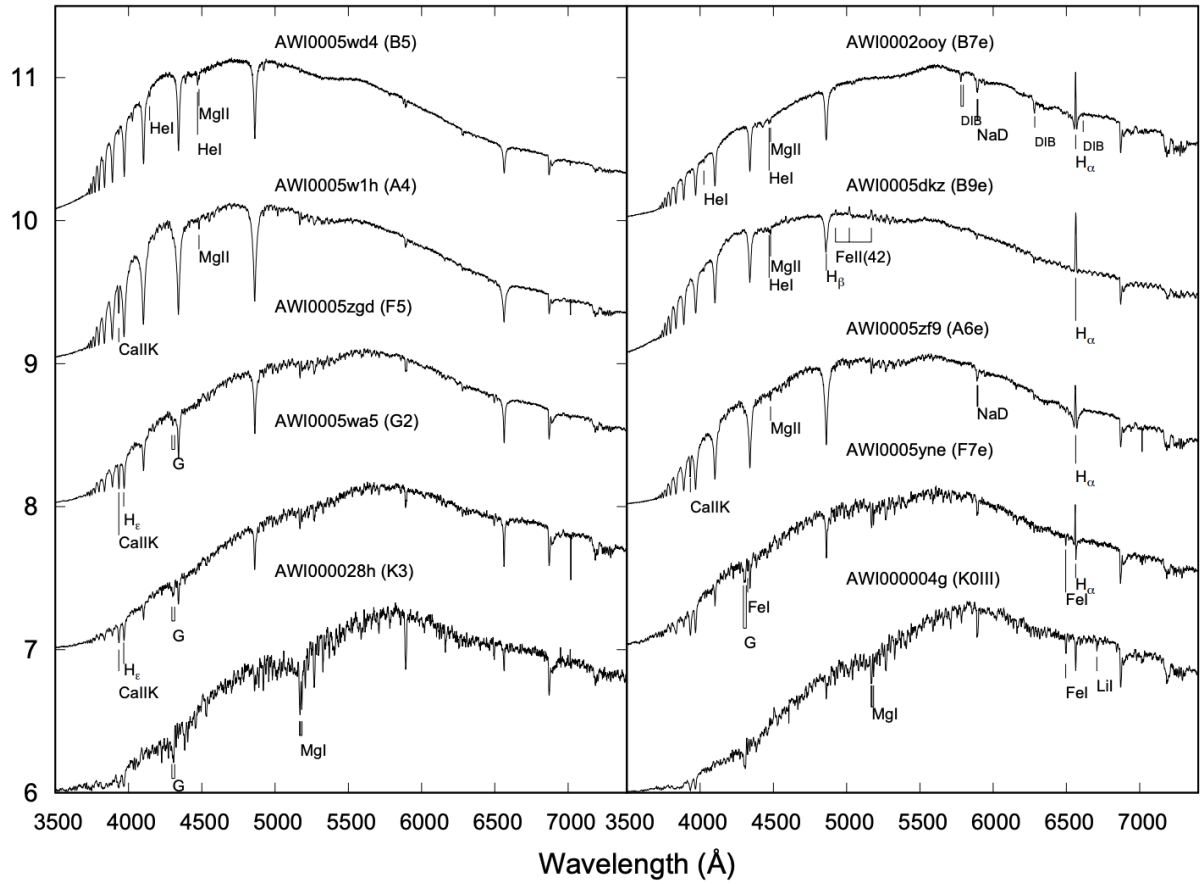

Figure 1. Sample FAST spectra of some of the Disk Detective candidates (taken from Bans et al. 2020). The object labeled AWI0002ooy and AWI0005dkz in the graph on the right share many similar spectral features, but they could be two very different objects. Measuring their variability could be one way to tell them apart.

Using spectral observations, levels of W1-W4 excess, GAIA parallax (absolute magnitudes can be calculated), and other factors, Bans et al. (2020) later organized

the candidates with spectral follow-up into the following categories: Debris Disks, late type Disks, Herbig Ae/Be(HAe/Be) and Classical Be/Shell (CBe) stars, Young Stellar Objects(YSO), and Giant stars. Figure 2 shows some example spectra of the Disk Detective objects. Within the figure, the spectral features that are used for characterization are marked. All the five objects on the left panel are debris disk candidates. The top four spectra of the right panel are either Classical Be stars, Herbig Ae/Be stars, or transitional disks. The bottom spectrum is a K giant star with lithium absorption. The objects labeled AWI0002ooy and AWI0005dkz on the graph on the right share many similar spectral features and properties (Bans et al. 2020), but they could be two very different objects. Even with the additional spectral information and GAIA DR2 data, in some cases, the nature of these objects with IR excess cannot always be accurately determined (Bans et al. 2020). One important piece of information that can help add to the understanding of these objects is variability.

Our project focused on measuring the variability of the objects that the Disk Detective Science team obtained reliable optical spectroscopic data for. For these candidates, we aim to use measured variabilities to help classify the stars further and understand the types of candidates that the Disk Detective project is finding. In the work outlined in this thesis, we analyzed the WISE archival data and also obtained observations using Emory's 24-inch telescope to help constrain the variability of the Disk Detective candidates with known spectral types from Bans et al. (2020). Our goal

in studying the variability for our candidates can mainly be summarized as the following three aspects:

1. Better separating the populations of objects with IR excess from Disk Detective. For example, there is an overlap between Herbig Ae/Be and Classical Be stars, as well as an overlap between extremely luminous active young stellar objects like FU Ori stars and giant post main sequence stars. Variability can be an important clue in separating these populations with more confidence.

2. Variability can shed new light on existing categories of objects with IR excess. Giant stars, which often have poor or unavailable parallax data, can potentially be identified by their periodic variability. Studying what type of giants are in the Disk Detective set not only sheds light on the population of giants stars that have IR excess but could help inform further searches for circumstellar disks (particularly around late type stars) on what types of objects could give rise to false positives.

3. By observing a large number of candidates, we hope to make some surprising new discoveries. For example, binary systems are a heavily studied topic as it connects to planet formation in binary systems. Though rare, variability might be one of the only ways to confirm new debris disk candidates as binaries, as the Disk Detective team did not obtain enough spectra of high enough resolution to detect binaries spectroscopically.

Of our candidates from the Disk Detective data set, we used archival WISE data to study their variabilities. We also observed some of the candidates with Emory's 24-inch telescope in order to look for short and long-term variability. The archival data analysis and the observations we did are very complementary approaches. The observational data we gathered provides an important check to validate the variability we found with the archival analysis, and the archival analysis also helps us identify future high priority targets to observe. The nature of our candidates and the type of variability that we expect to find are discussed in chapter 2. The details of these WISE archival data and Emory's observation data are further discussed in chapter 3. Analysis of this data as well as the results are given in the later chapters.

Chapter II. Variability Among The Disk Detective Objects

A variable star is a star whose brightness (or its apparent magnitude) changes as observed by us at different times. The variation may be caused by changes in the amount of light an object produces (these are known as intrinsic variables) or by something that blocks the light (known as extrinsic variables). The categories that Bans et al. (2020) sorted the Disk Detective candidates into are likely to show specific types of variability. In this chapter, we review the object types and their possible variability, and explain the specific objects and variability type we aimed to target.

2.1 Debris disks

As the main targets of the Disk Detective project, the criterion used in Bans et al. (2020) to categorize the candidates with IR excess as Debris disks is mainly composed of three aspects. First of all, the object should sit on the main sequence. The Disk Detective team used the Gaia M_G vs. B-R Hertzsprung-Russel diagram to make this selection. Second of all, spectroscopically, the debris disks should have no Balmer series emission lines, where the objects with those emission lines are more likely to be Classical Be/shell stars or Herbig Ae/Be stars. The third constraint is that the debris disks candidates should ratify W1 - W4 < 2.7. This is because stars lose their infrared excess over time which means stars with large infrared excesses should be better classified as young stellar objects than older debris disks (Bans et al. 2020).

As mentioned before, debris disks are actually the real targets of Disk Detective. However, we mainly focused our observations on the Classical Be stars, Giant stars, Herbig Ae/Be stars, and Young Stellar Objects. The main reason is that being the closest thing to just regular main sequence stars, the host stars in the debris disks systems are less likely to themselves be variable. Additionally, while they could also be hosts of exoplanets (one of the reasons why finding debris disks is interesting) and the planet transits give rise to short intervals of variability that we would be unlikely to discover by chance observation. In the presence of a binary companion star, one star may eclipse the other as they orbit around their common center, causing a reduction in the total emitting flux. Eclipsing binary systems require that the system has a particular alignment relative to us (the orbital plane of the stars needs to be at an inclination of 90), so we expect that the chance that we could catch these systems with a low number of observations (due to the limited weather condition) from Emory or by looking at the WISE archival data is very low.

2.2 Be Stars (CBes)

Classical Be stars are B-type stars close to the main sequence but thought to be near the end of their lives. They are frequently characterized by having emission lines (usually strong Balmer lines) within their spectrum (Jaschek, Slettebak, & Jaschek 1981). Be stars are thought to be rapidly rotating and rotation is thought to be the main feature that contributes to the production of the circumstellar medium. The circumstellar gas around is formed by material from the star that is thrown off by

their rapid rotation (called a decretion disk) and may not be spherically symmetric (Porter et al. 2003). The decretion disks formed around them can give rise to the infrared excess that Disk Detective selects for.

It is very common for classical Be stars to have long-term variations of the circumstellar emission and absorption lines. In addition, however, Be stars also have short-term variability whose timescales range from minutes to a few days, especially in most early-type Be stars (Porter et al. 2003). The variability that we could expect to find for Be stars are summarized as follows:

- *Pulsating stars* swell and shrink which affects their brightness. Pulsations can be split into: radial modes, where the whole star swells and shrinks together; and non-radial modes, where some parts of the star swell while some of the other parts shrink. The short-periodic line profile variability of Be stars can be attributed to non-radial pulsation on timescales between 0.5 and 2 days (Porter et al. 2003).

- *Rotational Modulation* is due to ordinary starspots, where the spots are regions with a lower temperature than the surrounding photosphere. Stars with starspots may show variations in brightness as they rotate and expose the brighter areas of the surface to our sight of view. Rotational modulation also arises from the circumstellar environment. The easiest way to maintain such rotational modulation is provided by an oblique magnetic field (Porter et al. 2003). Stars with ellipsoidal (or weird) shapes may also show variation in brightness as they rotate and expose different areas of surfaces to our sight of view (Porter et al. 2003).

- *Long-term variability* arises from the variation in the circumstellar environment of Be/Shell stars as they can both lose and rebuild their decretion disks. This process will lead to the long term and gradual variations of the circumstellar emission and absorption lines (Porter et al. 2003), but also the infrared brightness as the decretion disks are what produce the IR excess.

- *X-Ray Flares* may arise from the magnetic fields threading from the star through the disk. The combination of an azimuthal field with a dense disk creates a magnetic dynamo in the disk that can lead to flux changes. The differential rotation between star and disk causes magnetic stresses that may eject high-velocity plasmoids. These plasmids can impact on the object's surface and cause the hard X-ray flares. This occurs on even shorter timescales (few minutes), and the amount of plasmoids ejected is irregular (Porter et al. 2003). While X-ray flares are not something we can detect, there could be correlated variability in the IR or optical that we might see.

Periodic variations of Classical Be stars have been attributed to both nonradial pulsation (NRP) and rotational modulation (RM). These two variabilities are what we mostly expect to be present in our candidates.

2.3 Herbig Ae/Be stars (HAeBes)

Herbig Ae/Be stars are pre-main-sequence stars (younger than 10 million years) of spectral types A or B (Waters et al. 1998). They are surrounded by obscuring circumstellar medium. For example, they can be embedded in gas-dust envelopes. The Infrared excess of the stars is due to their circumstellar dust. The spectral energy distribution (SED) of Herbig Ae/Be stars is dominated at IR wavelengths due to their large amounts of circumstellar medium (Waters et al. 1998). However, sometimes HAeBes do not have large amounts of circumstellar medium, and these HAeBe are classified as the group III objects (Hillenbrand et al. 1992). The group III Herbig Ae/Be stars have weaker infrared excess but still can have prominent Balmer emission lines, as such they are very likely to be confused with the Classical Be stars (Bans et al. 2020).

The optical continuum of Herbig Ae/Be stars can vary on different time scales. Variability of Herbig Ae/Be stars is mainly caused by the variations in the amount of circumstellar dust between our sight of view and the star. Some of the Herbig Ae/Be stars show a color reversal when fading (after reaching a certain magnitude, the star becomes bluer while continue to fade). The color reversal effect may due to an increased contribution from scattered light to the total flux (Wenzel 1968, Zatsjeva 1973, Evans et al 1989, Bibo & Th´e 1990, Voshchinnikov & Grinin 1992). These variations demonstrate that the dust around the Herbig Ae/Be stars are not smooth but clumpy (Waters et al. 1998). Herbig Ae/Be stars also have a second type of

variability that shows long-term fading or brightening, often covering decades. These variations are related to FU Ori outbursts or to gradual changes in the degree of circumstellar extinction. Additionally, variations at low amplitude (<0.5 magnitudes in V) may also be observed, probably due to photospheric or chromospheric activity or stellar pulsations (Waters et al. 1998).

2.4 Giant stars

Giants are stars with a larger radius and luminosity than a main-sequence star of the same surface temperature (the larger luminosity mainly comes from the larger surface area). Giants lie above the main sequence on the Hertzsprung–Russell diagram and can be easily identified by their colors and absolute magnitudes if their distance is known. In Bans et al. (2020), any objects that were 2.5 (or more) magnitudes more luminous than the GAIA main sequence were classified as giants.

Giants tend to be pulsational variables. Though there are many categories and subcategories for giant star variables, the two categories that are most widely used in the literature are Cepheids and RR Lyrae variables.

- Cepheid variables: Cepheid variable stars are supergiants with luminosities 500-30,000 times greater than the luminosity of the Sun. They present regular radial pulsations (i.e., the star expands and contracts) with periods ranging from 1 day to 50 days, and they can be distinguished at great distances (Caltech 2020). We have a total of 181 Giant stars candidates and we have 55 objects with bad

parallax data (e.g. with high error bar) and only 7 of them have “spectral types and luminosities that would be Cepheid-like (i.e. with Mg < -4 and spectral types ranging from F-G).”

- RR Lyrae variables: RR Lyrae variables are horizontal branch stars with periods ranging from a few hours to 2 days (Swinburne 2020), where the horizontal branch is a stage that follows the red giant branch for stars with masses that are similar to the Sun's. They sit in the instability strip of the Hertzsprung-Russell diagram. Their instabilities cause their size to change periodically. This change in size also changes the temperature of the star which in turn leads to their change in variability as well.

2.5 Young stellar objects (YSOs)

Young stellar objects (YSOs), as the name suggests, are stars in the early stages of their life. Note that the Herbigs are also YSOs, and they are just of an earlier (hotter) spectral type. The reason Bans et al. (2020) separated the HAeBes as their own category was because as blue B/A type stars, they could be mixed up with Be stars. The stars that had spectral types later than A (i.e. F-M) were left under this remaining blanket YSO category in Bans et al. (2020). YSOs are often embedded in an obscured region like molecular clouds (within or near interstellar gas and dust).

There are many types of variability associated with YSOs, we use the descriptions from Herbst et al. (2012). All periodic variables with cool spots are classified as type I variables, irregular variables with hot spots are classified as type II variables, and irregular variables suffering occultations are classified as type III variables.

2.6 Our Targeted Variability

In general, based on the discussion above, we expect that most of the variability that we could characterize in this preliminary work should be on timescales shorter than a month (though we have plans to assess long term variability, see Chapter 7). Preferentially, our observations focused on things that would be short term variables and that are easy to detect.

In the sense that variability can further help us classify objects better, our observations are also planned with a preference for the type of candidates that are easily mixed up with others. For example, FU Ori is a pre–main-sequence star that is very luminous, so much so that even though they are likely rare, we might mix them up with some of our giants. They will have very irregular “outburst”-like variable events that display an extreme change in magnitude and spectral type (Lee et al. 1996). However, they are less likely to be periodically variable (as giants tend to be). Since FU Ori stars and giants can show Balmer line emission (Lee et al. 1996), we chose to observe objects with Balmer line emission and luminosities consistent with the object being an FU Ori star or a giant star. We hope that the variability may help ultimately help identify the object.

Recall that all our objects with Hα emission and spectral types A/B are either Herbig Ae/Be stars or Classical Be stars. To further separate Herbig Ae/Be stars from Classical Be stars we can check the variability they present. From the summary of the type of variability above, the pulsations' light curve of Classical Be stars tends to be regular and in a sinusoidal shape. However, the amount of dust doesn't tend to change regularly, thus, the light curve of a Herbig Ae/Be star should normally change irregularly. In this sense, if we detect any periodic variability from HAeBe candidates that behaves or seems like pulsational variability, we should recheck whether we have misclassified the object as a HAeBe or not.

Chapter III. Data Collection

3.1 WISE multi-epoch data

WISE is a 16 inches diameter infrared space telescope in Earth orbit with a 47' X 47' field of view. It was designed to perform an all-sky astronomical survey with images in W1 (3.35 μm), W2 (4.60 μm), W3 (11.56 μm), and W4 (22.09 μm) wavelength range bands. WISE began its survey in 2010 January. After its hydrogen coolant depleted (Sept 2010), a mission extension called NEOWISE Post-Cryogenic was conducted as the second all-sky coverage. These two epochs' data were packaged as the ALLWISE Data Release (Wright et al. 2010). WISE is currently searching for near-Earth objects under a mission call NEOWISE-R. The four years data of NEWOWISE-R has also been released.

We queried and downloaded all the available photometric data from WISE and NEOWISE using the platform IRSA (NASA/IPAC INFRARED SCIENCE ARCHIVE). The data is unevenly distributed over time (as shown in figure 2) and the method of finding the period will be discussed in the later chapters.

AllWISE data are points on the graph whose X-axis value are smaller than 56000 (it had fewer dates of coverage than NEOWISE). ALLWISE observations of an object typically involved 2-5 images per day when observed (timescales sampled ~ hours). The daily observations were spaced out typically 2-5 days a week (sampled timescales

~ days) and the entire procedure (taking images several hours apart, for several days during a week) was repeated about 3 times during the ALLWISE data was collected for.

NEOWISE started 4 years after WISE and it covered several years (4-5) of data, hence most data points are NEOWISE. It has similar coverage to the timescales outlined in the ALLWISE above (i.e. ~3-5 images per day, for a few days a week, spaced out across ~3-4 times per year). Since NEOWISE did this for 4-5 years, so there are roughly 5 times more data from NEOWISE than ALLWISE.

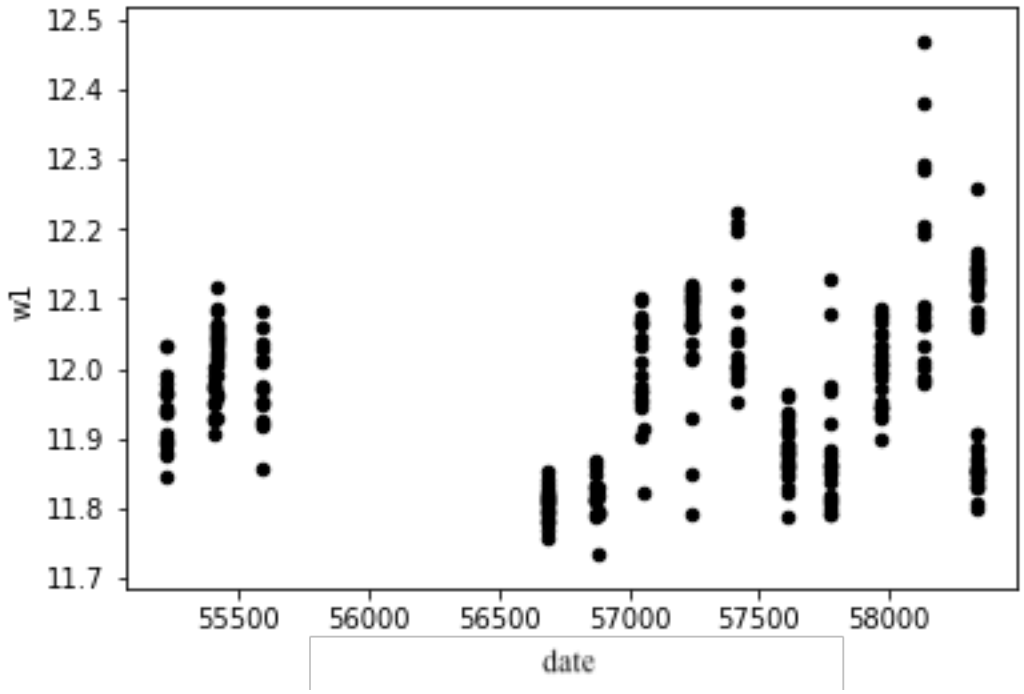

Figure 2. Raw data of object J234919.0+664211.4 (discussed in Chapter 6). The Y-axis is the apparent magnitude (brightness) in the W1 band and X-axis represents the Modified Julian Date in units of days (the label "date" applies to all the figures later in this paper unless specified).

3.2 Emory Observational data

Observation was conducted with a DFM Cassegrain telescope and this Cassegrain is fully controlled by a computer system and custom software. We have used two different cameras for observation. Most of the observations are conducted with SBIG ST-10 and it combined with the telescope to have a 6' x 9’ field of view. The original camera is Apogee Alta U47 with a 10' x 10' field of view and it has higher sensitivity. The Apogee camera was sent to repair and reinstalled on January 27th, 2020. Our observations are conducted at a different wavelengths (R band with effective central wavelength 634.9nm) from the WISE wavelengths.

Observations are planned based on objects’ RA (right ascension) and Dec (declination) values. The culmination is the instant of time of the transit of a celestial object across the observer's local meridian and this is the time that the object can achieve the highest height in one’s local sky. For an observer with latitude (L) at the northern hemisphere, an object's altitude (A, and also its maximum height) at its upper culmination is given by $A = 90^\circ - L + \delta$ where δ is object’s declination. We wrote code in python to help planning our observations. Each object’s culmination time and azimuth at culmination are outputted, where azimuth is the horizontal direction of a star or other astronomical object in the sky. Based on the culmination time and azimuth, observable objects will be filtered out for a specific time and date we aim for. The key point here is to find optimal objects that are not in the direction

of city light sources and with a culmination time between 8 p.m to 2 a.m. We need to keep updates our observable objects list as the objects we observed in one night are not observable at the same time some days or weeks later. This is because due to the rotation of the Earth as well as its orbit around the sun, we don't face the same sky every day (stars rise 4 minutes earlier each day).

Some additional preparation work must be done before we actually conduct the observation. The main work here is to build the field of view, e.g. finding suitable known check stars and reference stars needed for differential photometry (see Chapter 4), and deciding how to point the camera, etc.

Due to the limited field of view of our telescope, we search for check stars and reference stars on VizieR for our objects within about 10 arcmins[1]. A good check/ reference star is the star with similar apparent magnitudes to our target objects. One problem we faced is that many of our objects (especially the Be stars) were so bright, that we often couldn't find a good comparison star in the field of view. We gave up and avoided observing a lot of these objects. When possible, we tried to find alignments that placed our object and any reference stars in the center of our frame. The reason for trying to get the objects near the center is that the telescope won't track perfectly which means object near the edges of the frame could be lost from

[1] The field of view of the first camera we used was rectangular, 9' by 6' minutes. So it presented more of a challenge than the Apogee we mentioned above.

image to image. Below is one sample field of view (with labels) that we create for our objects, and the rest of the frames we created are presented in Appendix I.

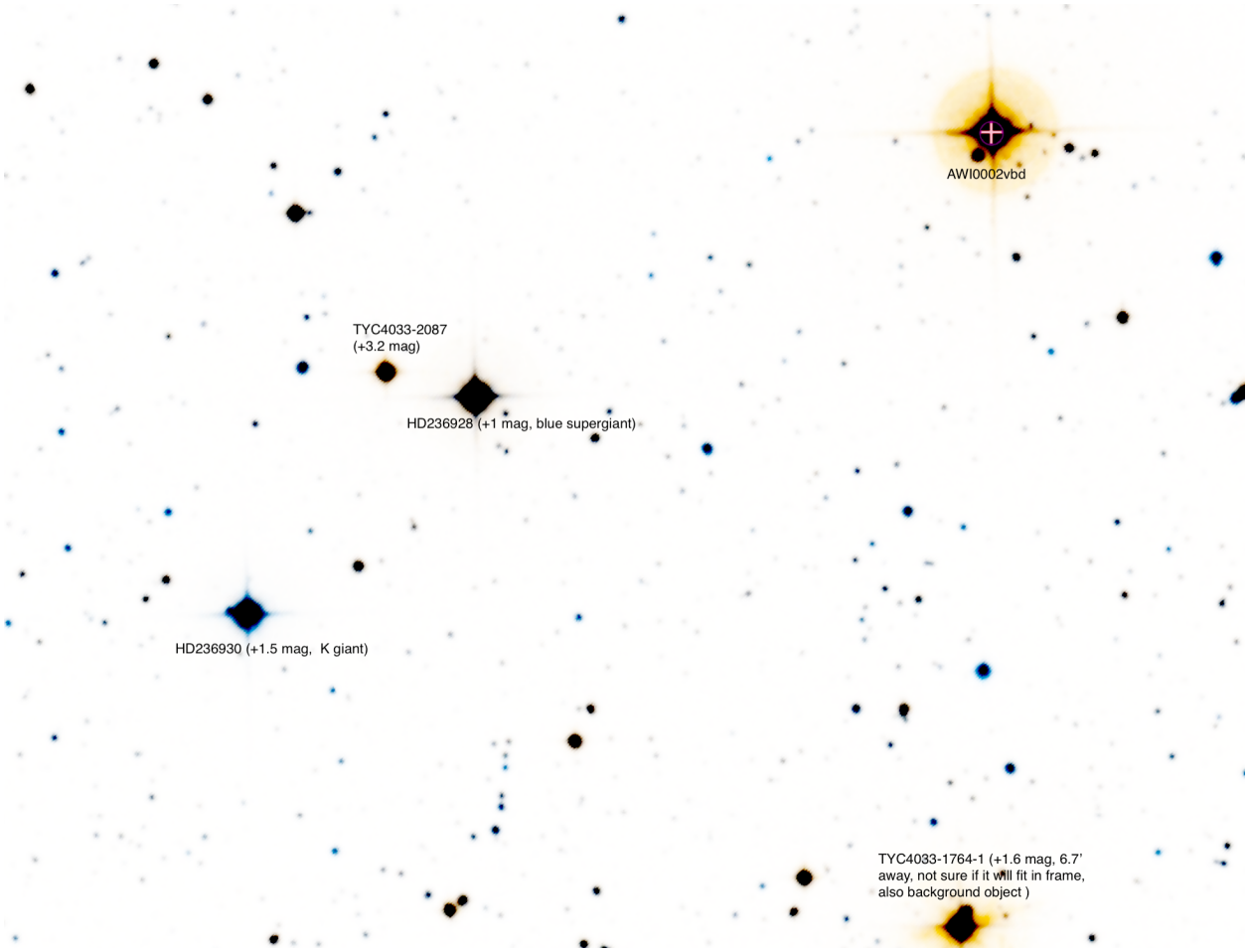

Figure 3. Sample field of view for AWI0002vbd. Comments and labels are given for our reference and check stars.

Due to the limited clear nights, only few candidates from our object list are observed with our Emory's 24-inch telescope, and they are summarized in the table below:

	Oct 17-18	**Oct 23-24**	**Nov 1-2**	**Nov 9-10**	**Nov 20 - 21**	**Nov 24 - 25**	**Nov 25 - 26**	**Dec 18-19**	**Dec 19-20**	**Feb 07 - 08**	**Feb 22-23**	**Feb 29- March 1**
AWI0002d9y									XL	O	XL	XL
AWI0002ozm									XL			
AWI0002v3v					O		O	O	O			
AWI0005w5z						XL			O			
AWI0005w6c								O	XL			
AWI0005yjf			XL	XL	O		O		O	XL		
AWI0019iw			XL	XL	O		O	O				
AWI0019pi		O	O	O	O		O	O				
AWI0002ooy			XL	XL	O		O	O				
AWI0055kz	XL	XL			O		O					
AWI0034wa								O				
AWI0002vbd							O	O				
AWI0005d8u												XL

Table 1. Summary of our observation. (Notes: O = observed; XL = observed for longer than an hour)

The data analysis of our observational data can further check and validate the periodic variability that we find with the WISE archival data. If a variable is periodic due to pulsations, it is likely to happen at all wavelengths. On the contrary, any variation that occurs just in the infrared band or far beyond the R band will not be able to be detected by our observations. While we expect some of our archival light curves to match up with our observations in some cases, there are additional reasons why the archival variability and observational data may not show similar behavior. We discuss the comparison of the archival and observational data on a case by case basis in chapter 7.

Chapter IV. Data Reduction

Photometry is a technique for measuring the flux of light radiated by astronomical objects. The light measurement relies on electronic devices such as a CCD photometer or a photoelectric photometer to record the light collected with a telescope.

The raw data recorded by the CCD depends on the characteristics of the detector, the telescope optics, the characteristics of the filter used to observe light in a specific wavelength range, as well as the effects of the atmosphere and sky brightness when the data are taken. When calibrated against other light sources of known intensity and color, we can measure the brightness or apparent magnitude of the astronomical objects. In order to use the data for science, several corrections need to be applied to account for these effects. The corrections needed to account for the effects of the instrument can vary from night to night, and corrections to account for variations in the atmosphere and sky brightness will vary throughout the night. Calibration data of various types are taken to make these corrections. For the data reduction process, we have used the software MaxIm DL (Cyanogen Imaging, 2020), Astro -ImageJ (Karen A. et al. 2017) and our own written python code.

Calibrations

All data from CCDs are affected by factors other than the astronomical object we are taking data for. These factors can include noise from the electronics, variations in the detector, dust in the optics, excess light from the sky, and turbulence in the atmosphere. Below are the three calibrations that should be done once per observing night, which remove the common instrumental effects on the raw data:

- Bias frame**:** A bias frame is a zero-length exposure with the shutter closed. Bias usually doesn't change from night to night but we still take an average from a sample of 20. Bias information is subtracted from the image

- Dark frame: Dark current, or thermal noise, is due to sources other than starlight. For example: heat from the electronics can create spurious charge on the chip. The exposures are made with the shutter closed so that no light falls on the detector which means that all the recorded signal is due to dark current. Since the dark current builds up over the exposure, darks should be taken with the same exposure time as our science images. Biases are also subtracted from the dark frames before the darks are applied for calibrations.

- Flat frame: A flat frame is simply an image of how the light fell on our optics. It is created by taking an image of a uniformly illuminated flat surface, with an exposure time long enough to provide a strong signal on the detector, but short enough that it remains well below the linearity limit of the CCD. Each flat frame also contains bias and dark information that is subtracted during the calibration process. Unlike biases and darks, flats are not subtracted from the science frames,

they are instead divided. Below is a sample of our calibrations. We can see clearly that the frame becomes better after we impose the calibrations.

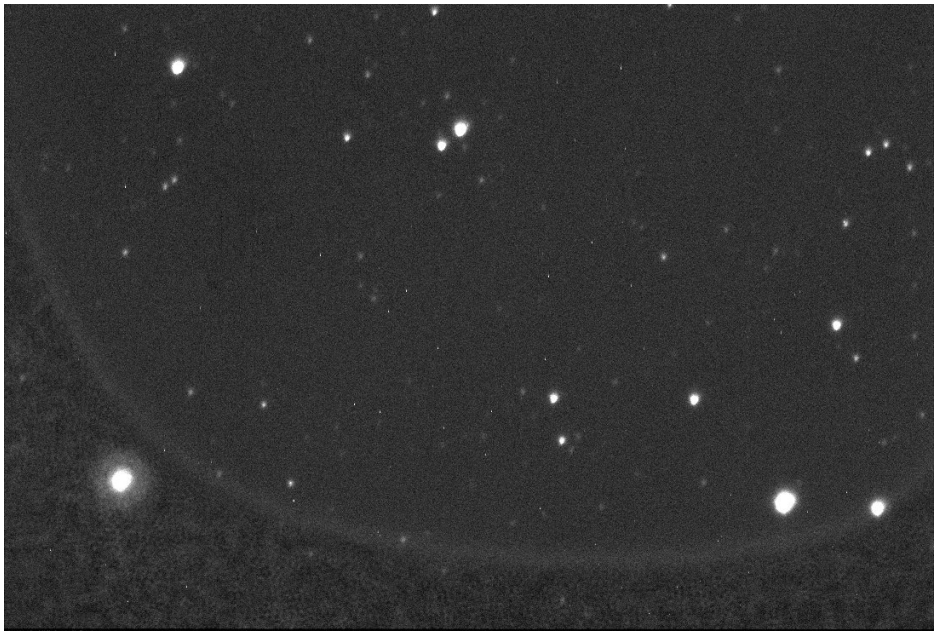

Figure 4. Raw image taken by Emory's 24-inch telescope

Figure 5. Calibrated image taken by Emory's 24-inch telescope

Photometry

We mainly used aperture photometry for our data reduction where aperture photometry is the measurement of light that falls inside a circular aperture of a certain size. We calculated the aperture photometry value (flux) by taking into account the local background subtraction.

Before we start conducting the photometry to measure the magnitudes, we need to pick a good size for our aperture. If the size is too big, we may include the light from neighbor stars (as shown in figure 6):

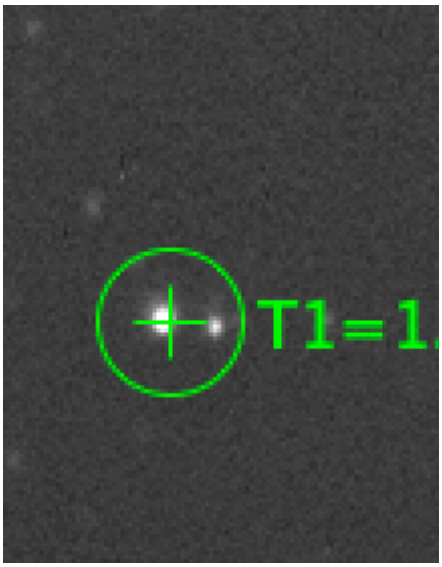

Figure 6. A sample aperture that contains neighbor stars

The most optimal aperture is to include most of the light from the star but with only a little light from the background as shown in figure 7 below:

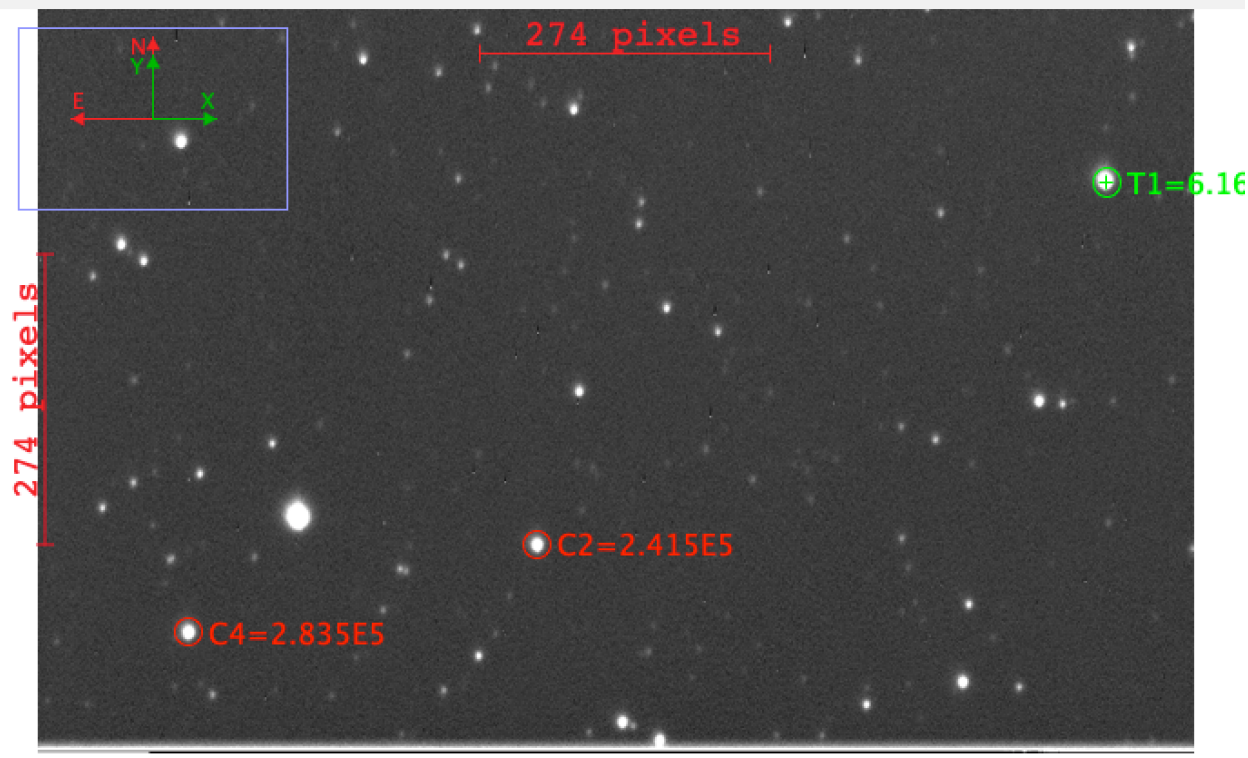

Figure 7. A sample frame with optimal aperture

Additionally, we also have to set the radii of the annulus to measure the local background sky values for each star. It doesn't matter if the annulus contains light from one or two stars. It's fine as long as the majority of the area are purely background sky.

After we are able to find the correct aperture photometry value of each object, we then find the magnitude of our target object with the help of differential

photometry. We use a star with known apparent magnitude as the reference star to measure the apparent magnitude of our target object. We conduct differential photometry where we calculated the relative flux by division (flux1/flux2). The hazards of differential photometry and our solution to them can be summarized as follows:

- Our main challenge here is to let our annuli track our object between each shot of images. The frame shifts under the bad tracking of our telescope. Within our written python code, we fixed this issue by roughly finding the center of the object within a rectangular area where we assume the brightest pixel is the center. We track the object by finding the center (brightest pixel) of the object in each image. Additionally, the software MaxIm DL and Astro -ImageJ also provide the feature to automatically align image by image based on the same pattern of the stars (two stars have same angular separation) within each image.

- Due to the limited field of view of our telescope's camera, it's hard to find good reference stars within our frame. Sometimes, there's only one good reference star in the frame and the reference star may also be a variable. To avoid this problem, we use another star as the checked star to see if the star is actually a variable or not. However, in some cases, the only available check stars in the frame were much less bright than the target and the reference and so there is a large error associated with using them.

- Another hazard we face is that doing longer term differential photometry is tricky. Our target may have short term periodic variability and the reference star may stay

flat over the night, but two weeks later the reference may have changed when we observe the target again. The check stars can help to tell us the behavior of our reference stars, but we still run into issues in cases where there aren't enough comparably bright check stars in the frame.

Chapter V. Identification of periodic variables from the Archival Data

To identify periodic variables from the WISE and NEOWISE data, we used the Lomb–Scargle periodogram with python's package *gatspy* (General tools for Astronomical Time Series in Python). The Lomb-Scargle periodogram is a well-known algorithm for detecting periodic signals in unevenly distributed data. In general, the Lomb-Scargle periodogram can efficiently compute the oscillating period of a Fourier-like power spectrum estimator from an unevenly-sampled data (Jacob et al. 2017).

The algorithm tries different folding of the data for different periods until it finds the "best" period. Least Squares Methods is also used sometimes it involves fitting a model to the data at each candidate frequency, and selecting the frequency with the maximized likelihood (Jacob et al. 2017). However, this algorithm can fold certain irregular variability to maybe look periodic. Our observations can be helpful in identifying when the Lomb-Scargle light curves may be misleading, and occasionally studying the *unfolded* archival data sheds light on the periodogram analysis.

Based on the observation timescales of the WISE data we discussed at the end of chapter III, we covered the periods between 0.1 to 30 days in our analysis as we don't have enough data spread out over long timescales.

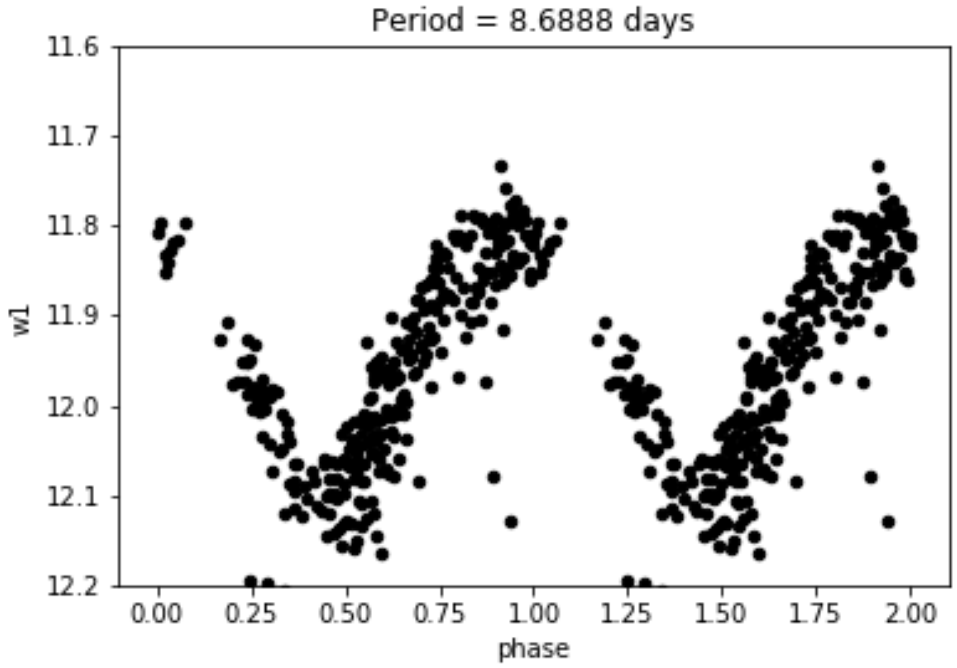

Figure 8. The reproduced light curve with WISE archival data. The Y-xis is the apparent magnitude (brightness) in the W1 band and X-axis represents the phase of the object. Note that "phase" on the X-axis means the particular appearance or state for cycle of changes and phase from 0 to 1 depicts one full cycle (the label "phase" applies to all the figures in this paper later unless specified).

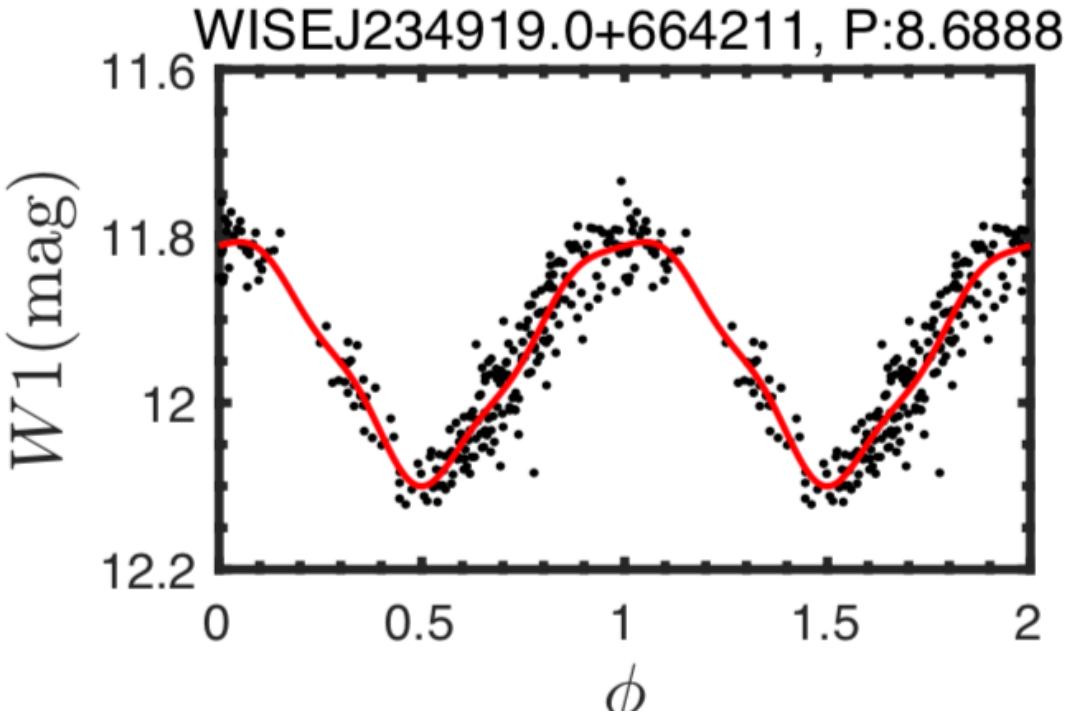

Figure 9. Chen's published light curve (Chen et al. 2018)

Before we applied the Lomb-scargle analysis to our candidates and classified our found variability into specific classes, we tested our algorithm of finding period with an existing result that is published by others. Here, we compared our results with the results from Chen et al. (2018). In this paper, ALLWISE and NEOWISE-R data were used to detect periodic variables (applying the Lomb–Scargle periodogram to find the period) . Chen et al. (2018) found 50,282 periodic variables and an additional 17,000 suspected variables.

Several objects' light curve has been reproduced with the package mentioned above and they largely coincide with what Chen et al. (2018) published. The two figures above are samples of the comparison between one of our reproduced light curves with the corresponding published light curve. Note that "phase" on the X-axis means the particular appearance or state for cycle of changes and phase from 0 to 1 depicts one full cycle (the label "phase" applies to all the figures in this paper later unless specified).

Although the period we found coincide with Chen et al.'s published value, the objectives and analysis of our project is different from this paper's. The algorithm in Chen et. al (2018) for finding periods is more precise (namely as it involved iteratively running periodograms for different subjects of the archival data, a process that was too time-consuming for us to focus on). Also, they mainly focus on the objects that are located in the Galactic plane and near the equatorial poles, and objects that they

studied are high-probability variables (i.e., with AllWISE Source Catalog keyword ‘var_flg’ = 6, 7, 8, or 9) (Chen et al. 2018). Sources with W1 < 8 magnitudes or W2 < 7 magnitudes are not used in their analysis. On the contrary, over 50% of our candidates are bright with infrared excess (W1 < 8). Additionally, they did not attempt to specifically identify any variable with IR excess, where they defined “IR excess” as W1-W2 > 0.12 x (J-K), a condition that over 60% of our candidates meet (note J-K are the 2MASS bands). Therefore, we expect that most of our candidates are not in their analysis.

As Chen et al. (2018) noted there are zero-point differences between ALLWISE and NEOWISE-R data, resulting in a systematic difference of ~ 0.01 mag and a statistical scatter of 0.03–0.04 mag for 8 < W1 < 14 magnitudes and 7 < W2 < 13 magnitudes. Magnitudes errors near .02-.04 magnitudes are typical of ALLWISE and NEOWISE photometry, thus we caution that low amplitude variability of less than <.05 magnitudes is difficult to identify with the archival data. However, it may be possible to confirm even apparent low amplitude variability with good observational data.

Chapter VI. Results of WISE archival data

6.1 Stars with no significant variability

Below are some sample objects that don't show significant variability (the figures on the left represent the raw archival data while the figures on the right are the results after folding). Note: As the variation in the raw archival data is small, we pick the folded results that give a relatively stable and continuous W1 magnitude over time (a horizontal line) that displays no variability. Thus, the period indicates below may not actually be the true period of the object and the period may come from the noise.

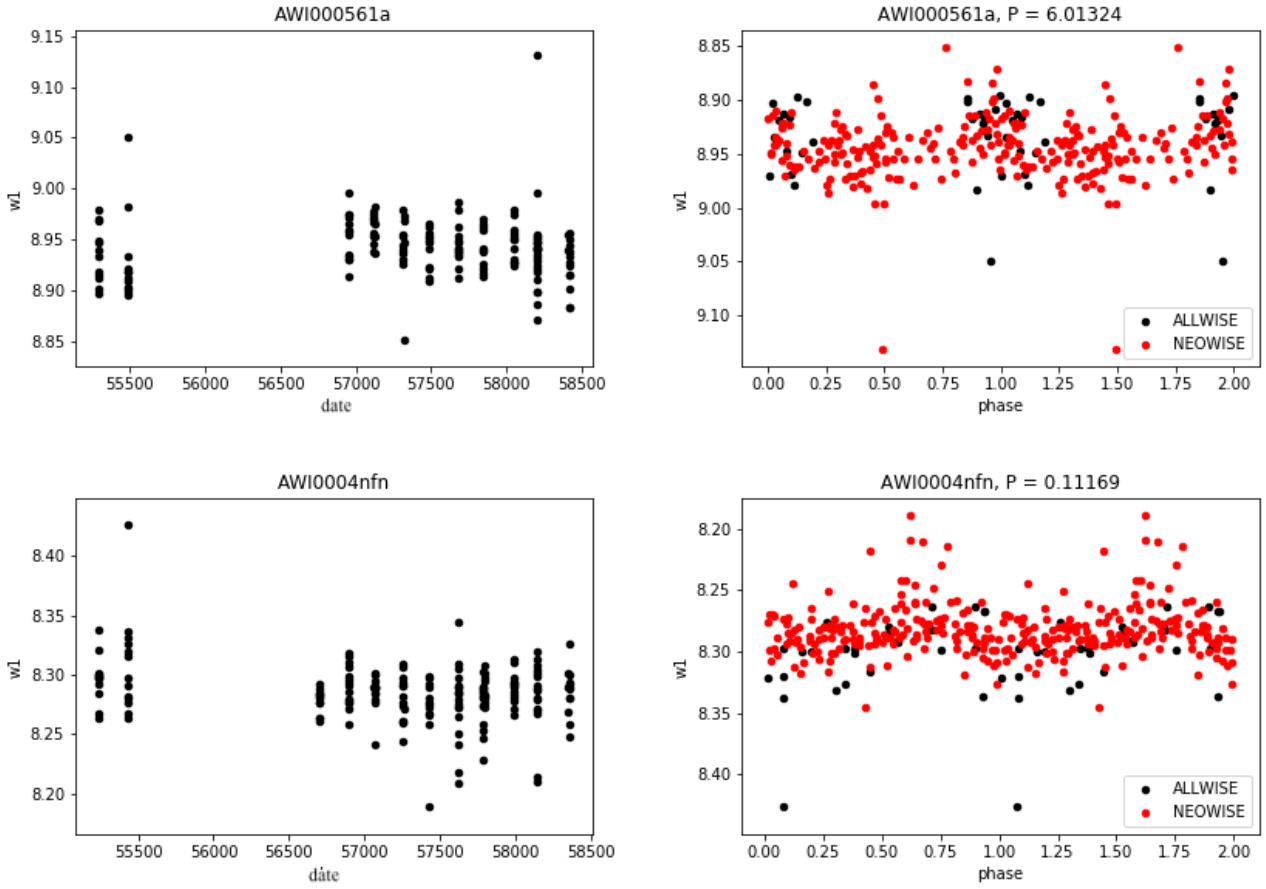

Figure 10. The figures on the left represent the raw archival data while the figures on the right are the corresponding folded results. From the unfolded archival data, we can clearly see that the variation of W1 magnitude (vertically) among each day (horizontally) is stable and relatively the same over time. On the contrary, from figure 2 on page 17, we can see that the variation of magnitude from one day to the other is not stable or not on the same level.

	CBe	HAe/Be	YSO	Giants	Debris Disk
No significant Variability	12	7	4	17	87
Non-periodic Variable	22	20	41	154	74
Periodic Variable	3	5	10	10	0
Total candidates	37	32	55	181	162

Table 2. Summary of variations of the candidates. No significant Variability refers to the number of objects that don't show significant variability (stars whose variation in magnitude < 0.2 magnitudes in raw archival data).

Table 2 above summarizes the variations of the different type of candidates. The first row (**No significant Variability**) refers to the number of objects that don't show significant variability. We defined the non-significant variability as the stars whose variation in magnitude < 0.2 magnitudes in unfolded archival data. We visually go through each object in the raw archival data that isn't folded and pick out the objects with variation < 0.2 magnitudes. We didn't include the counts of the periodic variables whose variation < 0.2 magnitudes into the No significant Variability category. The figures above are some examples of stars with non-significant variability. The second row (**Non-periodic Variable**) simply represents the number of candidates that are variables with variation > 0.2 magnitudes but are not periodic variables. In this sense, the sum of No significant Variability, Non-periodic Variable, and Periodic Variable should equal to the total number of candidates as indicated in the last row. Based on the numbers above, debris disk candidates seem to be less variable compared with other types of candidates.

From table 2, we can see that 50% of the debris disks showed some variability. That is very exciting and contrary to what we earlier argued in chapter 2 that debris disks would be less likely to be variable. Figure 11 shows some of the archival data for debris disks that didn't seem periodic but did seem variable.

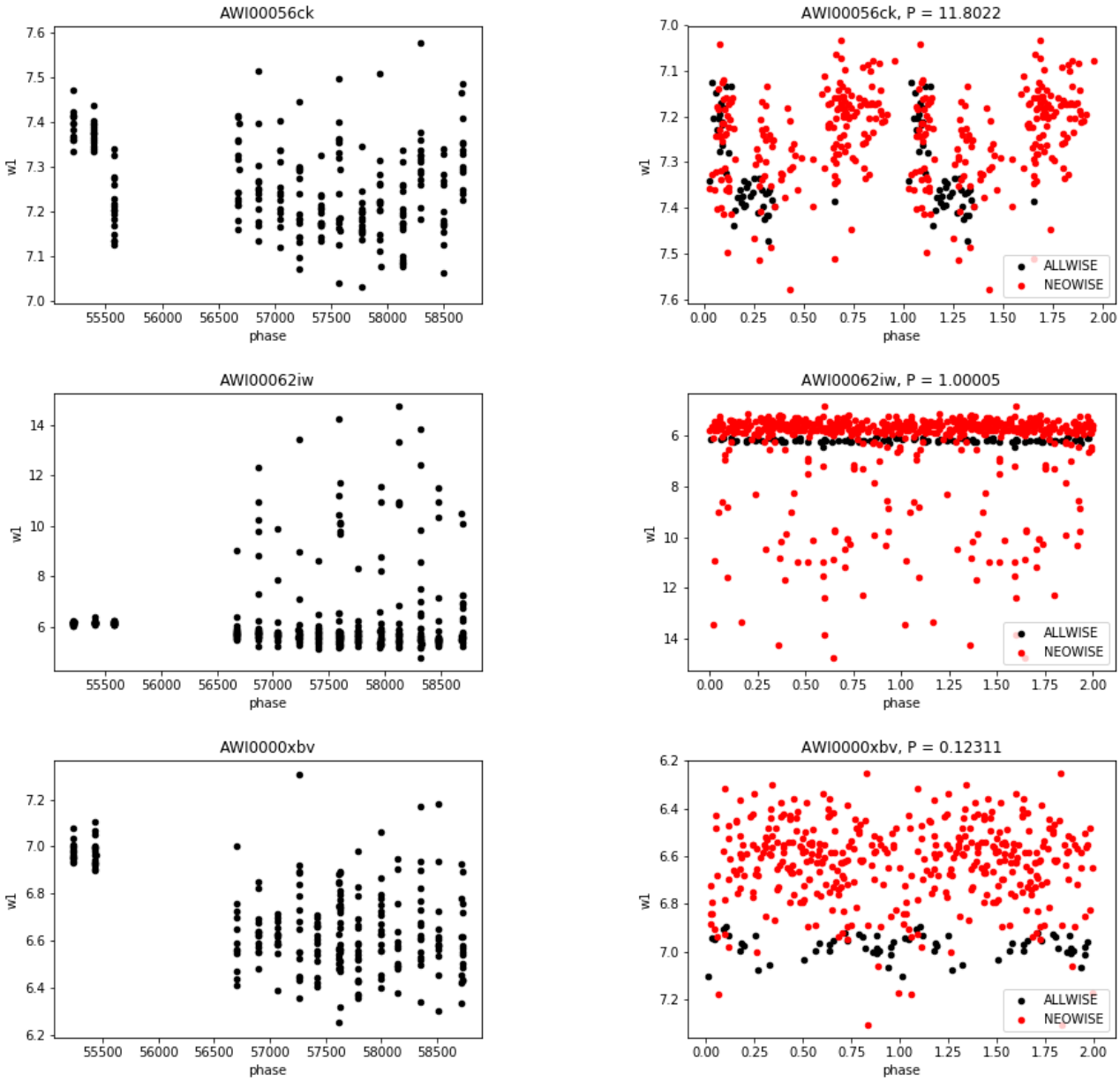

Figure 11. The figures on the left represent the raw archival data while the figures on the right are the corresponding folded results. From the unfolded archival data, we can clearly see that the variation of W1 magnitude is random and irregular over time. Compared with our non-variables in figure 10, the archival data here tend to spread out over the whole graph. Note that AWI00062iw is stable over time around W1 = 6 which gives similar folded result as shown in figure 10, but its variation in lower magnitude is irregular.

Among the other half of debris disk candidates, none of the objects show variability that would be associated with a binary system. It is still very unlikely that we are seeing binaries (which should be periodic) or exoplanets, so the irregular variability we detect in the debris disks could be due to stellar activity, or particularly in the WISE bands, it could be due to changes in the circumstellar material, which usually occurs on timescales of months to years (Hughes et al. 2018). Variability due to changes in circumstellar material is usually associated with the "extreme debris disks" (Hughes et al. 2018), so one thing we could check for (in the figure) is how the IR excess of our debris disk variables is different from that of our non-variables. We can further compare the light curves we found with the features described in Hughes et al. (2018) to further study these objects.

6.2 Stars with Periodic Variability

Zooid	Original categories	Period (days)
AWI0000ojv	Classical Be	10.9941
AWI0002vby	Classical Be	6.76700
AWI0003cp6	Classical Be	5.73532
AWI0000bh9	Herbig Ae/Be	3.27015
AWI0000zjo	Herbig Ae/Be	5.40783
AWI0002m6v	Herbig Ae/Be	11.8183
AWI0005ag4	Herbig Ae/Be	6.88799
AWI00023d1	Herbig Ae/Be	9.92286
AWI0002cu6	YSO	9.15151
AWI0003cr7	YSO	12.4250

Zooid	Original categories	Period (days)
AWI0005wfv	YSO	3.66641
AWI0005wh3	YSO	7.23738
AWI0005whz	YSO	7.88690
AWI0005wvk	YSO	6.47417
AWI0005yof	YSO	8.99355
AWI0005yos	YSO	3.77502
AWI00022vs	YSO	9.66980
AWI00062be	YSO	4.07511
AWI0000jo8	Giants	7.89374
AWI0000l70	Giants	4.41547
AWI0002d9y	Giants	5.68883
AWI0005b5v	Giants	4.52148
AWI0005dqb	Giants	0.12256
AWI0005lth	Giants	9.50741
AWI0005yjf	Giants	4.50451
AWI0005yly	Giants	3.59372
AWI0005zda	Giants	8.37874
AWI00056aj	Giants	197.792

Table 3. Summary of the variability we found

Among our candidates, we have found 3, 5, 10, 10 variables for CBe, HAeBe, YSO and Giant candidates respectively. All the newly discovered periodic variables are summarized in table 3 and a few of their light curves are discussed below (the full set of light curves for the table 3 objects are in appendix II).

Classical Be stars

Of the CBe candidates, we have found 3 periodic variables that take up one-ninth of the CBe pool. Figure 12 shows one sample periodic light curves we found with the WISE archival data. Periodic variations of Classical Be stars have been attributed to both nonradial pulsation (NRP) and rotational modulation (RM) (Porter et al. 2003), both of which may give rise to periods of around 2-10 days, which is what we see here. Be stars of early types have been found in surveys to show more short term variability than the later type Be stars (Labadie-Bartz et al.2017). Though we only have three detections, we note that they all show early type spectra, even though the Disk Detective population of CBe stars may be biased towards the later type objects (Bans et al. 2020).

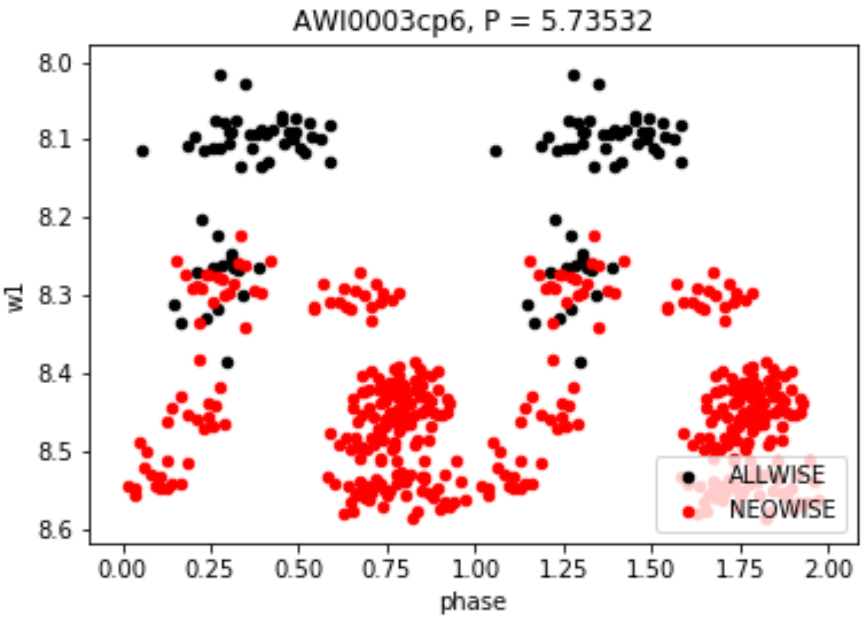

Figure 12. Periodic light curve of AWI0003cp6 with WISE archival data

The light curves' amplitude of the 3 variables we found, around ~.2 mag or more, are a little higher than the amplitude of non-radial pulsation variability (which typically is 10-100s of mille-magnitudes) (Labadie-Bartz et al. 2017). One possibility is that some of these objects are binaries, detailed study and models of the shape of the light curves may help better identify the root for the variability. Another hypothesis is that our periodograms could be misleading: note that the ALLWISE data and the NEOWISE data of AWI0003cp6 are well separated, indicating perhaps that this object may have had long-term variation (i.e. object got dimmer by the time the NEOWISE data was taken, remember, ALLWISE and NEOWISE are 4 years apart). It's not uncommon for Be stars to have long-term variability and changes on timescales of years. One way to possibly weed out the long-term changes would be observing and obtaining a light curve ourselves over the presumed 5 day period and compare its shape to the curve generated by the periodogram analysis (we cannot easily find the amplitude of variability because our observations are at a different wavelength). Alternatively, we could check other archival data and see if there's a trend of dimming across years in other bands.

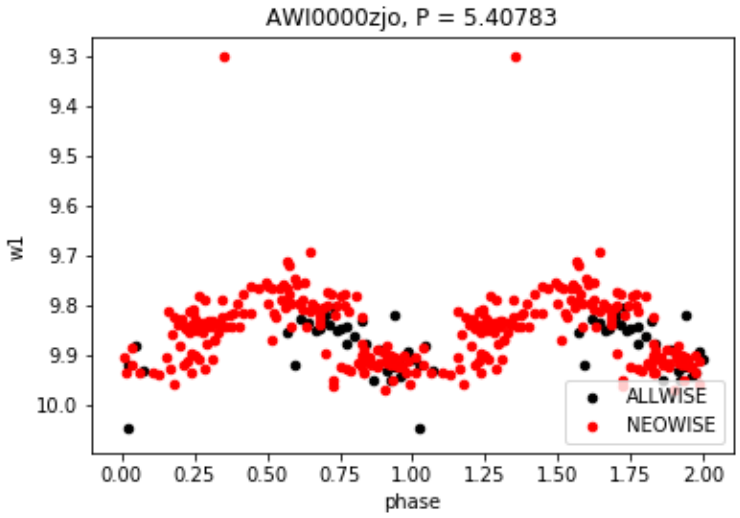

Figure 13. Periodic light curve of AWI0000zjo with WISE archival data

Herbig Ae/Be

We have found five variables from Herbig Ae/Be candidates that take up one-sixth of the HAe/Be pool. Several of the variables have a very symmetric sinusoidal shape of their light curves. As discussed before, Herbig Ae/Be star normally have irregular variability (Waters et al. 1998), but based on the symmetry of many of the light curves, the phase folding is less likely to have been fooled by an irregular variability or transient variability. The exception is AWI00023d1, which shows a separation of the ALLWISE and NEOWISE data in its folded curve and less of a sinusoidal shape. It is possible that this object had an irregular and brightening event. Some of these candidates could be rotational or pulsational variables based on the light curves, and we have to further study these objects as they might be Classical Be stars (given the difficulty of separating the two types of objects discussed in chapter 2). According to the spectral classification given by Bans et al. (2020), the spectral type of AWI0000bh9[2], AWI0000zjo, AWI0002m6v, AWI0005ag4, AWI00023d1 are A2, A0, A0, A4, B8 respective, where all these objects are either early A type our late B type stars. Additionally, four of the objects (all except the AWI0000zjo), have H alpha emission and significant infrared excess (they are group I objects in the Hillenbrand et al. (1992) classification). While it is possible that more than one of these 5 objects are misclassified as HAe/Be instead of CBe stars, AWI0000zjo is the likeliest candidate due to its weaker IR excess. Additionally, the Herbig Ae/Bes could be binaries (as could the CBes). The other short term variability in Herbigs could be due to stellar

[2] AWI000bh9 is a *known* type of variable which has a SIMBAD reference as a Alpha2 Canum Venaticorum.

activity (sunspots etc), but they tend to not be stable over long periods. Thus, we would expect the ALLWISE and NEOWISE data to not be so well folded together.

YSO

We detected 10 variables within the young stellar objects candidates. Due to their periodic variabilities, they would be best described as the “type I” variables of YSO according to Herbst et al. (2012) as mentioned in the second chapter.

According to Herbst et al. (2012), type 1 objects (periodic variables with cool spots) are thought to be from stellar activity (sunspots, etc.). But Herbst et al. (2012) mention that while these look periodic, stellar activity changes over the timescales of several months. So it is a mystery why our folded data (which includes two data sets that are 4 years apart) would show the same stellar activity periodicity in the NEOWISE and ALLWISE sets. We currently plan to apply the same periodogram to these objects again using just the NEOWISE data and just the ALLWISE data (which spans a shorter total timescale) respectively to see if there are any cleaner or different results. According to Herbst et al. (2012), sunspot caused periodicity is usually at the ~.1 -.2 magnitude level, and some of the YSOs are consistent with that while some are a bit higher. By looking at some of the unfolded data for these candidates, AWI00062be (shown in figure 14) might have long term irregular changes mixed in there.

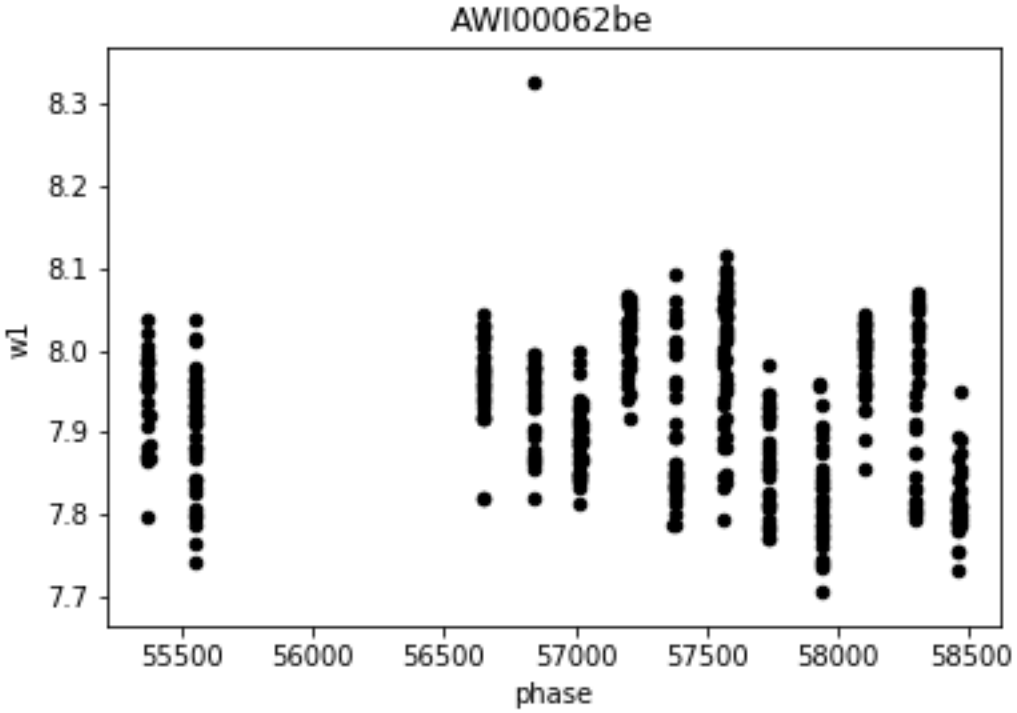

Figure 14. Raw data of AWI00062be with WISE archival data

Giants

Among the giants candidates, we have detected 10 variables. The 10 candidates are also plotted on the HR diagram (figure 15) below. Note that some of them have been reddened by interstellar dust (which results in a further shift to the right on the HR diagram). Based on their position on the HR diagram and periods, we tentatively suggest that 4 of them may be Cepheids, 1 may be a W Virginis object (a subclass of the Cepheid variable that its pulsation causes changes in both temperature and size (AAVSO 2020)), 1 may be a long period variable (Mirae), 1 may be a RR Lyrae and 3 may possibly be cases of FU Ori type objects, or very luminous YSOs, that got

mixed up with giants. By correcting the reddening for these objects and re-plot them on the HR diagram in the future, we plan to have to better classification of these 3 objects.

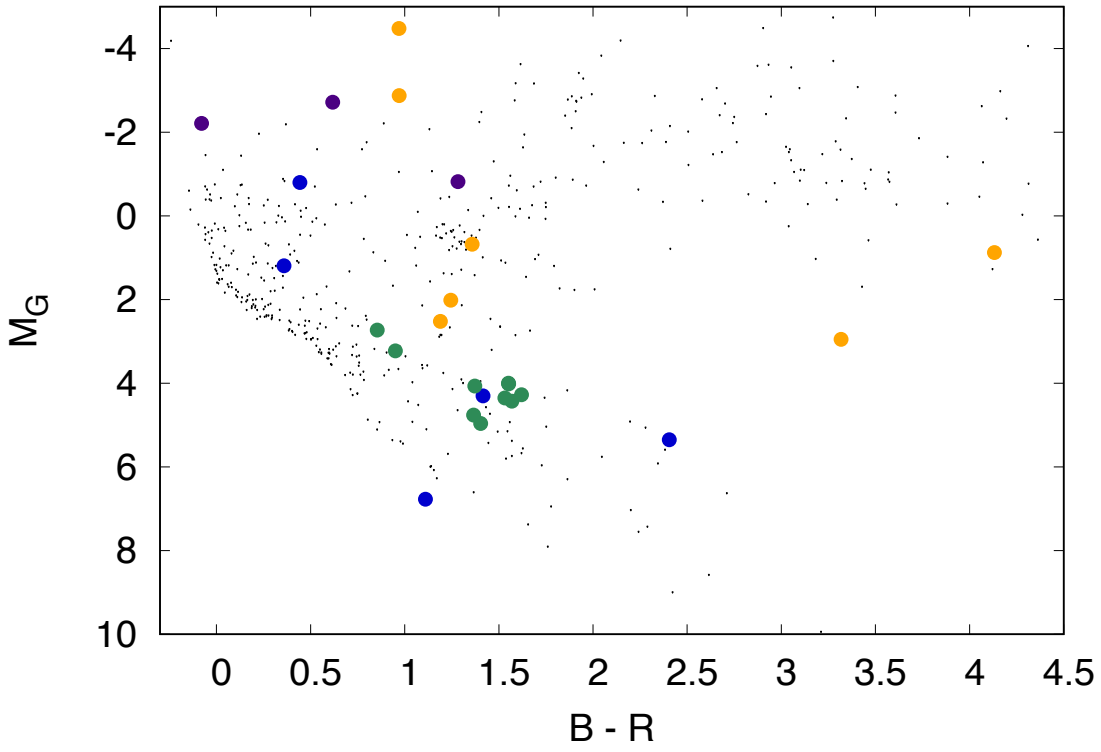

Figure 15. HR diagram for giants candidates. Background black points are all the Emory survey objects (with reddening and extinction not corrected for). The colored dots are variables from the archival survey (minus the 3 giants that don't really have good parallax data). Note: Purple points are CBes, blue points are Herbig Ae/Bes, green points are YSOs and yellow points are giants.

Chapter VII. Results from Emory Observatory

As discussed in chapter III, we observed some of the candidates with Emory's 24-inch telescope. We also conducted photometry analysis of our observation data. With the photometry analysis, we can further check the variability that we found with the WISE archival data. Apart from short term variability, we also look for long term changes with our observation. In order to look for long term variability, our strategy is to observe each candidate for more than 3 hours for the first time we observe them. Then, every time we conduct an observation, we will observe some of the objects we preciously observed for 10-20 minutes. In this sense, we will be able to have at least half of a light curve for some of the variable candidates that vary with periods of several days. However, in practice, we were not able to employ this strategy for every object due to changes in the weather and telescope availability.

The figure below is an example of the comparison between our observational data as well as the periodic light curve we found with the WISE archival data. We directly folded our Emory's data after photometry by the period we found with the Lomb-Scargle analysis. We can see that they largely coincide with each other except that the phase is off by roughly 0.25 and at phase = 1 the object shows a minimum with WISE archival data while a maximum with Emory's observational data. Additionally, the amplitude of the WISE archival data, when converted to magnitudes, would give about an R band magnitude amplitude of .07-.1 mag, and that's smaller than the archival analysis amplitude by about a factor of 2. Granted they are in

different wavelengths, so they might truly be different. Further observation on this object can help us to find out whether the maximum at phase = 1 (plot on the right of figure 16) is an error due to photometry or the periodic curve found with archival data is a coincidence.

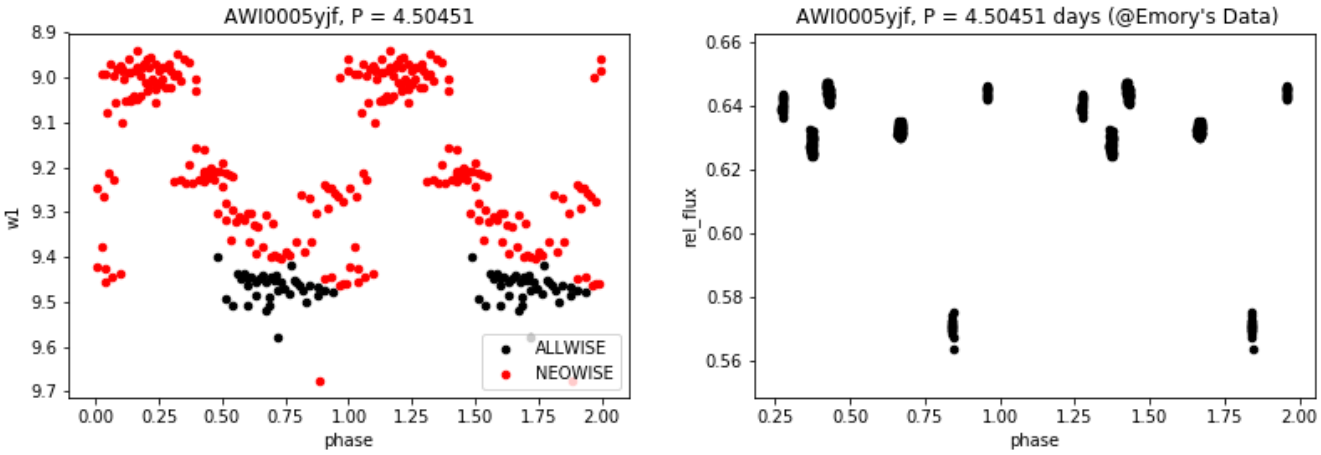

Figure 16. Periodic Light curve found with the WISE archival data (on the left) and the folded results on Emory's observation data. The plot on the right has the relative flux (between the target object and the reference star) on Y-axis.

For another candidate, AWI0002d9y, our observation also helped us in determining its period. Below are two periods we identify for the object with the WISE archival data:

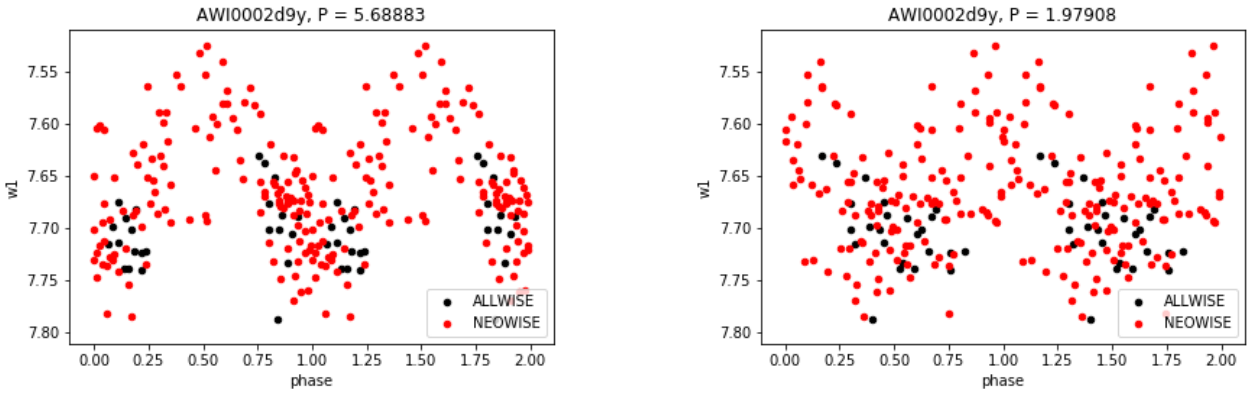

Figure 17. Periodic Light curves found with the WISE archival data.

It's hard to directly tell which one better describes the variation of the object. We folded our Emory's observation data both by the two periods we found. We find that by folding the data with p = 5.68883 days, the folded result (figure 15) coincides with the archival light curves of p = 5.68883. Note that the Y-axis value in figure 18 is different from the Y-axis value in the appendix, this is because the Y-axis of all the plots in Appendix III are normalized.

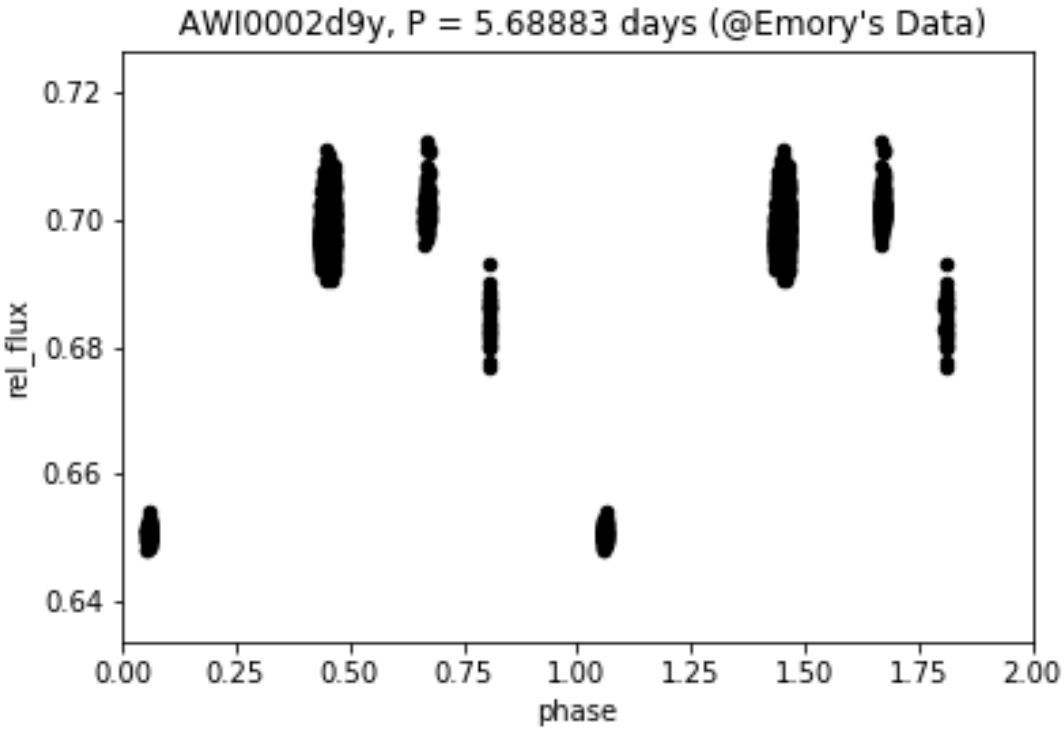

Figure 18. Periodic light curves found with the Emory observation data.

AWI0002d9y is problematic and the photometry result may not be accurate because the main reference star we fit in the frame every time (we experimented with different field of views for this star), turns out to look a bit variable. Also, there's a larger error bar associated with 2d9y because we may have to use a reference star that is much dimmer than the target.

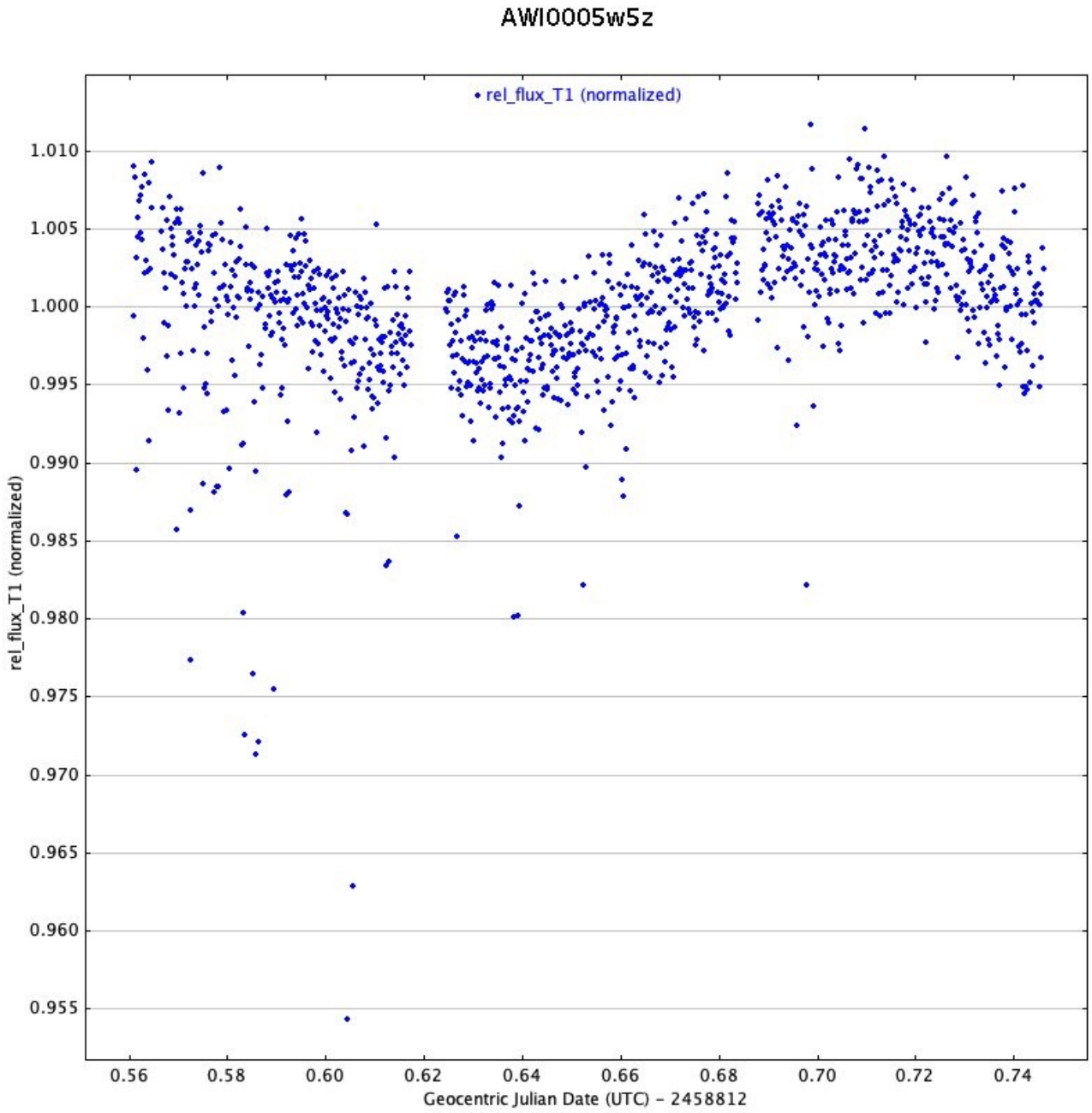

Figure 19. Calibrated differential photometry result for AWI0005w5c based on reference star 1. The Y-axis is the relative flux between the target star and the reference star, and X-axis represents the Geocentric Julian Date in units of days.

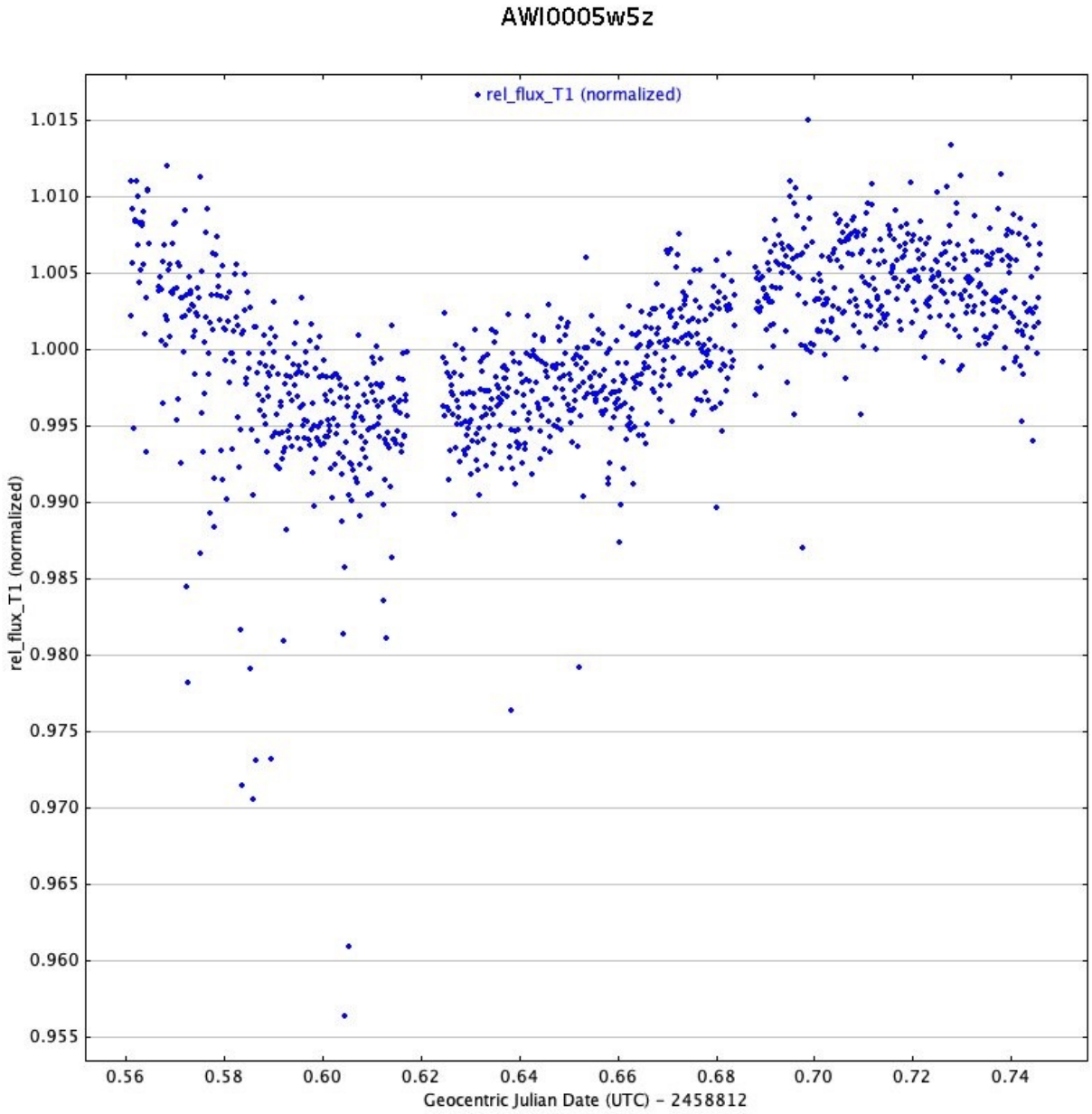

Figure 20. Calibrated differential photometry result for AWI0005w5c based on reference star 2. The Y-axis is the relative flux between the target star and the reference star, and X-axis represents the Geocentric Julian Date in units of days.

Figure 19 and 20 above are the results of differential photometry with two different reference stars (as shown in figure 21) for AWI0005w5z. We notice that the photometry under two different reference stars all gives a similar sinusoidal shape and phase. The gaps within the light curves of the two figures above are caused by our pause on observation. We observed some other objects during that period. Based on this result, we suspect that AWI0005w5z may be a short-term variable roughly with a period of 0.22 days. In order to further validate our light curve, the relative flux of the two reference stars is also checked and the result is given in figure 22:

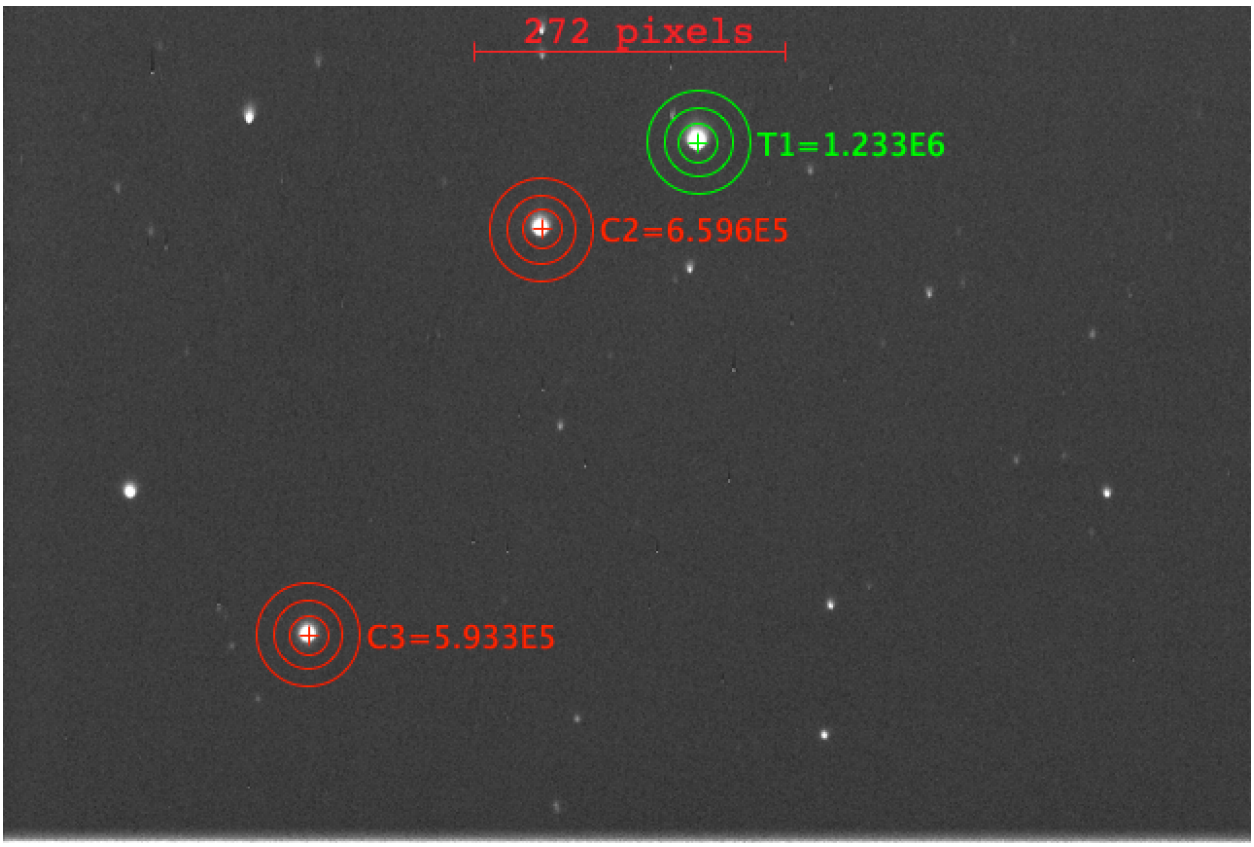

Figure 21. Field of view for AWI0005w5z. T1 is our target AWI0005w5z and C1, C2 are the two reference stars we used.

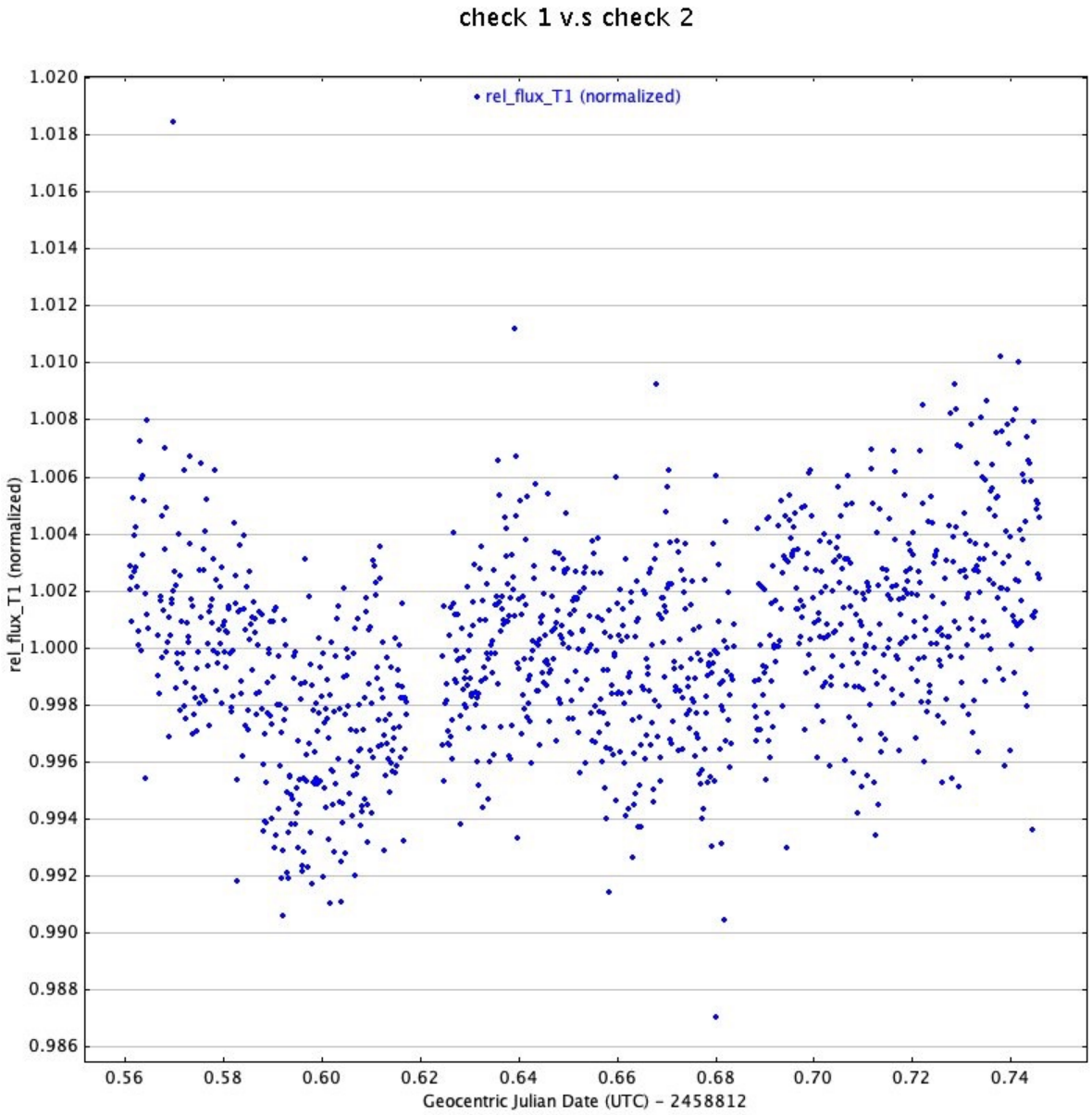

Figure 22. Differential photometry result for reference star 1 based on reference star 2.

Though there are some changes in the reference star with respect to the check star, neither seems to be changing in a way that would be giving rise to the sine-wave shape seen in the target. We also tried to apply our periodogram analysis for AWI0005w5z with only the NEOWISE data. However, no similar period has been found. One hypothesis is that the variations are so small in amplitude (and perhaps even

smaller in amplitude in the IR) that it's just not within the level of what we could hope to find with variations in WISE data. Thus, we plan to re-observe this object in the future to further validate the period we found here.

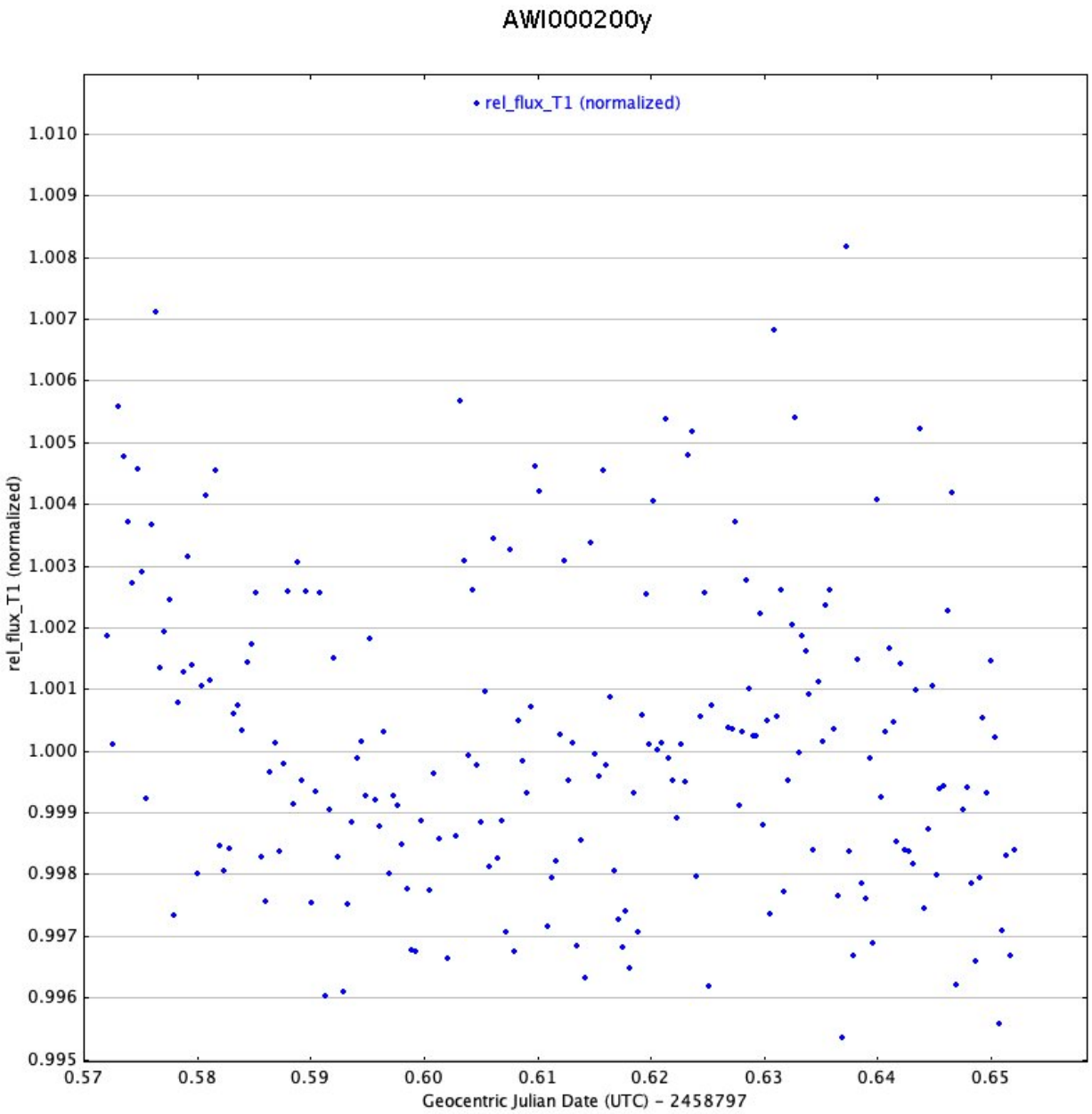

Figure 23. Calibrated differential photometry result for AWI0002ooy

Photometry results for the rest of the objects are given in appendix III. The check/reference stars we use are given in appendix I. Among all the 13 objects we observed, 3 of them are observed only one night. Photometry done by different reference stars (assuming it is not a variable) may give different results but should largely give the same tendency in the variation of magnitudes.

In general, AWI0002ooy needs more observation to collect more data. So far it doesn't seem to change enough to be significant across long timescales. The variation in one night is also not significant as shown in figure 23. AWI0002ozm looks pretty variable (as shown in figure) as there is a dip near the end of our observations. By checking the reference star and other stars in the image we find that this dip only happens to AWI0002ozm. AWI0002v3v shows different flux levels over time no matter which reference star we use. Thus, it seems to have significant long-term variation compared to the typical scatter in the data. It looks irregular as well, and we also see changes in the unfolded archival data. We definitely need more data on AWI0002vbd to see if it varies in long-term. AWI0005d8u doesn't seem like it has short-term variability on the order of hours, but we plan to still assess any long term variability with repeated observations. AWI0005w6c seems to be varying in a significant way. Also, the archival WISE data suggests that it varies irregularly. AWI0005w5z has an interesting low amplitude periodic variability, as we discussed above, but its long-term observation so far doesn't show signs of long term changes (just the short period oscillation). AWI00019iw looks pretty non-variable except for the second night (but we

noted that the second night on the target had periodic spotty cloud cover that might have affected the target and reference star differently). We only observed AWI00034wa over a very short timescale, so nothing to conclude about this yet at this moment. AWI00019pi looks like it may be varying slightly. This object is both near and far from a nebula and the galactic plane. As it is faint, it's more of a challenge to observe than some of the other objects (it is easy to accidentally get light from background stars included in the photometry). AWI00055kz definitely looks like it's changing (as is one of its reference stars though) both within one night (as shown in figure 25 below) and over a long time period. Every object mentioned in this paragraph we aim to further study in future work.

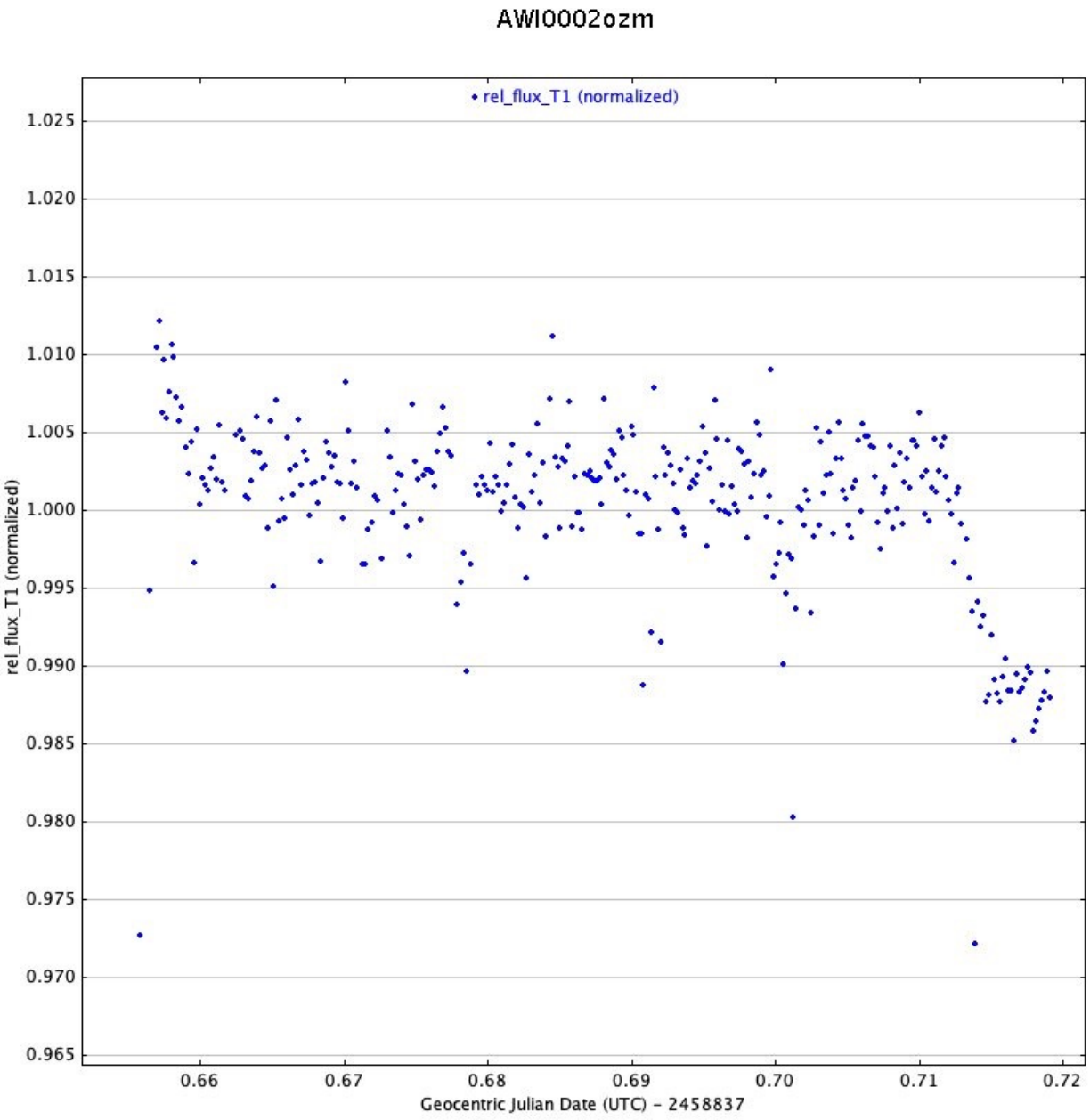

Figure 24. Calibrated differential photometry result for AWI0002ozm over one night

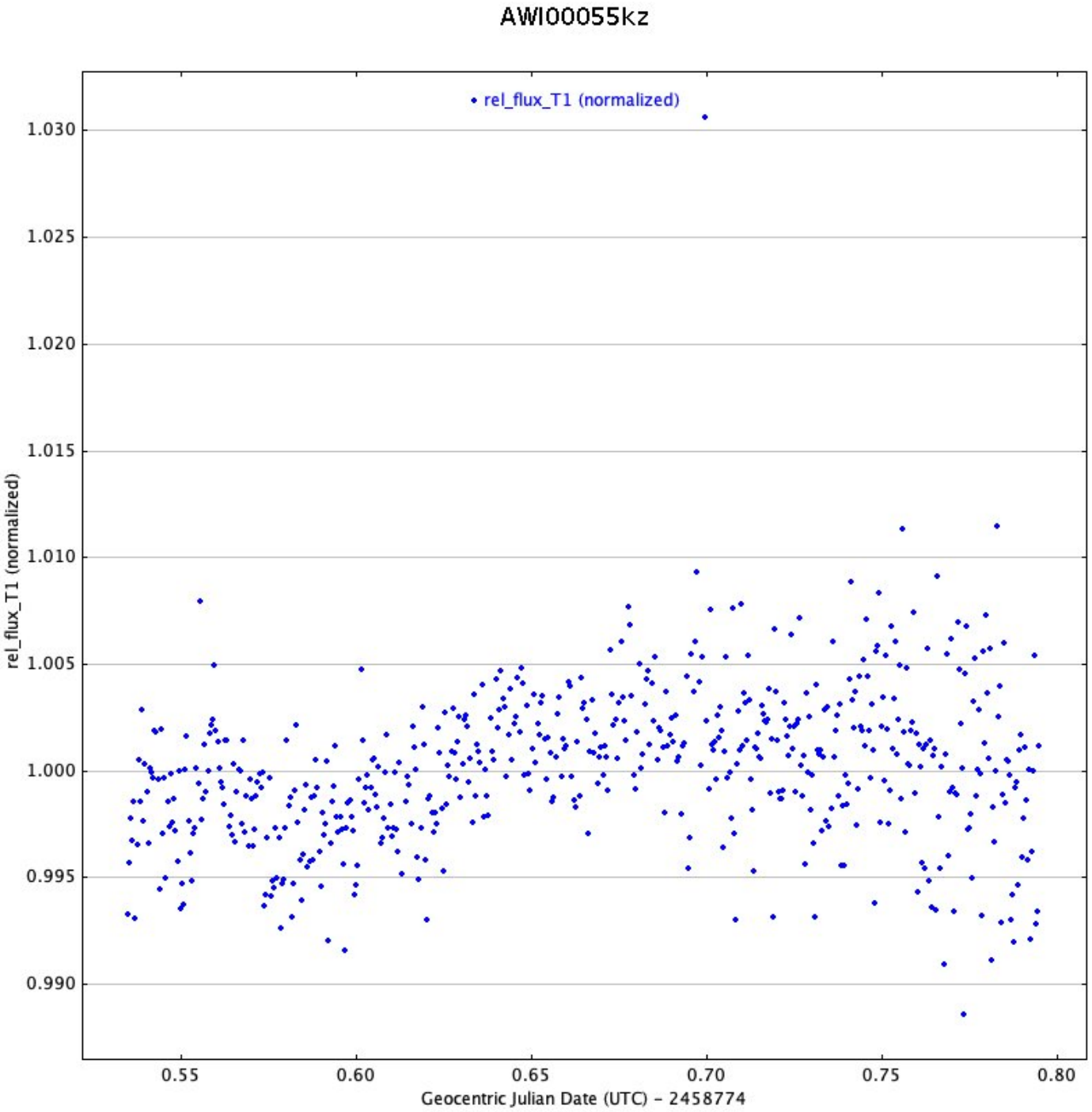

Figure 25. Calibrated differential photometry result for AWI00055kz over one night

Chapter VIII. Conclusions and Discussions

In this paper, we have used the ALLWISE and NEOWISE data to search for variability, both periodic and irregular. Several potential periodic variables are found with the WISE archival data. We also started a new program to monitor some of the candidates from Disk Detective for variability with Emory's 24-inch telescope. Two of the objects are found to be periodic variables with periods that agree with our analysis of the ALLWISE and NEOWISE data. Other potential periodic variables through our observations like AWI0005w5z were found. Several variables were observed that appear to be varying non-periodically (or perhaps varying with a long period that we would not yet be able to measure).

Our analysis of period identification can be improved in several aspects. We could more thoroughly vet the archival data and get rid of photometry with certain flags that might indicate the moon was nearby, etc. We could also do something to estimate the quality of the fit, i.e. making sure that we get the same period when we change the input data set a bit. Different models for maximum power spectral density fitting may give better results as well.

The classification of periodic variables can be further improved as well. The current classification is rough. We can include the color as a criterion to classify our variables, where we can adapt the star's intrinsic colors. Infrared excess can also be

included as a criterion for use. Additionally, each categories can be further separated. For example, Cepheids can be further separated into classical Cepheids (Cep-Is) and Type II Cepheids (Cep-IIs), and RR Lyrae can be further separated into Type-ab RR Lyrae (RRab), Type- c RR Lyrae (RRc) and so on.

We have found a lot of periodic variabilities among the Herbigs and YSOs and they are of interest to investigate. It may mean that some of our Herbigs are better classified as Be stars, but it also might somehow be a sign of long-lived quasi-periodic stellar activity, or that those stars are in binary systems.

Although our observational data collection is in its early stages, we have already made some new variable star discoveries. Further monitoring of these candidates and more of the Disk Detective objects of interest will help better classify these objects and shed light on the nature of variable stars with IR excess. Additionally, we have shown that assessing the archival data can be useful in identifying new variables, and can help to guide our future observations. Classification on periodic variables can be further studied to conduct a better analysis as well. Weather permitting, we also plan to observe more objects with Emory's 24-inch telescope to check the validity of the period we find as well as looking for long term period both for the objects we mentioned in this paper as well as for new objects.

References

AAVSO. W Virginis. Accessed April 5, 2020. https://www.aavso.org/vsots_wvir.

Appenzeller, I; Mundt, R (1989). "T Tauri stars". *The Astronomy and Astrophysics Review*. 1 (3–4): 291.

“Bias Frame Calibration.” Bias Frame Calibration. MaxIm DL. Accessed March 10, 2020. https://diffractionlimited.com/help/maximdl/Bias_Frame_Calibration.htm.

Bans, A., et al. 2020.

Caltech. “STARS, CEPHEID VARIABLE.” Stars, Cepheid Variable. Accessed March 19, 2020. https://ned.ipac.caltech.edu/level5/ESSAYS/Evans/evans.html.

Chen, X., Wang, S., Deng, L., et al. 2018, ApJ, 237, 2.

Evans A, Davies JK, Kilkenny D, Bode MF. 1989. MNRAS 237:695–705

GAIA. “GAIA'S HERTZSPRUNG-RUSSELL DIAGRAM.” ESA Science & Technology - Gaia's Hertzsprung-Russell diagram, n.d. https://sci.esa.int/web/gaia/-/60198-gaia-hertzsprung-russell-diagram.

Group, CfA Web Services. RG Research: Young Stellar Objects, May 16, 2006. **https://www.cfa.harvard.edu/rg/star_and_planet_formation/young_stellar_objects.html**.

Herbst, W., et al. 2012, JAAVSO, 40.

Hughes, A. Meredith, Gaspard Duchêne, and Brenda C. Matthews. “Debris Disks: Structure, Composition, and Variability.” Annual Review of Astronomy and Astrophysics 56.1 (2018): 541–591. Crossref. Web.

Jaschek, M., Slettebak, A., & Jaschek, C. 1981, Be Star Newsl., 4, 9

John M. Porter, Thomas Rivinius et al. 2003 ASP, 115, 12.

Karen A. C., et al. 2017. AJ, 153, 2.

Kenyon, S. J., & Bromley, B. C. 2002, ApJL, 577, L35.

Kuchner, M., et al. 2016, ASJ, 830, 2.

Labadie-Bartz, Jonathan et al. “Photometric Variability of the Be Star Population.” The Astronomical Journal 153.6 (2017): 252. Crossref. Web.

Lee, H., Scott J., et al. 1996, ARAA, 34:207-240

Matlab. “Lomb-Scargle Periodogram.” Accessed March 14, 2020. https://www.mathworks.com/help/signal/ref/plomb.html.

Samus N.N., Kazarovets E.V., Durlevich O.V., Kireeva N.N., Pastukhova E.N., General Catalogue of Variable Stars: Version GCVS 5.1, Astronomy Reports, 2017, vol. 61, No. 1, pp. 80-88 {2017ARep…61…80S}

“Simple Aperture Photometry by Hand.” Simple Aperture Photometry by Hand. Michael Richmond. Accessed March 11, 2020. http://spiff.rit.edu/classes/phys373/lectures/photom_2003/photom_2010.html.

Swinburne. “COSMOS - The SAO Encyclopedia of Astronomy: COSMOS.” Centre for Astrophysics and Supercomputing. Accessed March 19, 2020. http://astronomy.swin.edu.au/cosmos/R/RR Lyrae.

“Swinburne University of Technology.” Swinburne University of Technology>. Accessed April 12, 2020. http://astronomy.swin.edu.au/cosmos/R/RR Lyrae.

VanderPlas, Jacob T. “Understanding the Lomb–Scargle Periodogram.” The Astrophysical Journal Supplement Series 236.1 (2018): 16. Crossref. Web.

VanderPlas, J T., Ivezić, Ž., et al. 2015, ApJ, 812, 18.

Voshchinnikov NV, Grinin VP. 1992. Astrophysics 34:84–95

Waters, L., Waelkens, C., et al. 1998 ARAA, 36, 233–66.

Wenzel W. 1968. In Non-Periodic Phenomena in Variable Stars, ed. L Detre, IAU Colloq. 4:61–73

Wright, E. L., Eisenhardt, P. R. M., Mainzer, A. K., et al. 2010, AJ, 140, 1868

Zatsjeva GV. 1973. Var. Stars 19:63

Appendix I.

Figures below are the sample images (field of view) we took for each of the objects in table 1. All the objects are circled and labeled as “T1” and the reference/ check stars we used are labeled as “C1, C2, etc..”.

AWI00055kz:

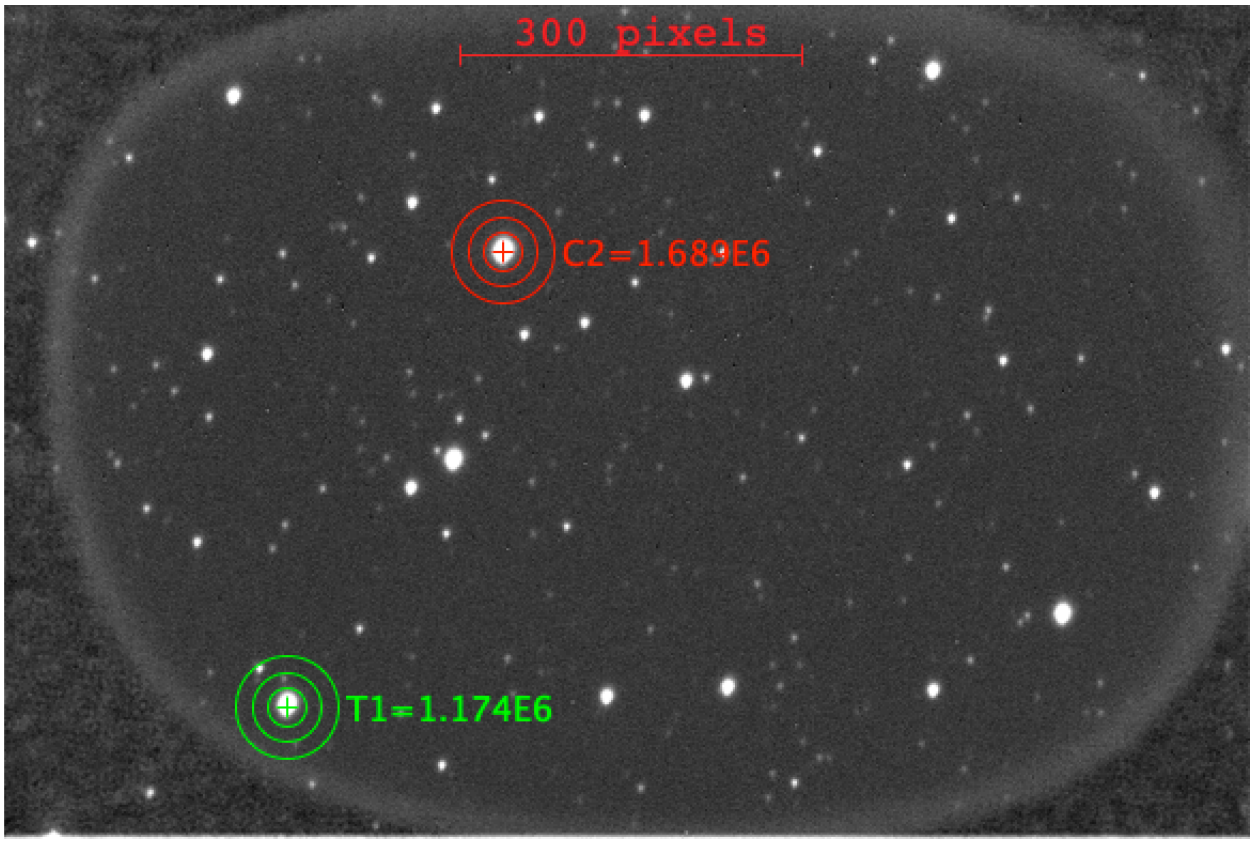

AWI0002d9y:

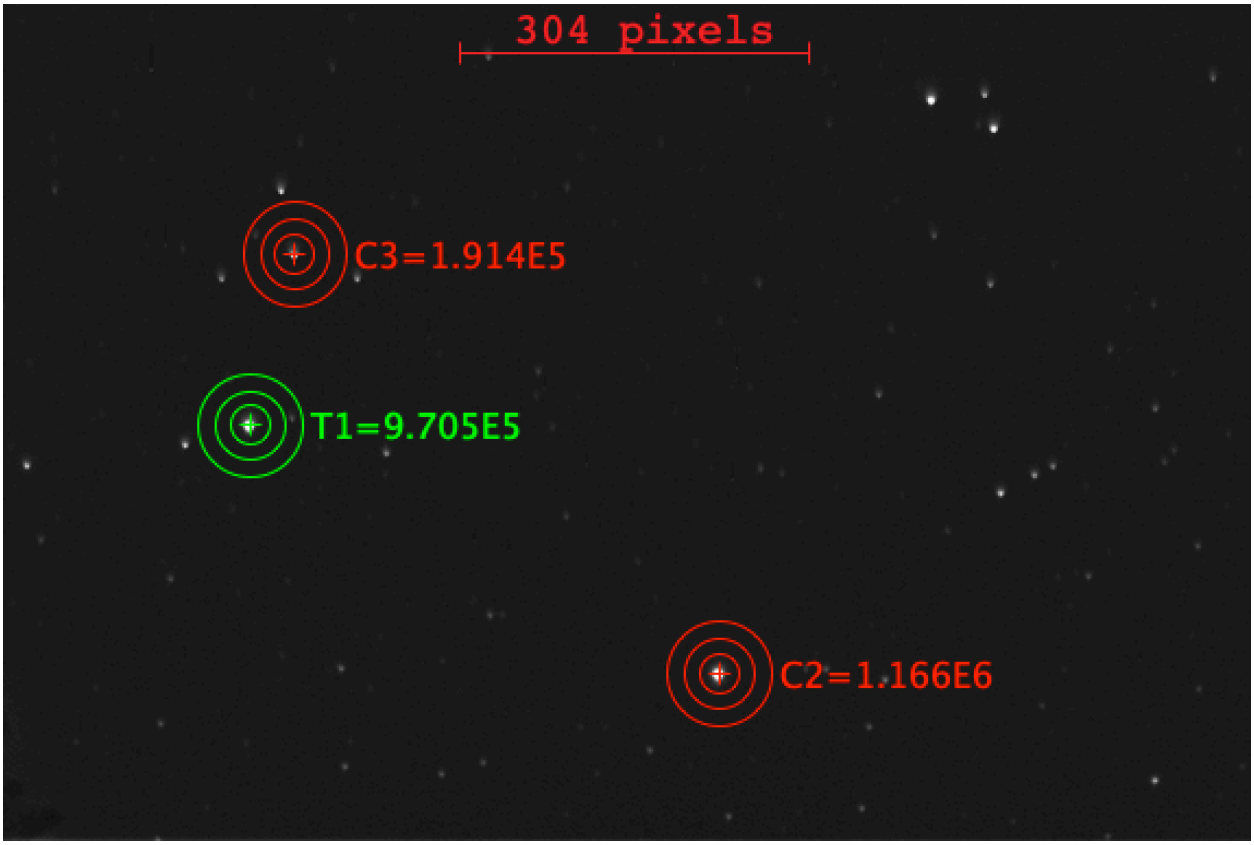

AWI0002ooy:

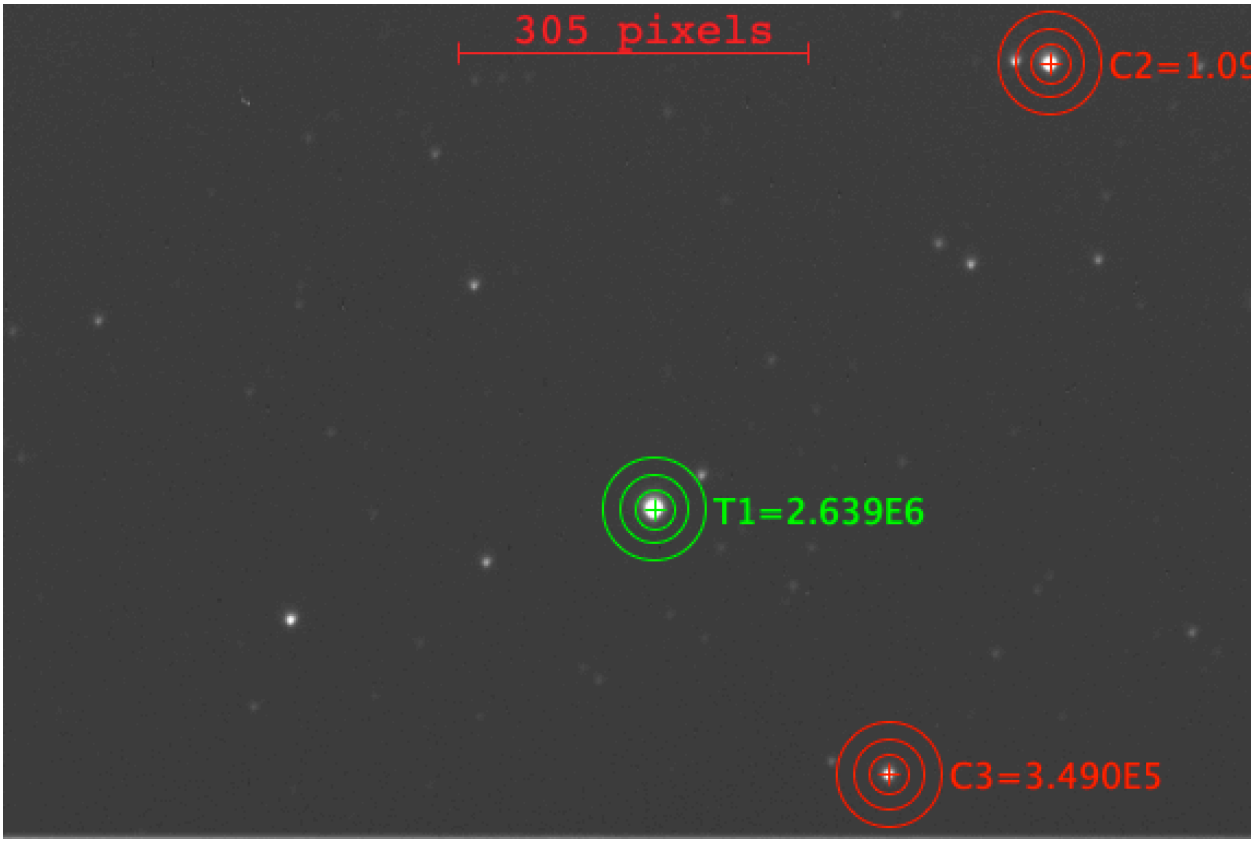

AWI0002ozm:

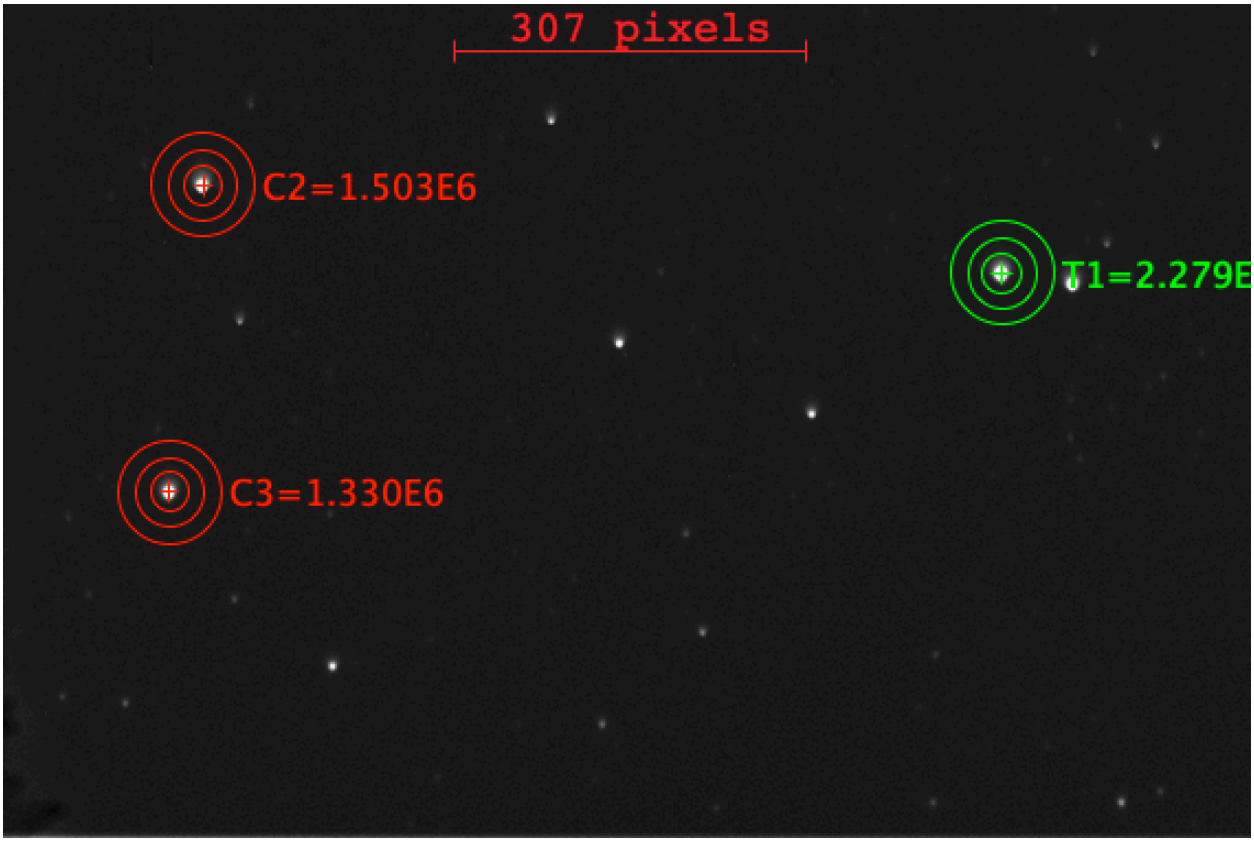

AWI0002v3v:

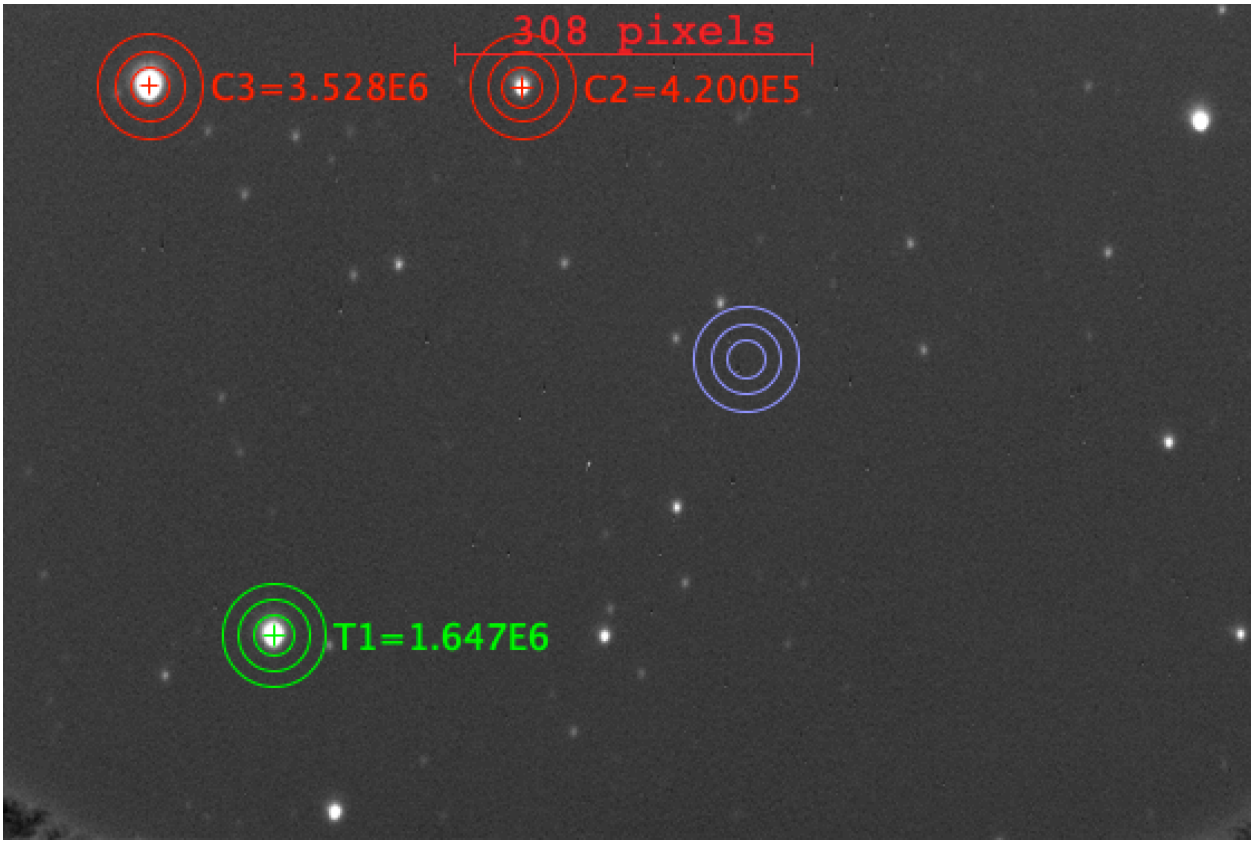

AWI0002vbd:

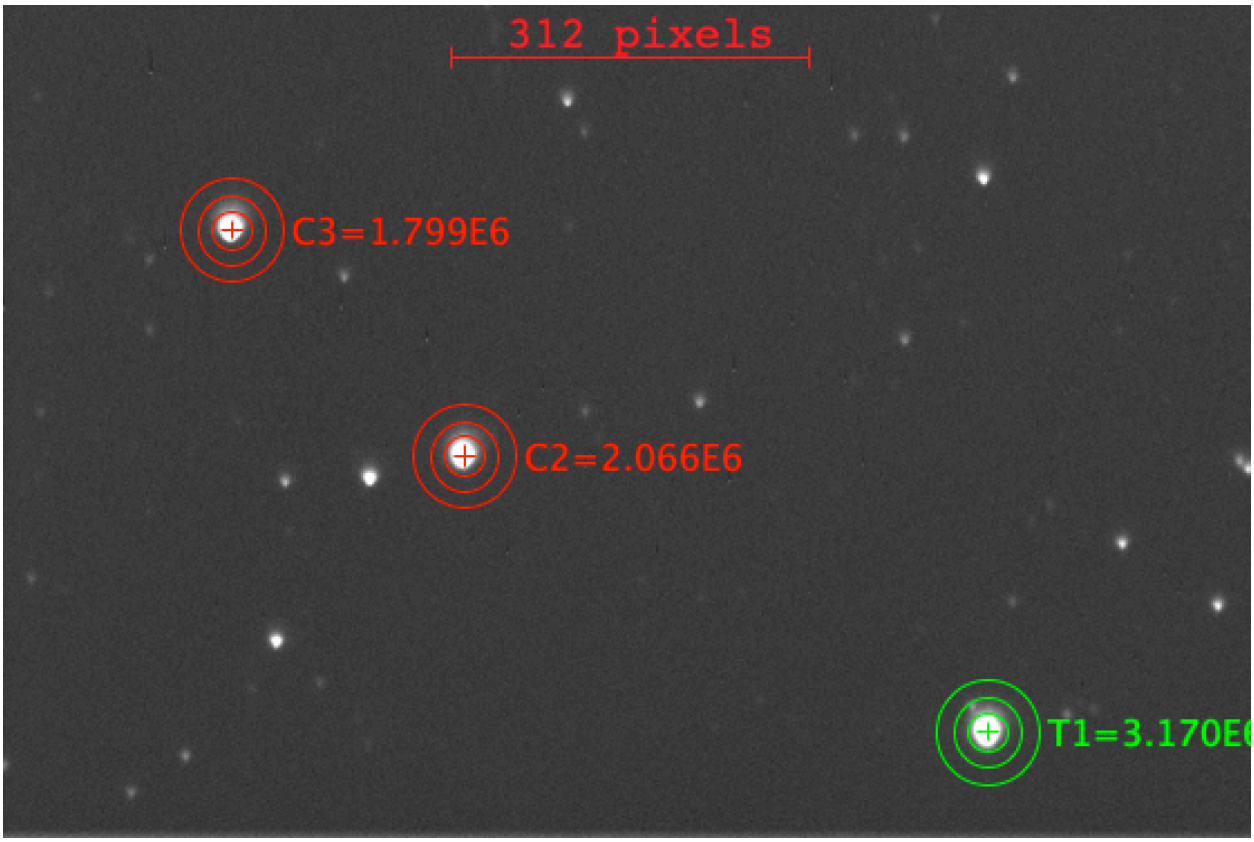

AWI0005d8u:

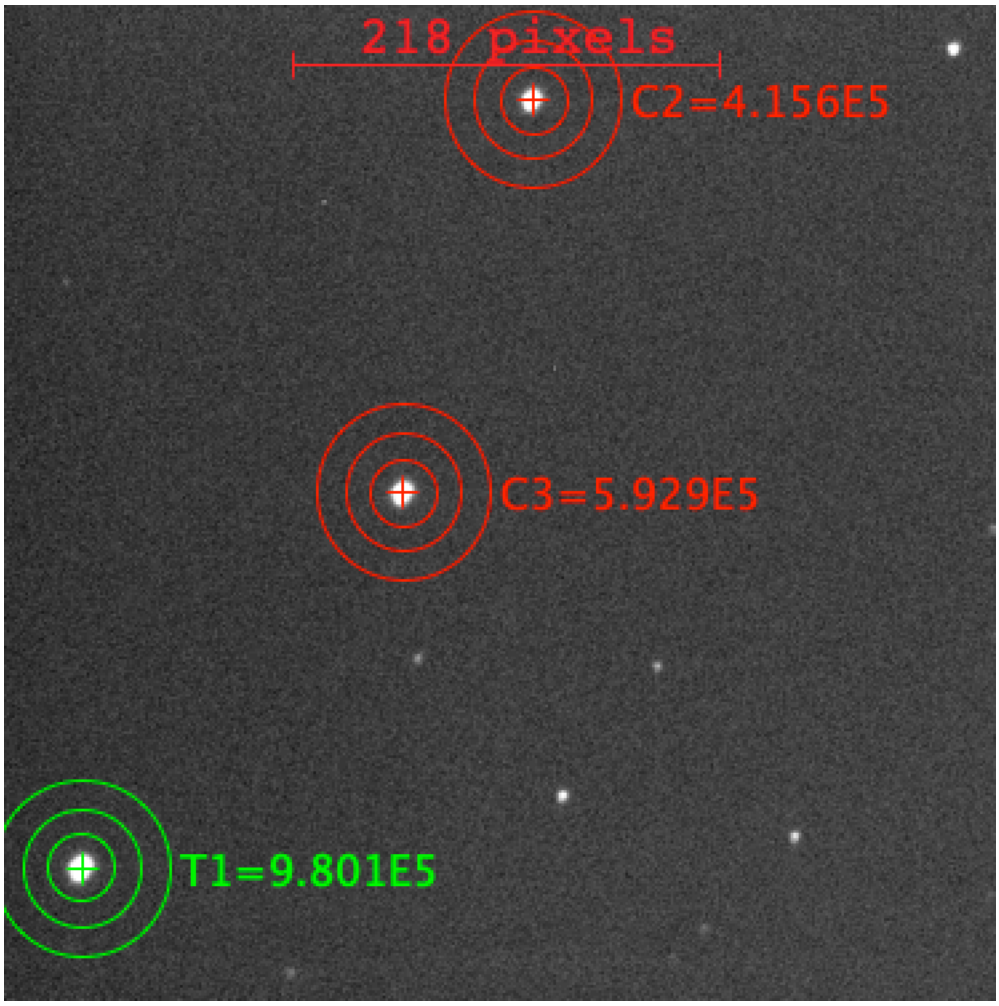

AWI0005w5z:

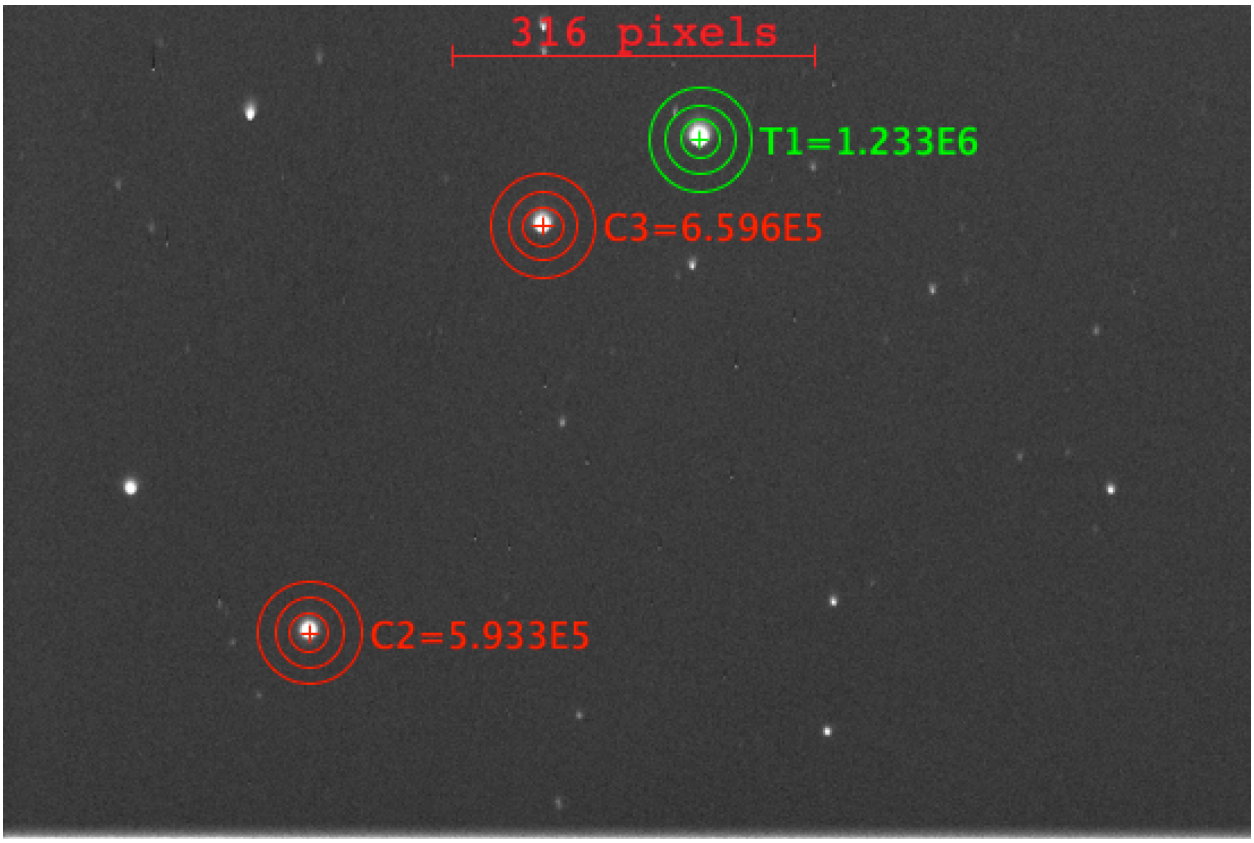

AWI0006w6c:

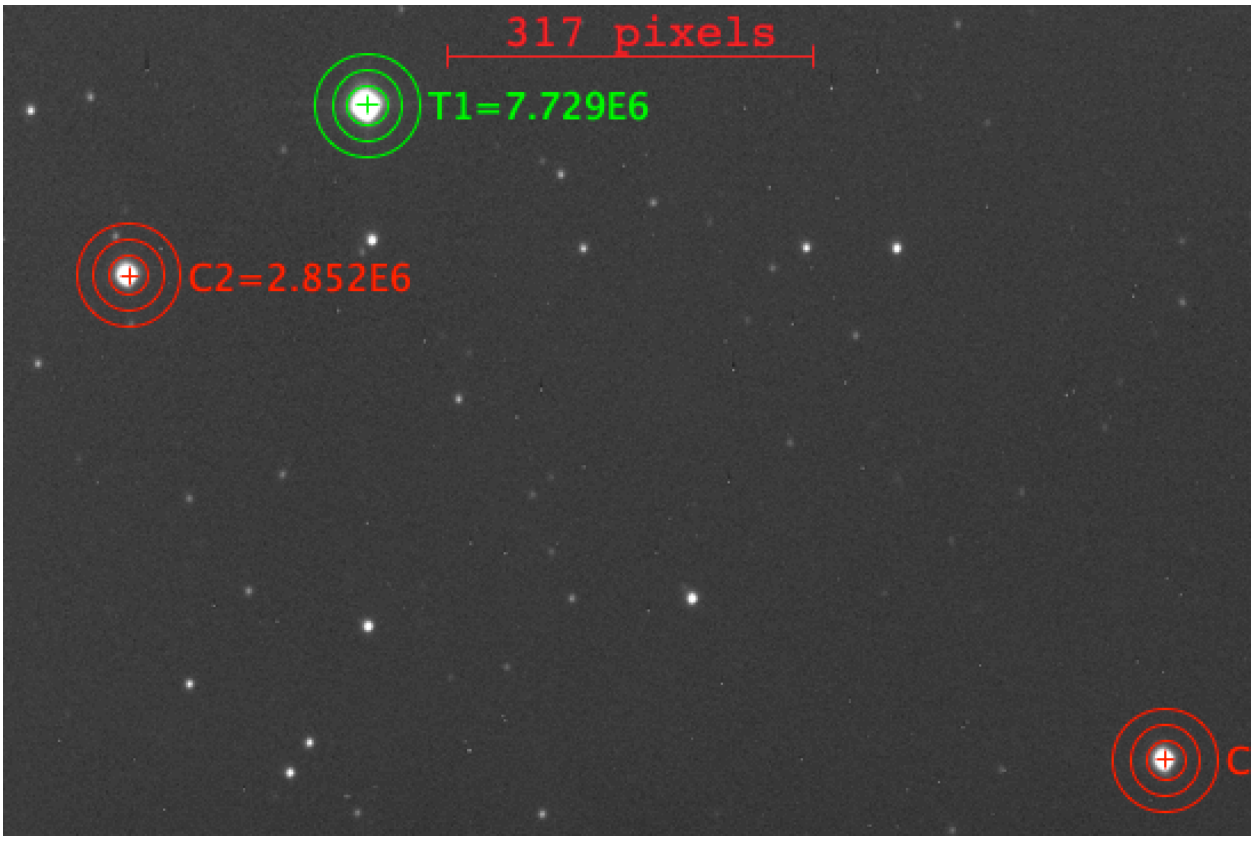

AWI00019iw:

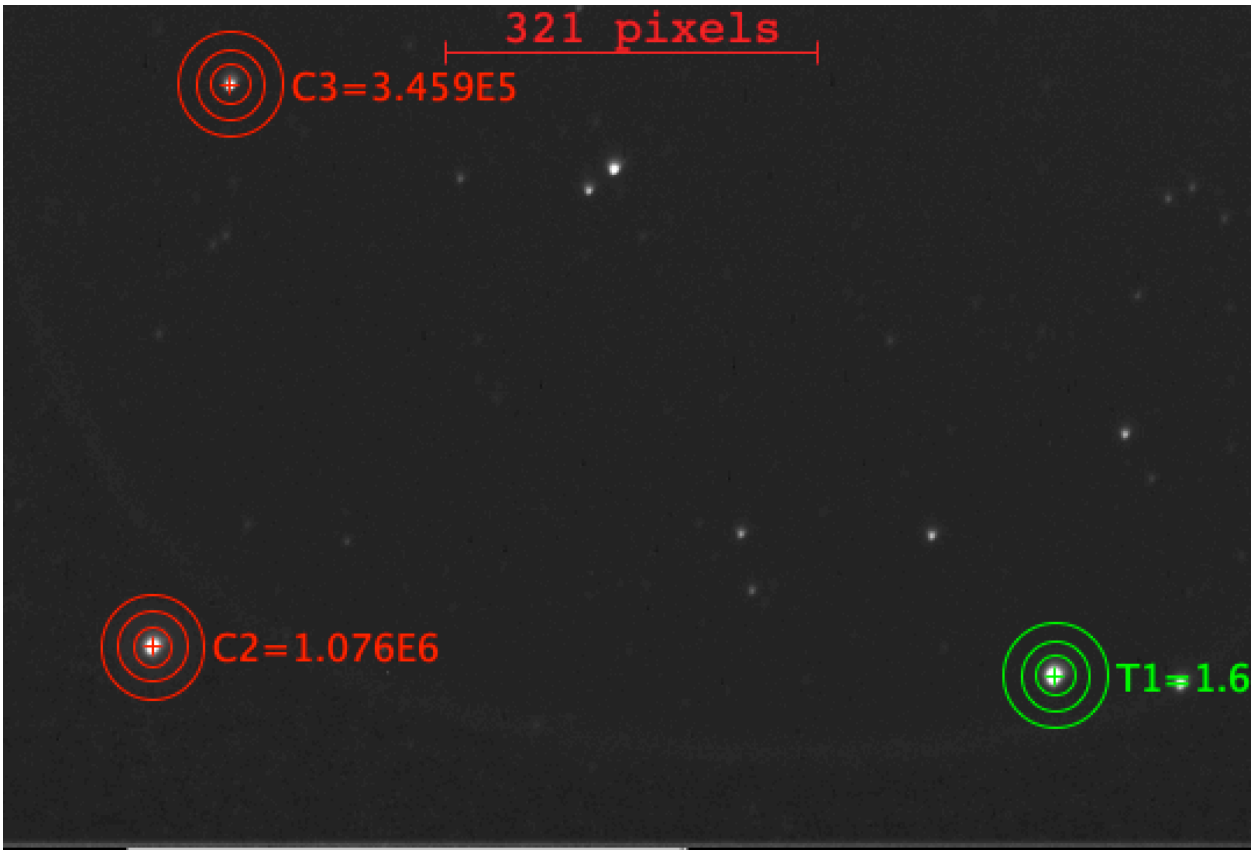

AWI0005yjf:

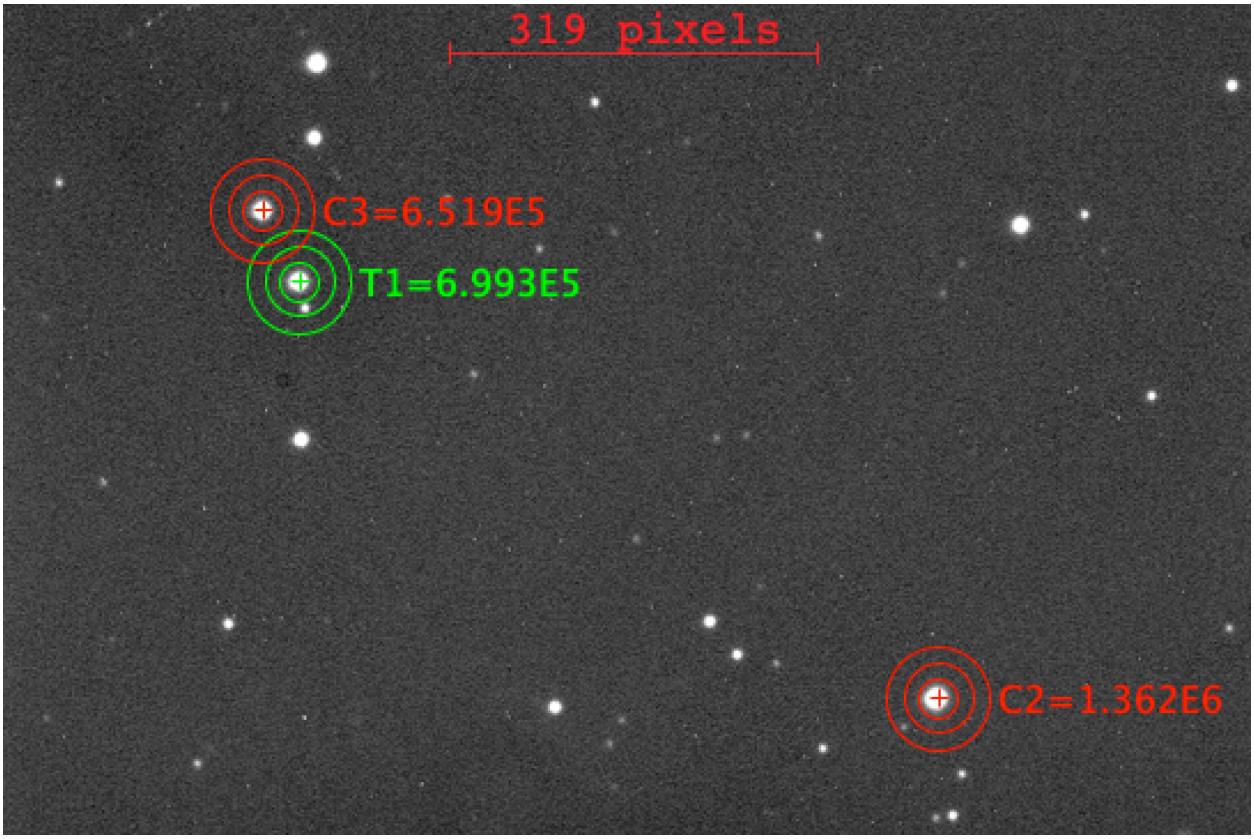

AWI00019iw:

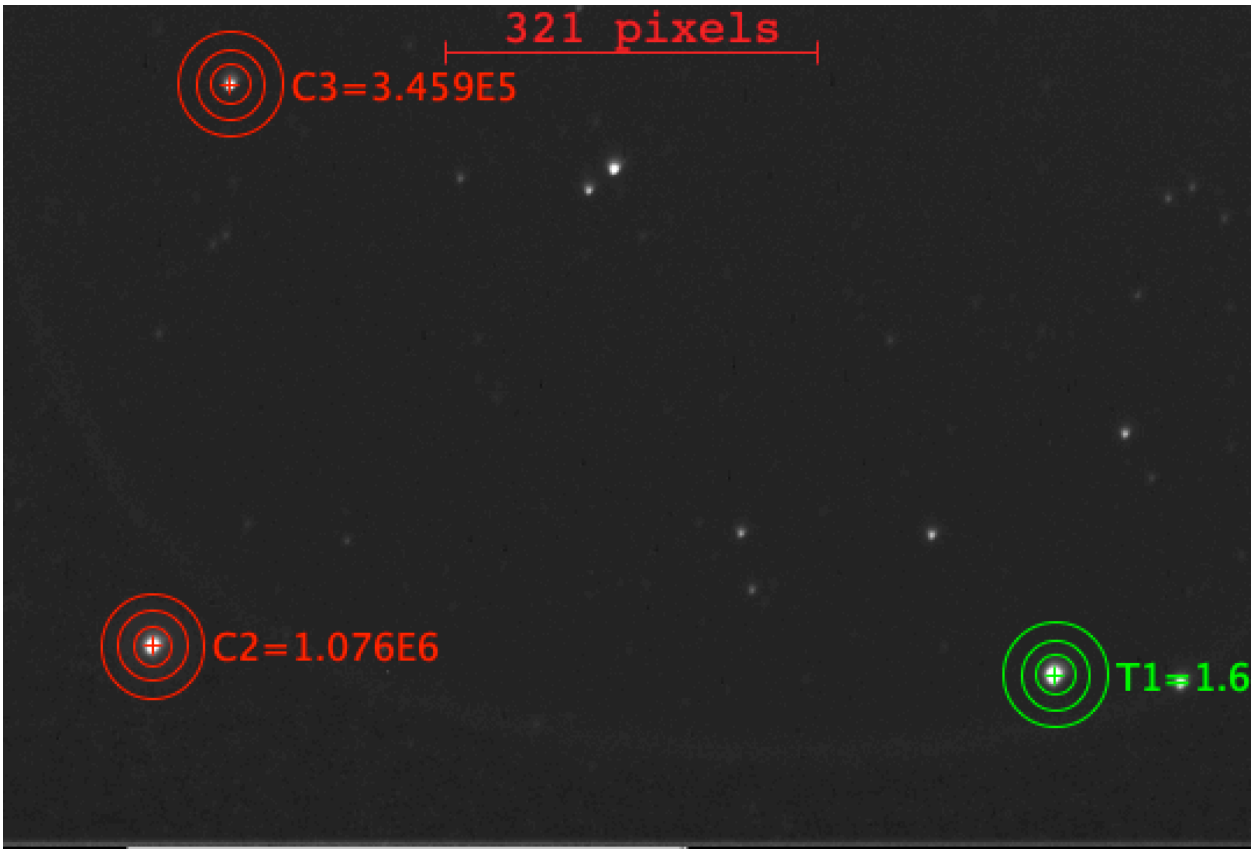

AWI00019pi:

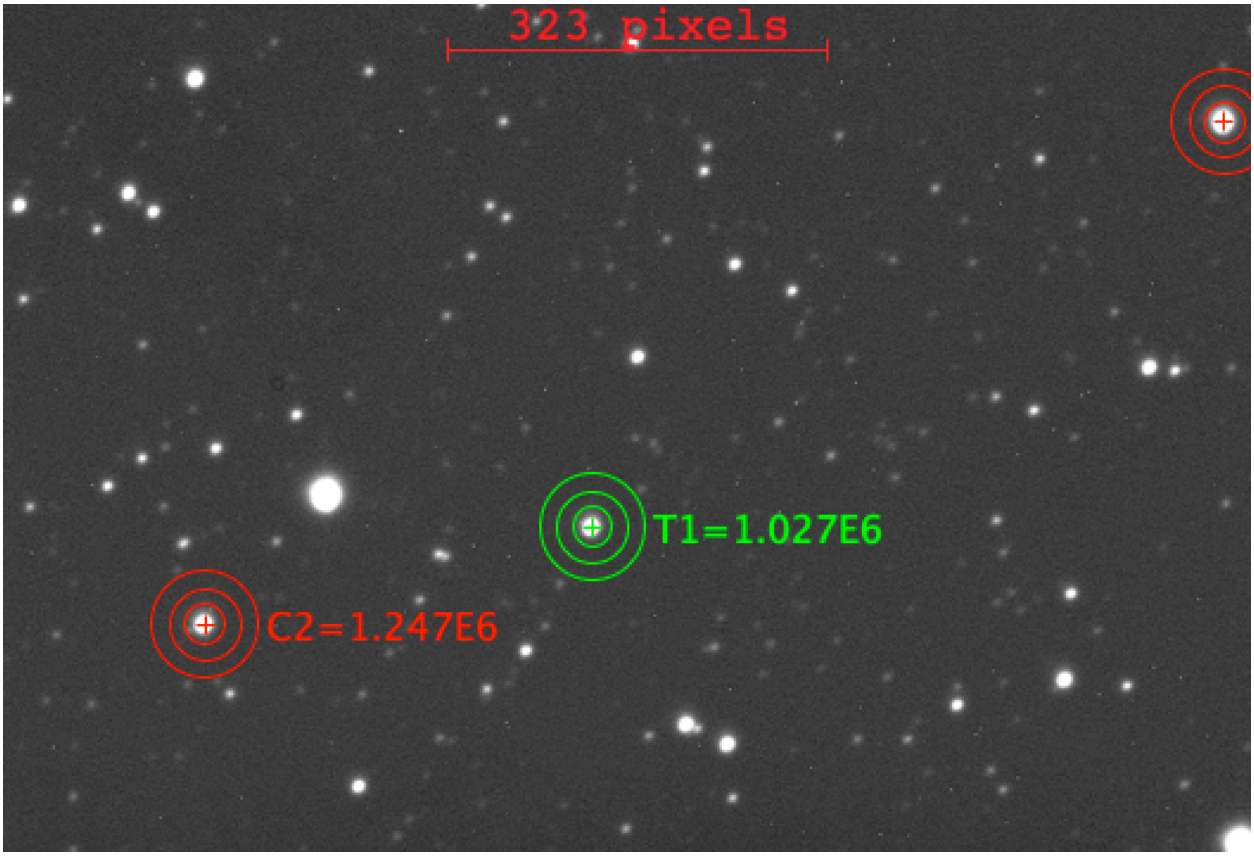

AWI00034wa:

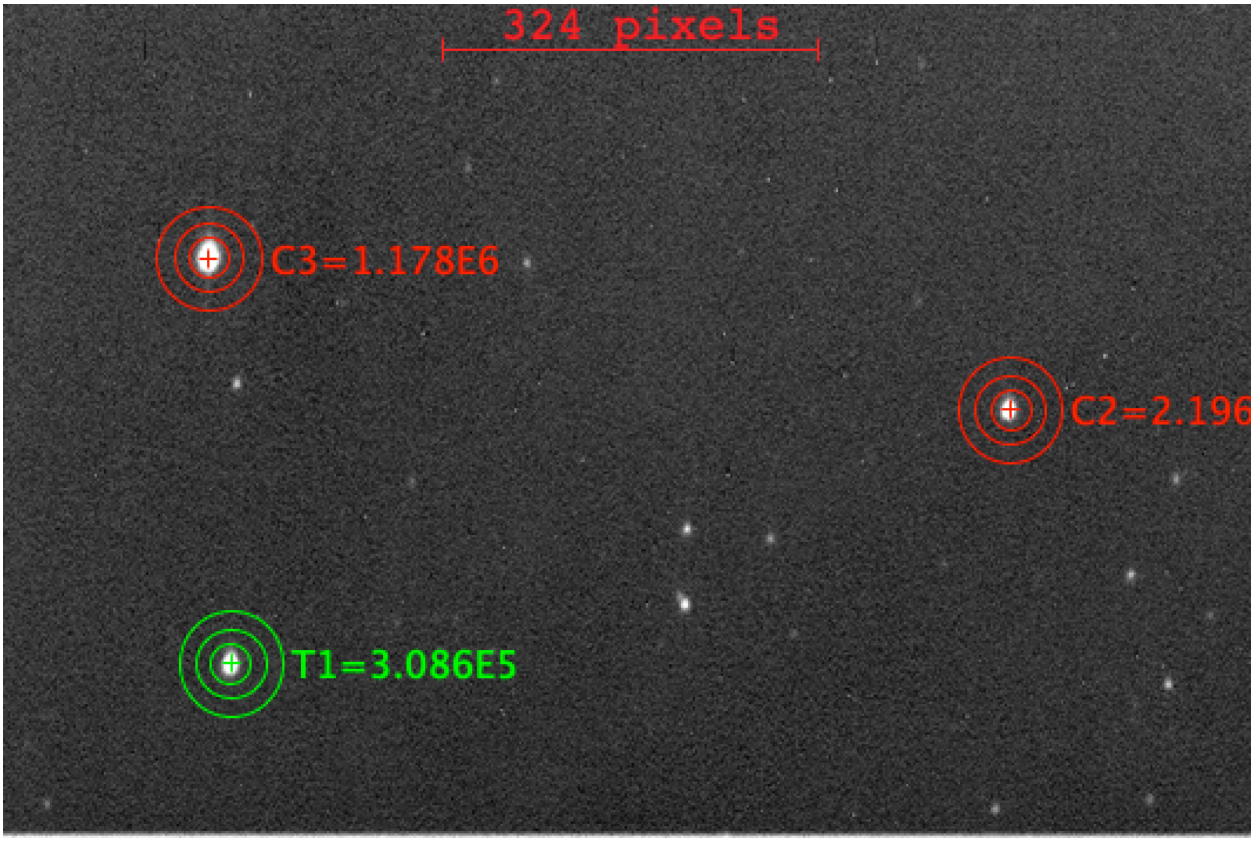

Appendix II.

Figures below are the light curves of all the periodic variables we found with the WISE archival data in table 2. Y axis plots the W1 magnitude and X axis represents the phase of the object. Note that "phase" on the x axis means the particular appearance or state for cycle of changes and phase from 0 to 1 depicts one full cycle.

Classical Be stars

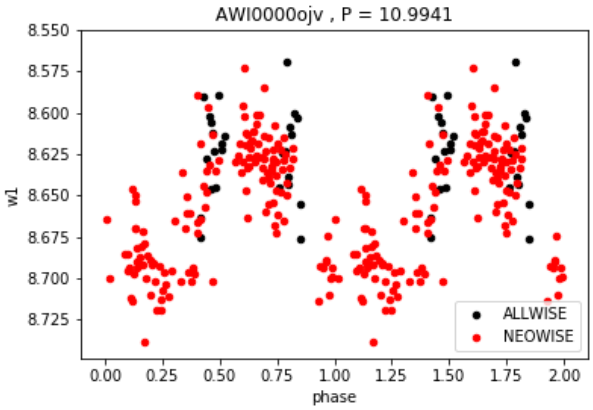

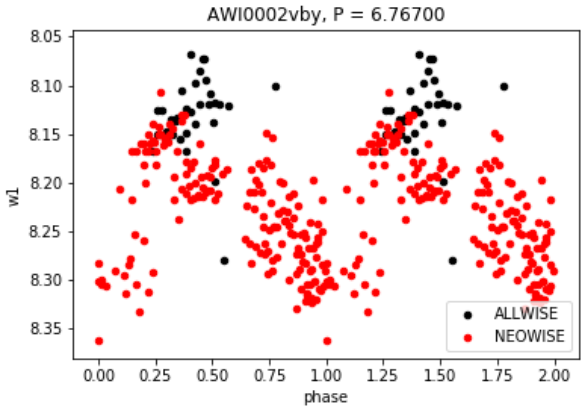

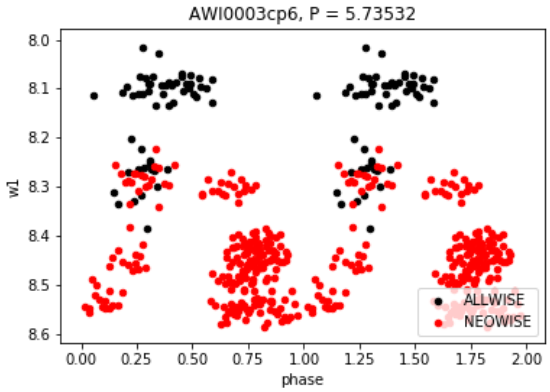

Herbig Ae/Be stars

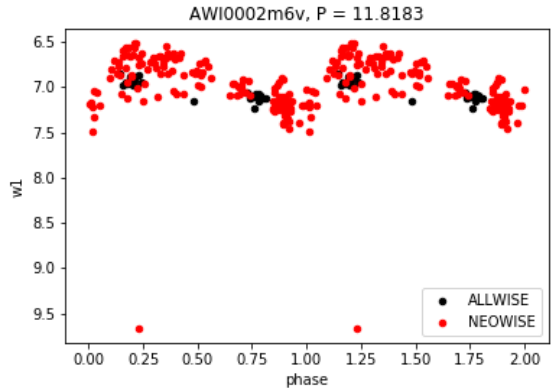

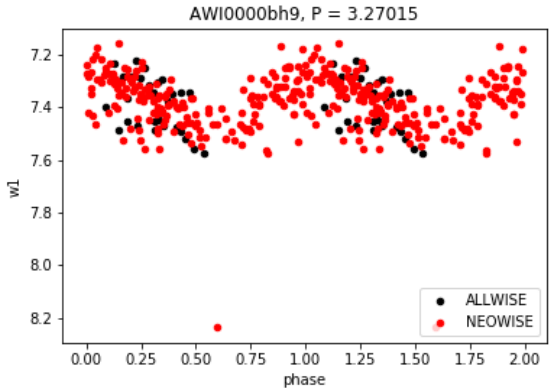

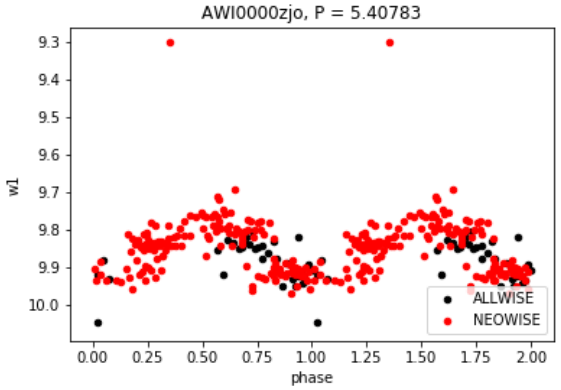

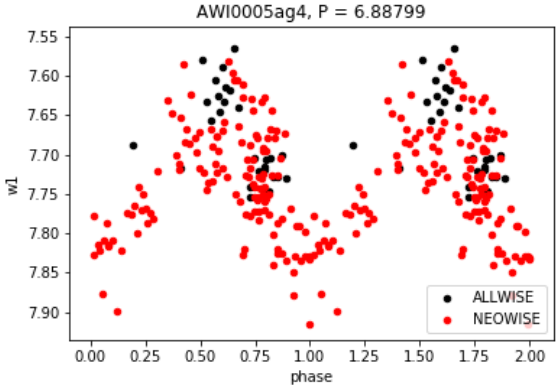

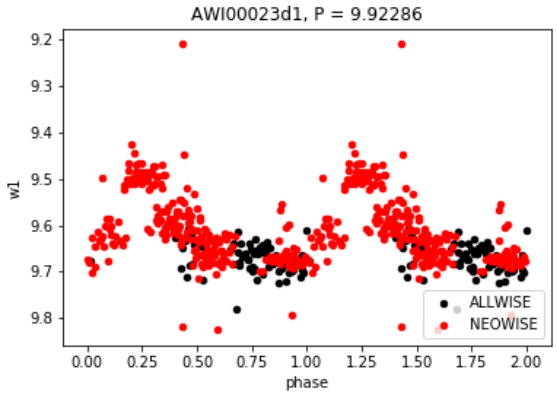

YSO

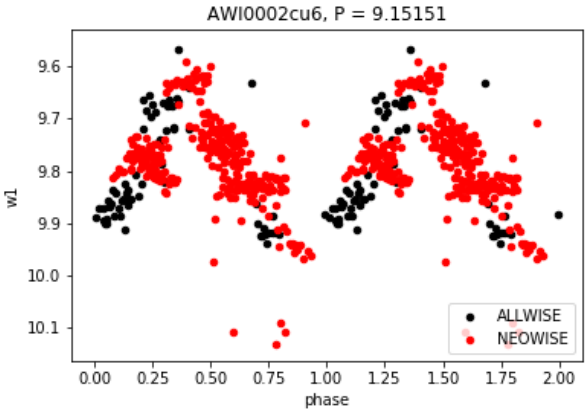
AWI0002cu6, P = 9.15151
w1
phase
ALLWISE
NEOWISE

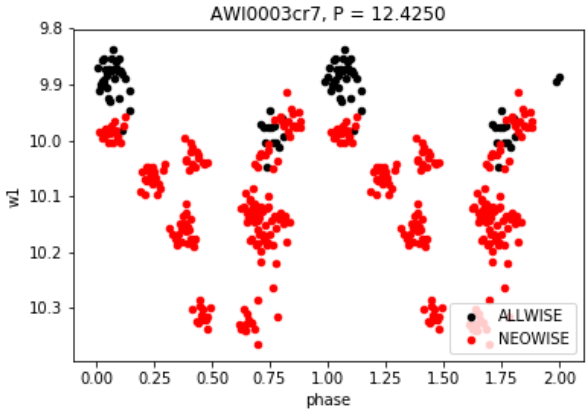
AWI0003cr7, P = 12.4250
w1
phase
ALLWISE
NEOWISE

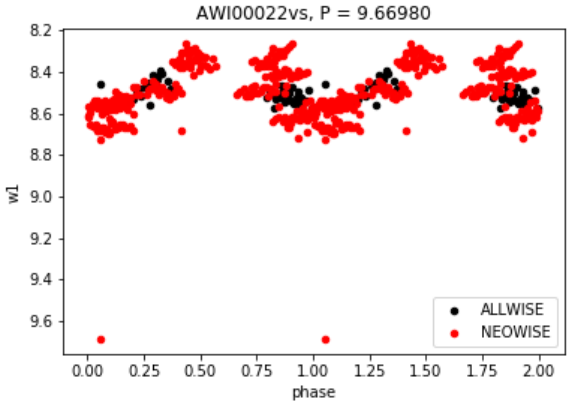
AWI00022vs, P = 9.66980
w1
phase
ALLWISE
NEOWISE

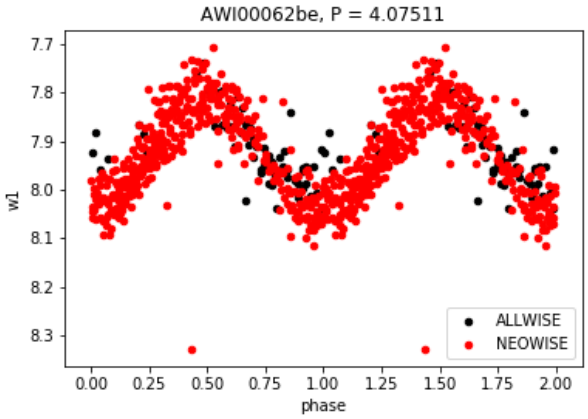
AWI00062be, P = 4.07511
w1
phase
ALLWISE
NEOWISE

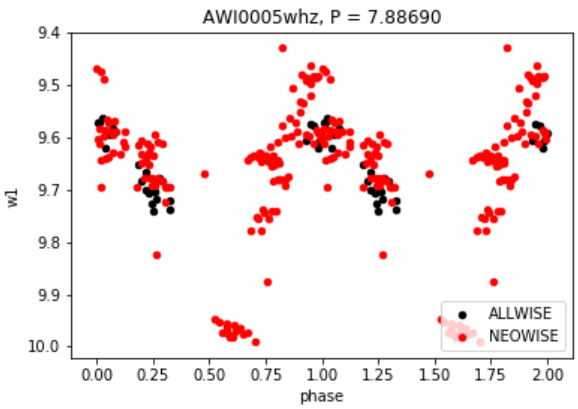
AWI0005whz, P = 7.88690
w1
phase
ALLWISE
NEOWISE

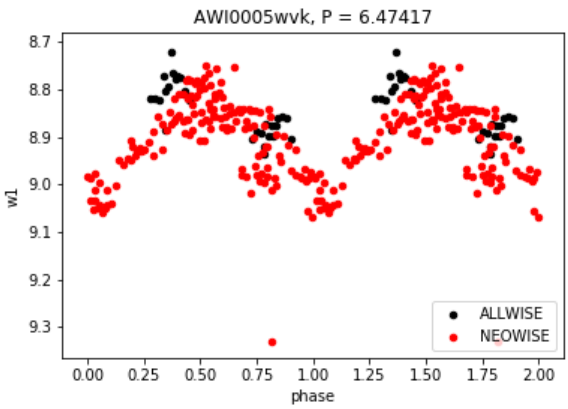
AWI0005wvk, P = 6.47417
w1
phase
ALLWISE
NEOWISE

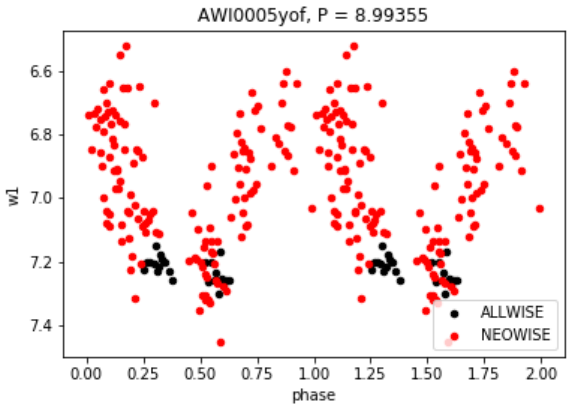
AWI0005yof, P = 8.99355
w1
phase
ALLWISE
NEOWISE

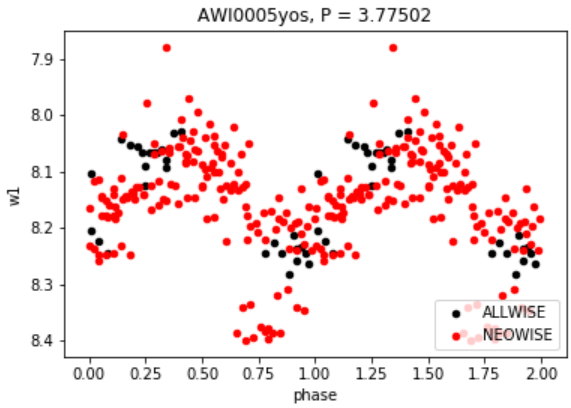
AWI0005yos, P = 3.77502
w1
phase
ALLWISE
NEOWISE

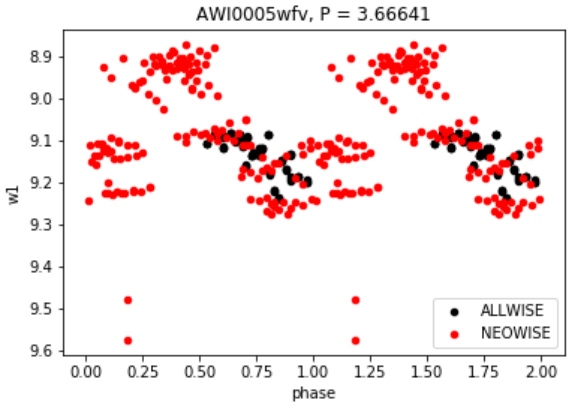
AWI0005wfv, P = 3.66641
w1
phase
ALLWISE
NEOWISE

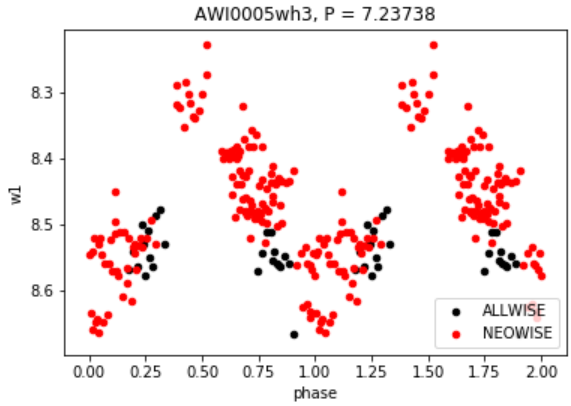
AWI0005wh3, P = 7.23738
w1
phase
ALLWISE
NEOWISE

Giants

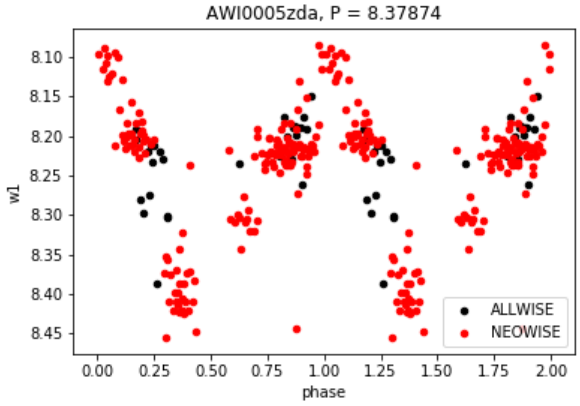
AWI0005zda, P = 8.37874
w1
phase
ALLWISE
NEOWISE

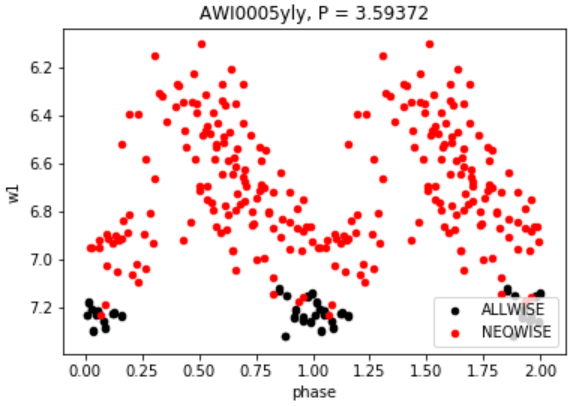
AWI0005yly, P = 3.59372
w1
phase
ALLWISE
NEOWISE

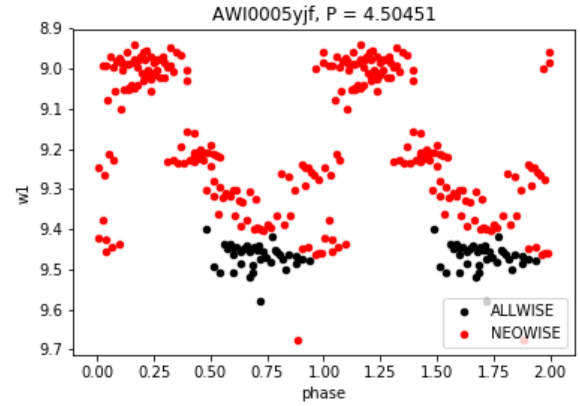
AWI0005yjf, P = 4.50451
w1
phase
ALLWISE
NEOWISE

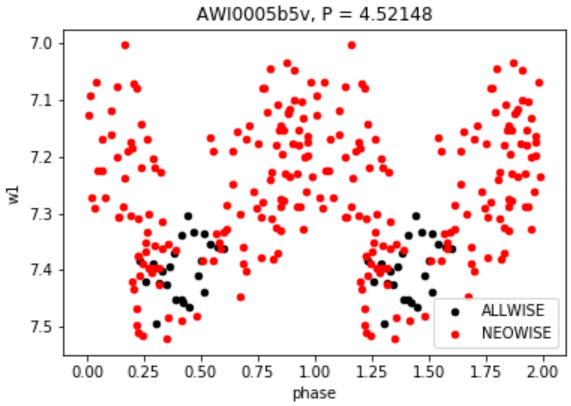
AWI0005b5v, P = 4.52148
w1
phase
ALLWISE
NEOWISE

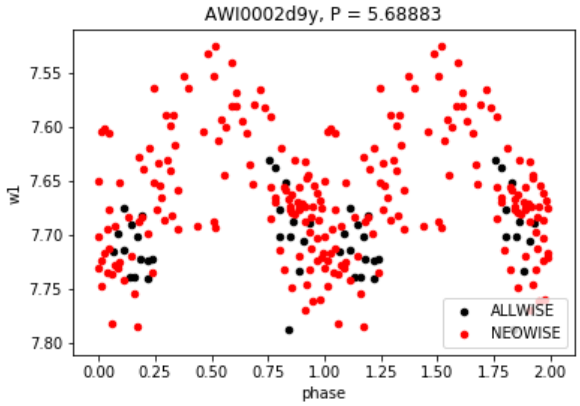
AWI0002d9y, P = 5.68883
w1
phase
ALLWISE
NEOWISE

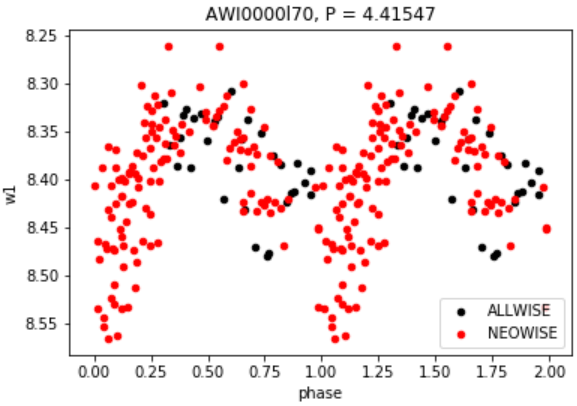
AWI0000l70, P = 4.41547
w1
phase
ALLWISE
NEOWISE

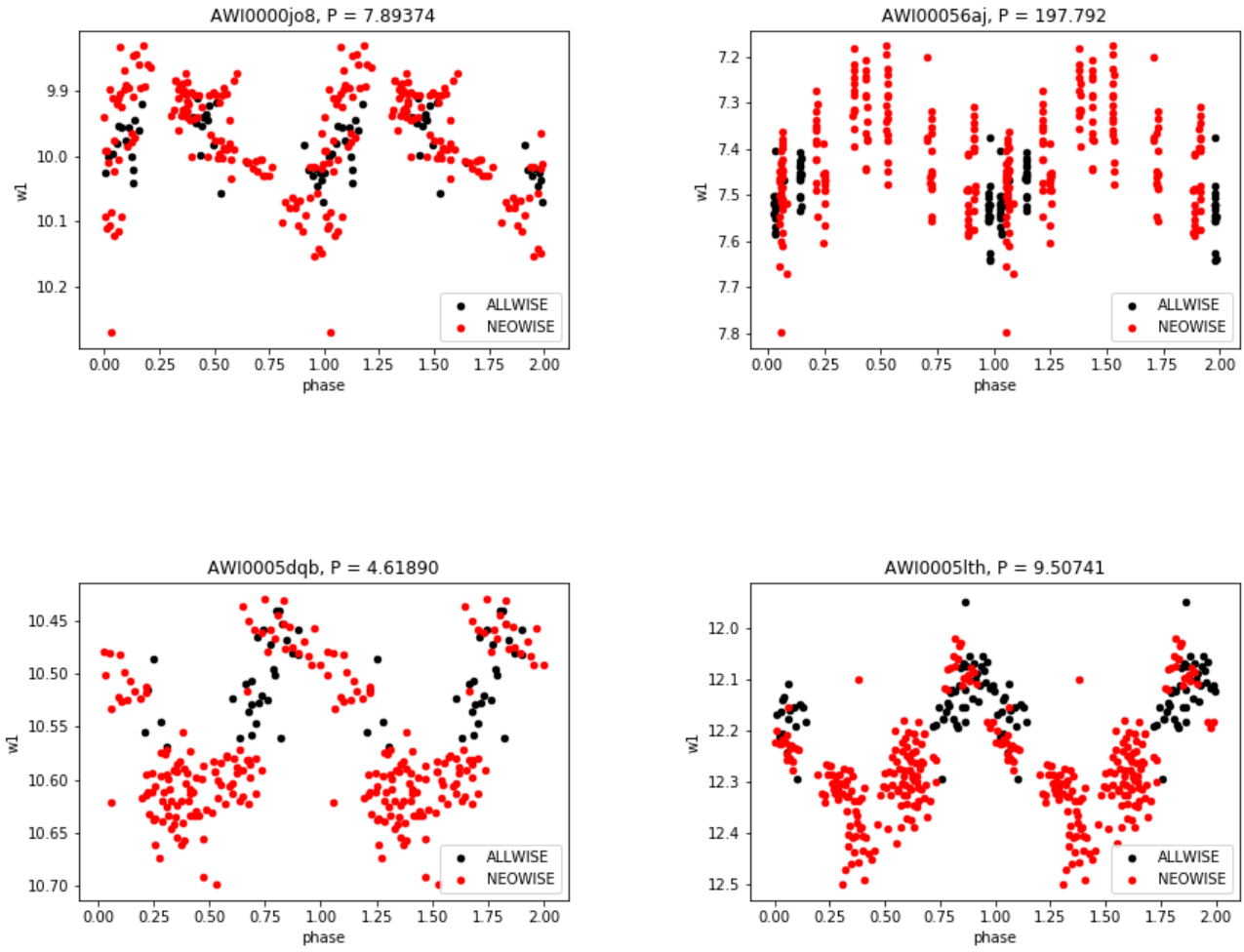

Figures. Periodic variables we found with the WISE archival data in table 2. Y axis plots the W1 magnitude and X axis represents the phase of the object. Note that “phase” on the x axis means the particular appearance or state for cycle of changes and phase from 0 to 1 depicts one full cycle.

Appendix III.

Figures below are the calibrated light curves for all the objects in table 1. Y axis plots the relative flux between the objects and the reference star (Flux_o - Flux_r) and X axis is the Geocentric Julian date.

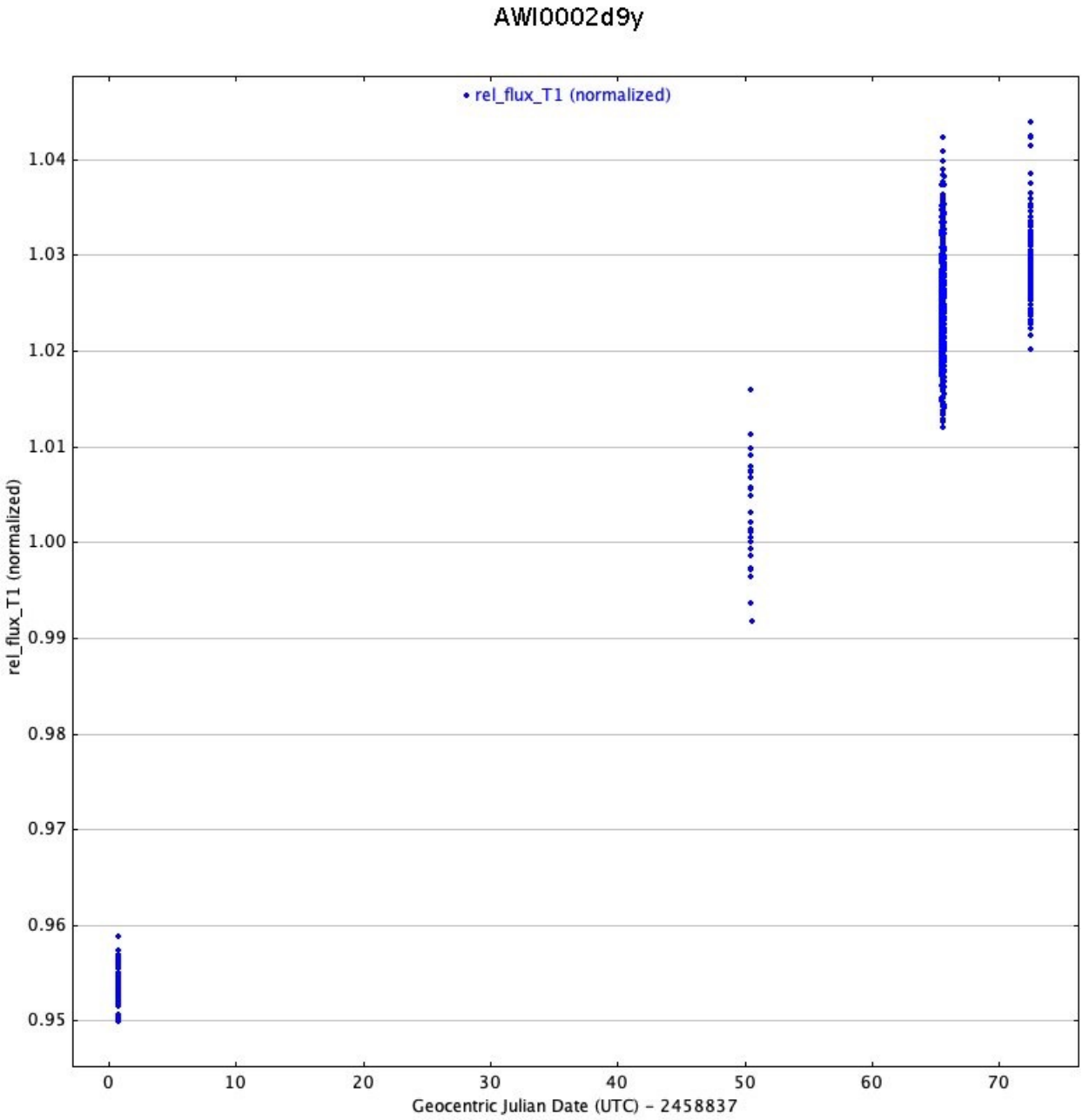

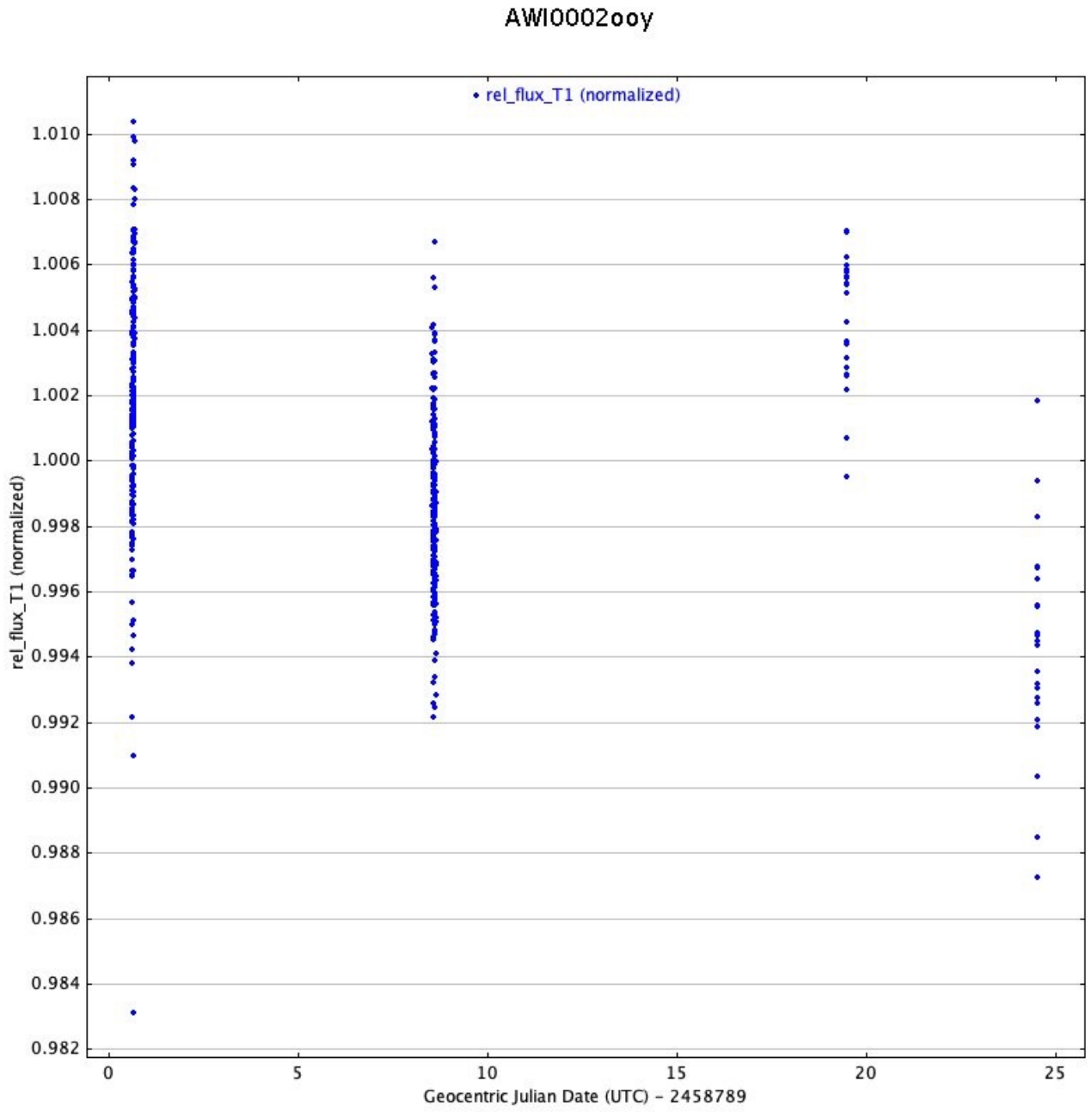
AWI0002ooy
rel_flux_T1 (normalized)
1.010
1.008
1.006
1.004
1.002
1.000
0.998
0.996
0.994
0.992
0.990
0.988
0.986
0.984
0.982
rel_flux_T1 (normalized)
0
5
10
15
20
25
Geocentric Julian Date (UTC) - 2458789

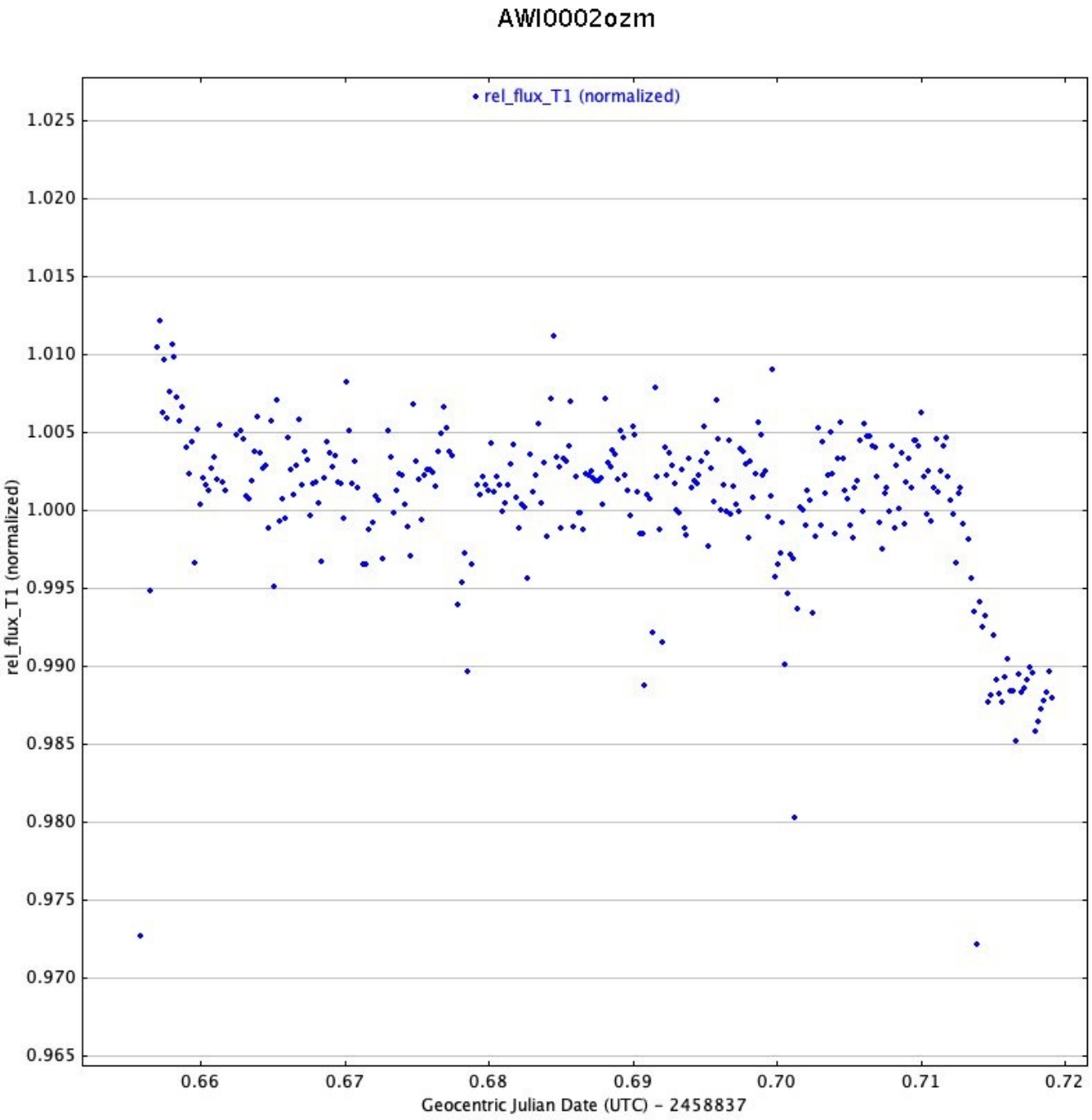
AWI0002ozm
rel_flux_T1 (normalized)
1.025
1.020
1.015
1.010
1.005
1.000
0.995
0.990
0.985
0.980
0.975
0.970
0.965
rel_flux_T1 (normalized)
0.66
0.67
0.68
0.69
0.70
0.71
0.72
Geocentric Julian Date (UTC) - 2458837

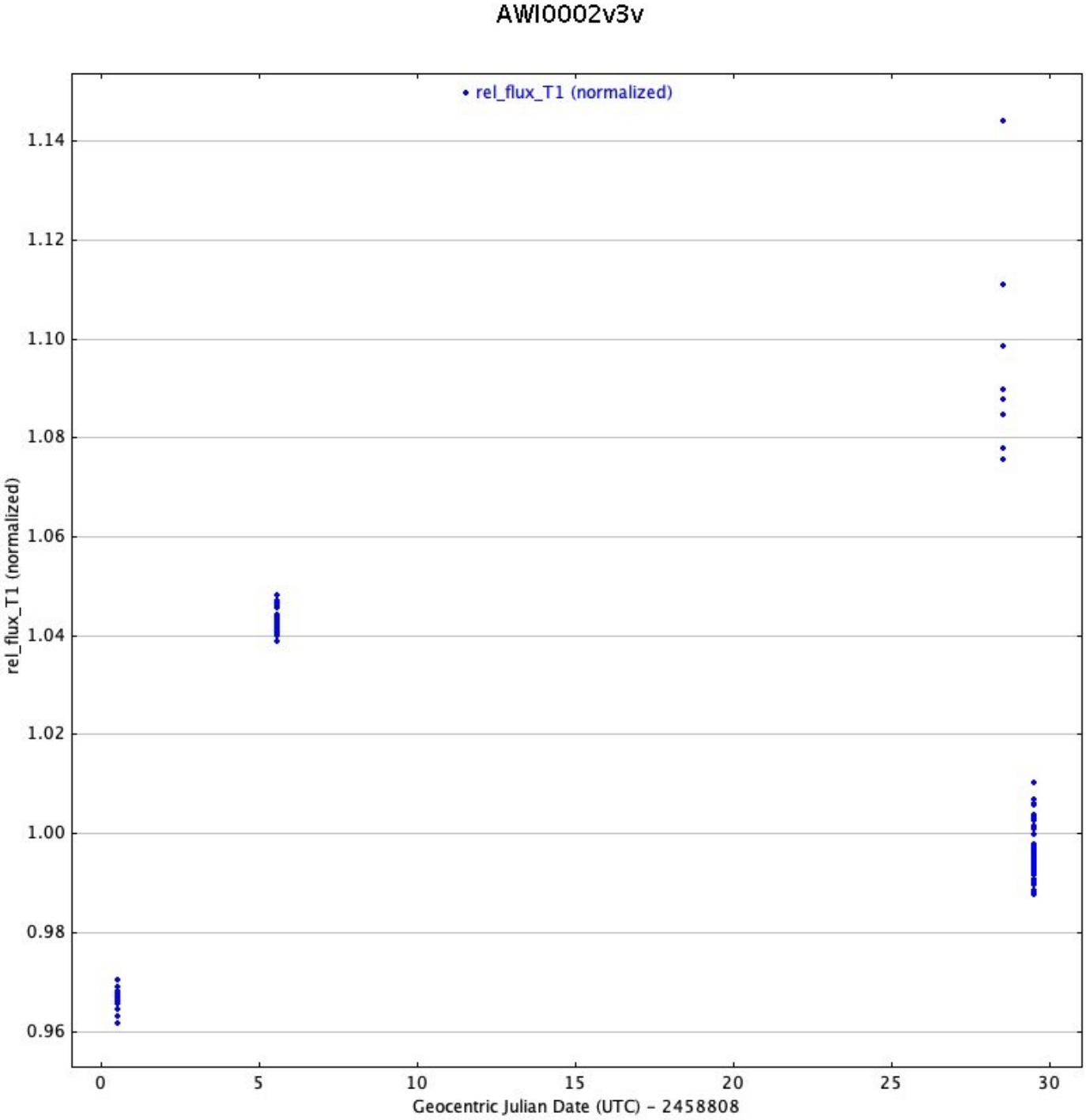
AWI0002v3v
rel_flux_T1 (normalized)
1.14
1.12
1.10
1.08
1.06
1.04
1.02
1.00
0.98
0.96
rel_flux_T1 (normalized)
0
5
10
15
20
25
30
Geocentric Julian Date (UTC) - 2458808

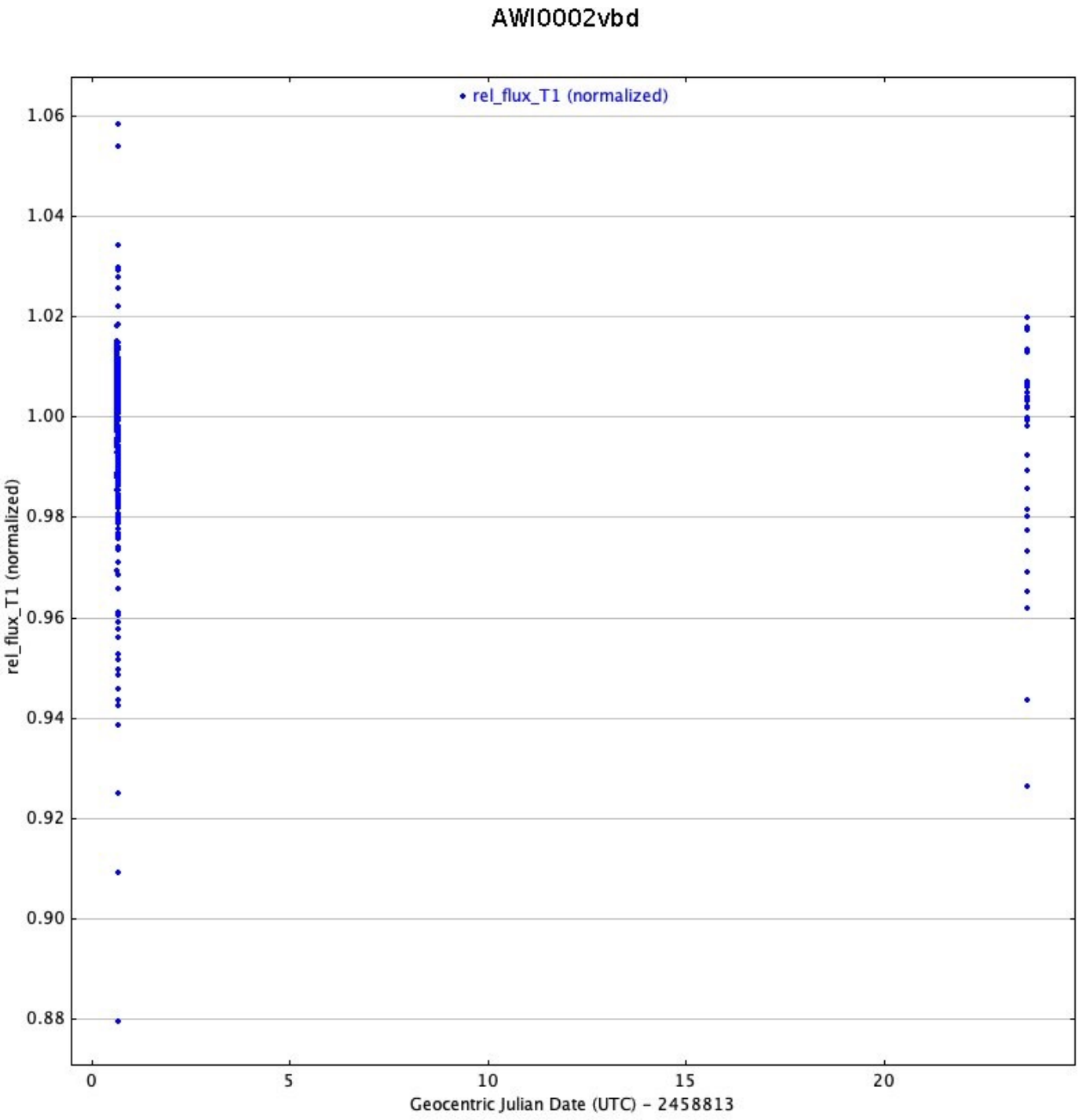
AWI0002vbd
rel_flux_T1 (normalized)
1.06
1.04
1.02
1.00
0.98
0.96
0.94
0.92
0.90
0.88
rel_flux_T1 (normalized)
0
5
10
15
20
Geocentric Julian Date (UTC) - 2458813

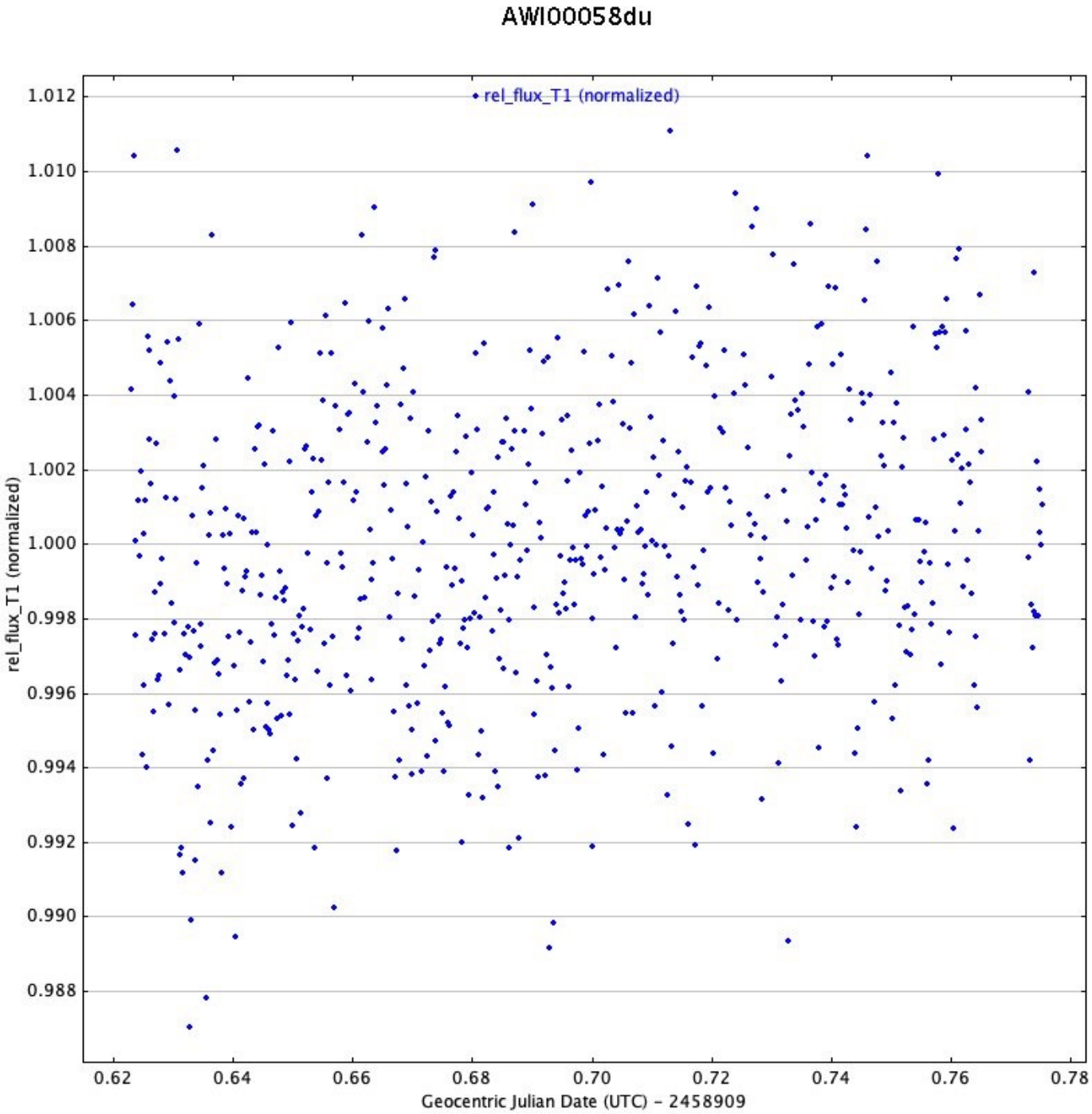
AWI00058du
rel_flux_T1 (normalized)
1.012
1.010
1.008
1.006
1.004
1.002
1.000
0.998
0.996
0.994
0.992
0.990
0.988
rel_flux_T1 (normalized)
0.62
0.64
0.66
0.68
0.70
0.72
0.74
0.76
0.78
Geocentric Julian Date (UTC) - 2458909

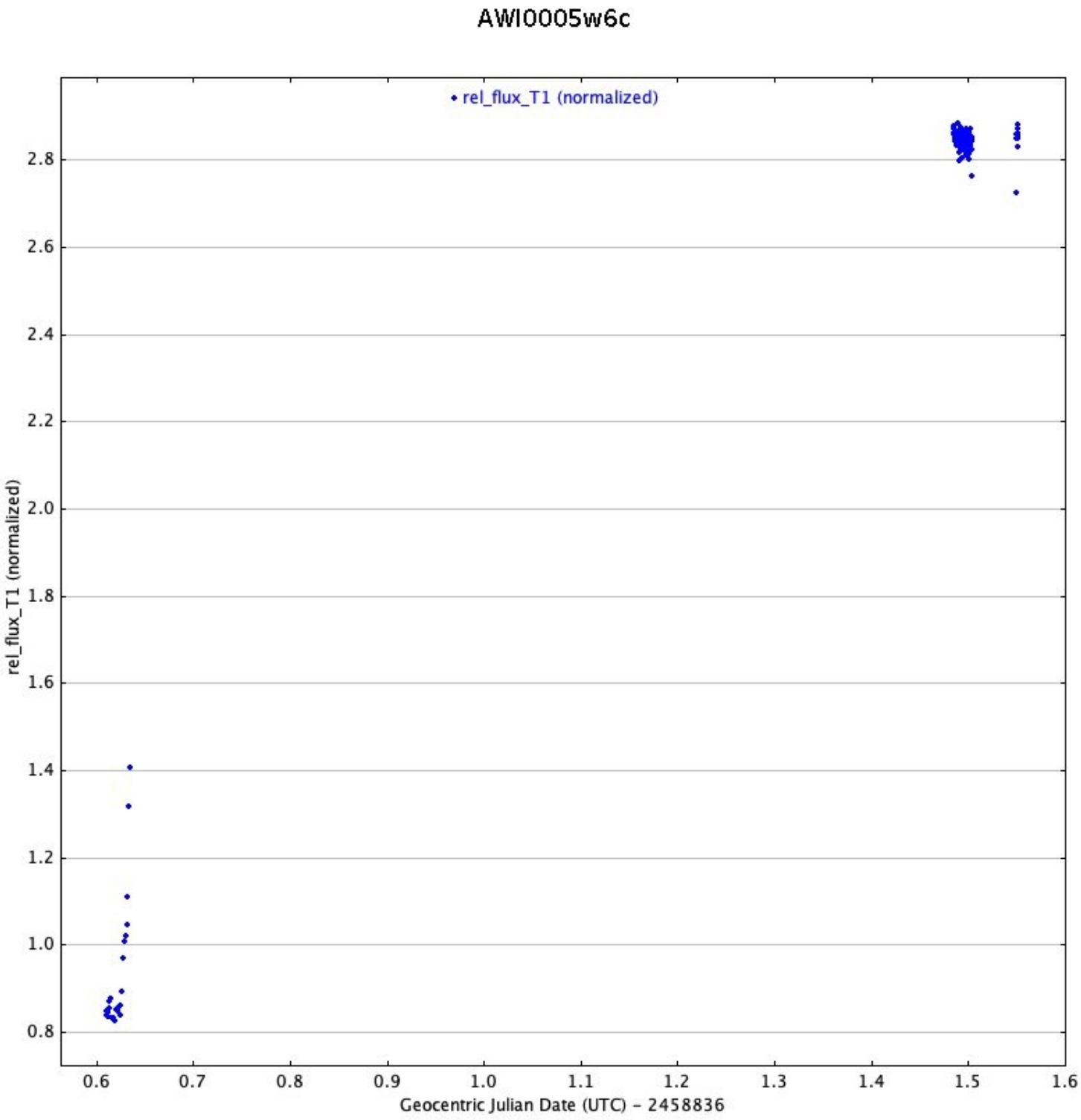
AWI0005w6c
rel_flux_T1 (normalized)
rel_flux_T1 (normalized)
2.8
2.6
2.4
2.2
2.0
1.8
1.6
1.4
1.2
1.0
0.8
0.6
0.7
0.8
0.9
1.0
1.1
1.2
1.3
1.4
1.5
1.6
Geocentric Julian Date (UTC) - 2458836

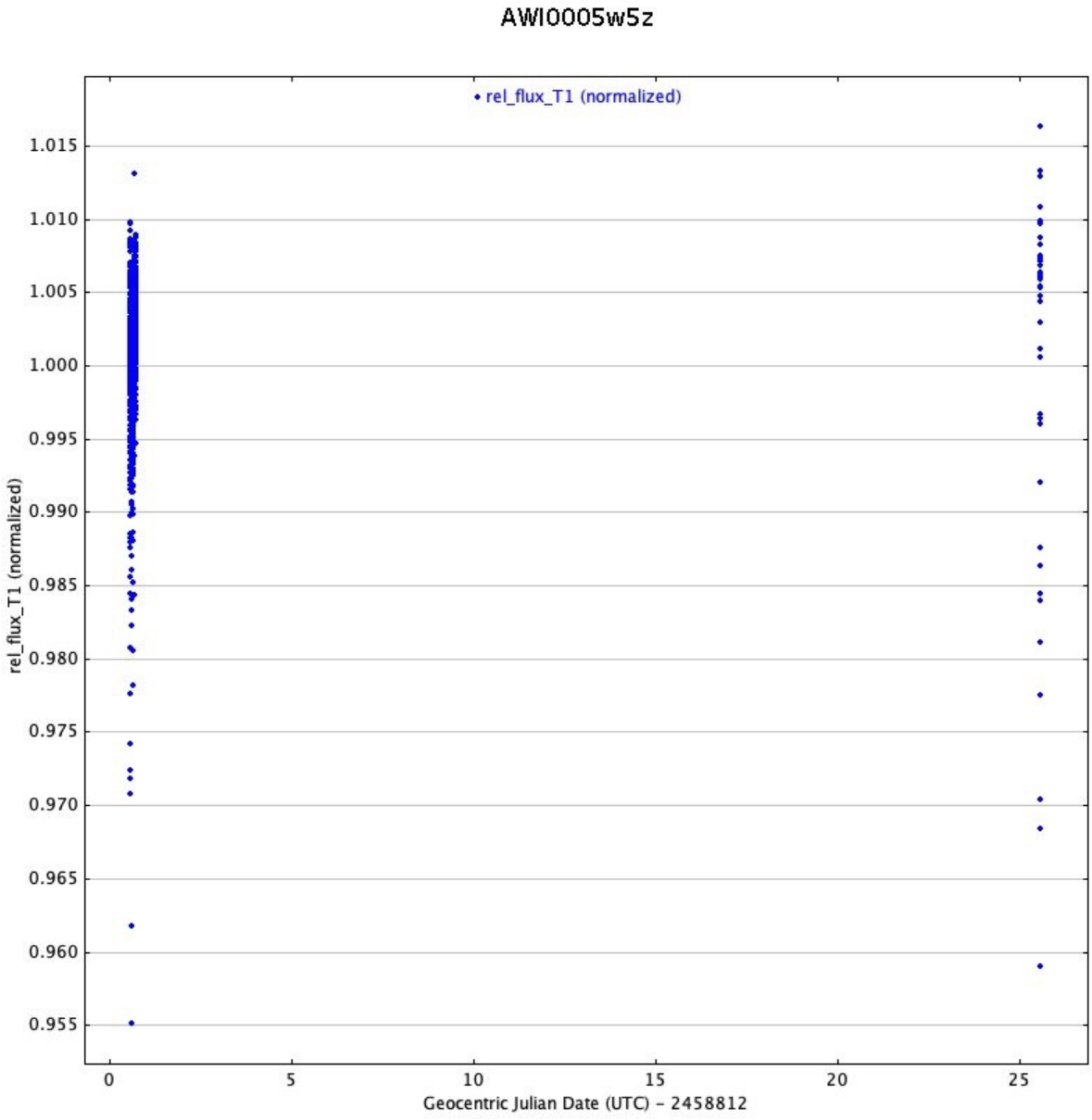
AWI0005w5z
rel_flux_T1 (normalized)
1.015
1.010
1.005
1.000
0.995
0.990
0.985
0.980
0.975
0.970
0.965
0.960
0.955
rel_flux_T1 (normalized)
0
5
10
15
20
25
Geocentric Julian Date (UTC) - 2458812

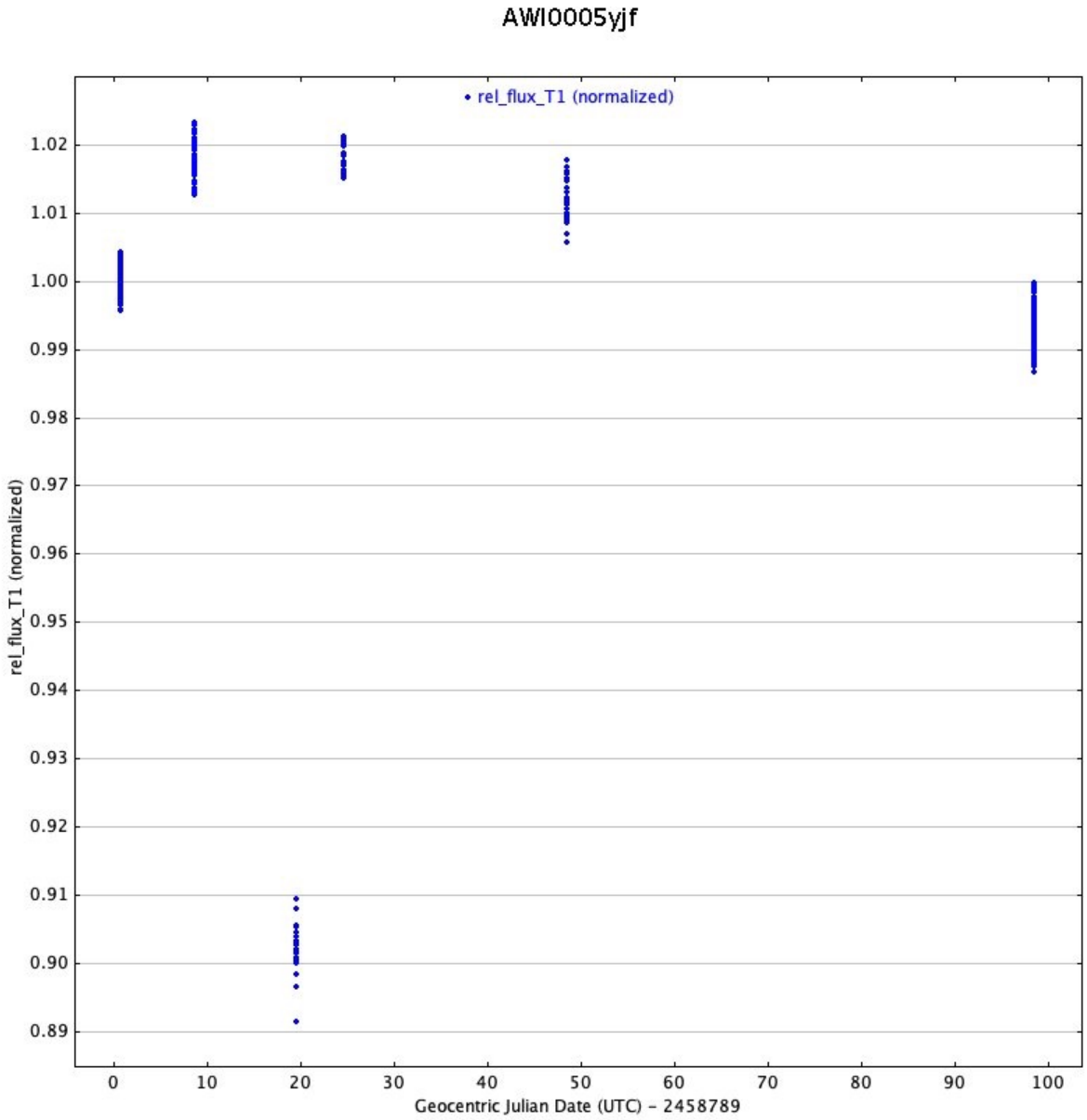
AWI0005yjf
rel_flux_T1 (normalized)
rel_flux_T1 (normalized)
1.02
1.01
1.00
0.99
0.98
0.97
0.96
0.95
0.94
0.93
0.92
0.91
0.90
0.89
0
10
20
30
40
50
60
70
80
90
100
Geocentric Julian Date (UTC) - 2458789

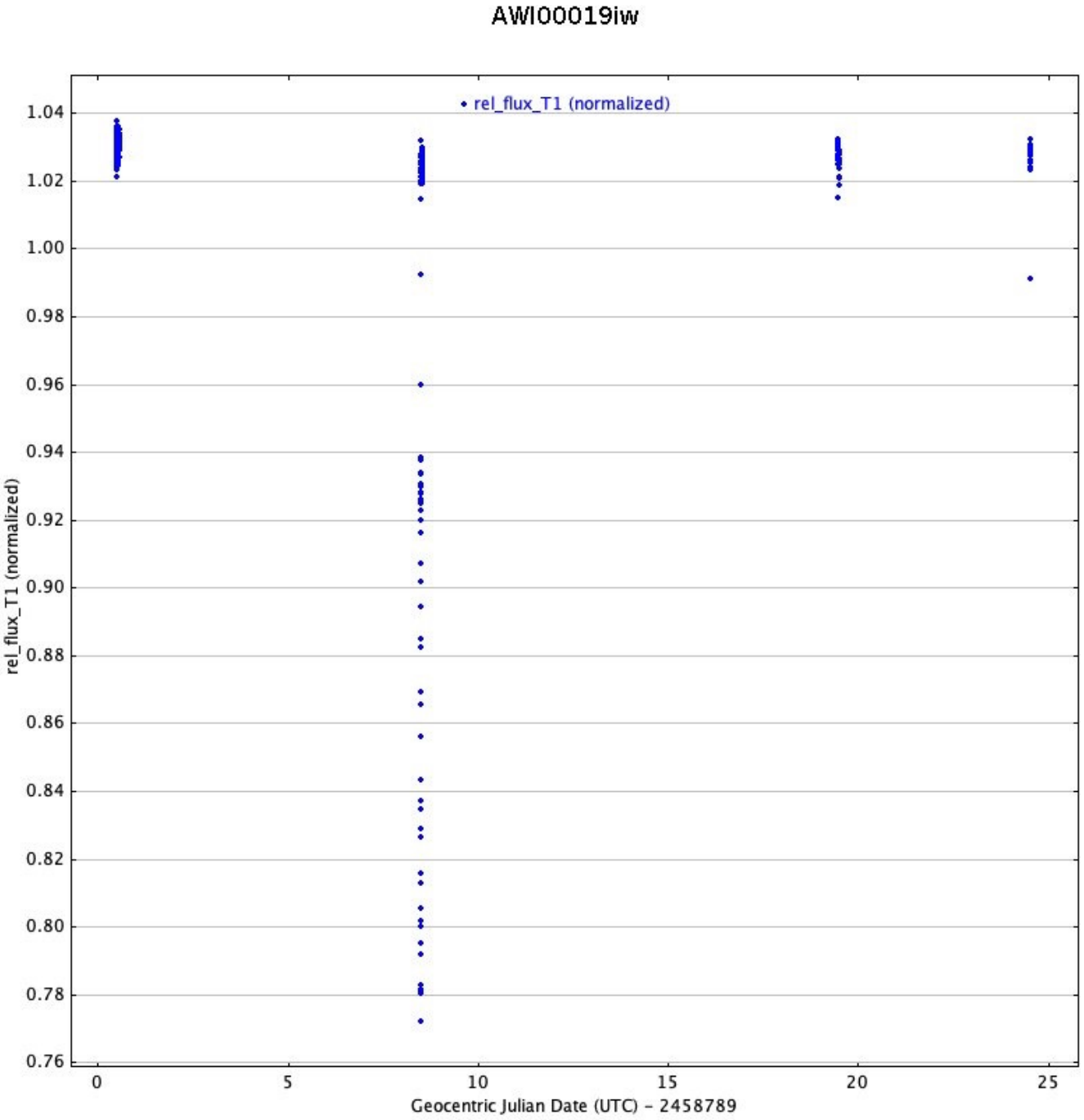
AWI00019iw
rel_flux_T1 (normalized)
1.04
1.02
1.00
0.98
0.96
0.94
0.92
0.90
0.88
0.86
0.84
0.82
0.80
0.78
0.76
rel_flux_T1 (normalized)
0
5
10
15
20
25
Geocentric Julian Date (UTC) - 2458789

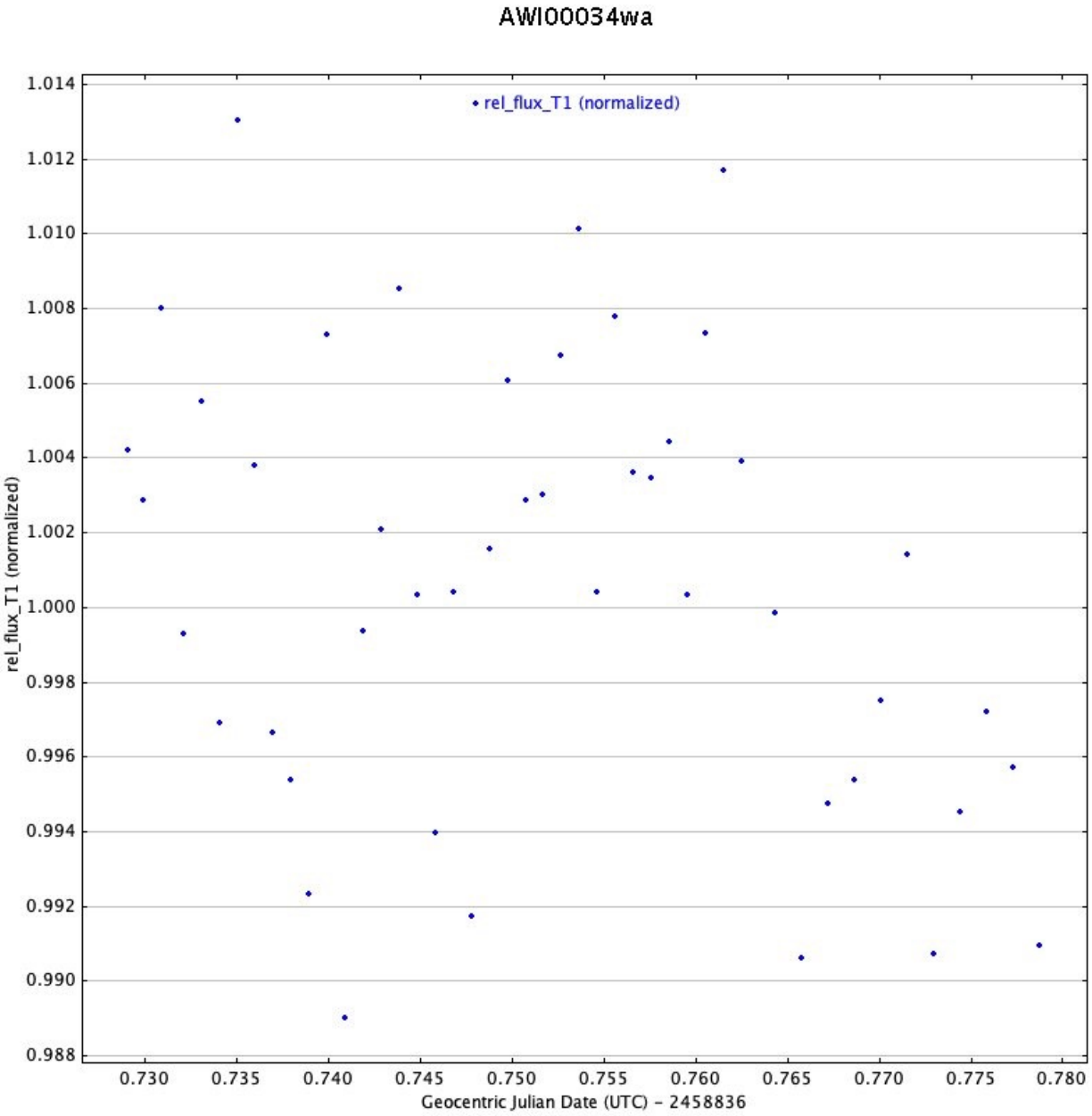
AWI00034wa
rel_flux_T1 (normalized)
rel_flux_T1 (normalized)
1.014
1.012
1.010
1.008
1.006
1.004
1.002
1.000
0.998
0.996
0.994
0.992
0.990
0.988
0.730
0.735
0.740
0.745
0.750
0.755
0.760
0.765
0.770
0.775
0.780
Geocentric Julian Date (UTC) - 2458836

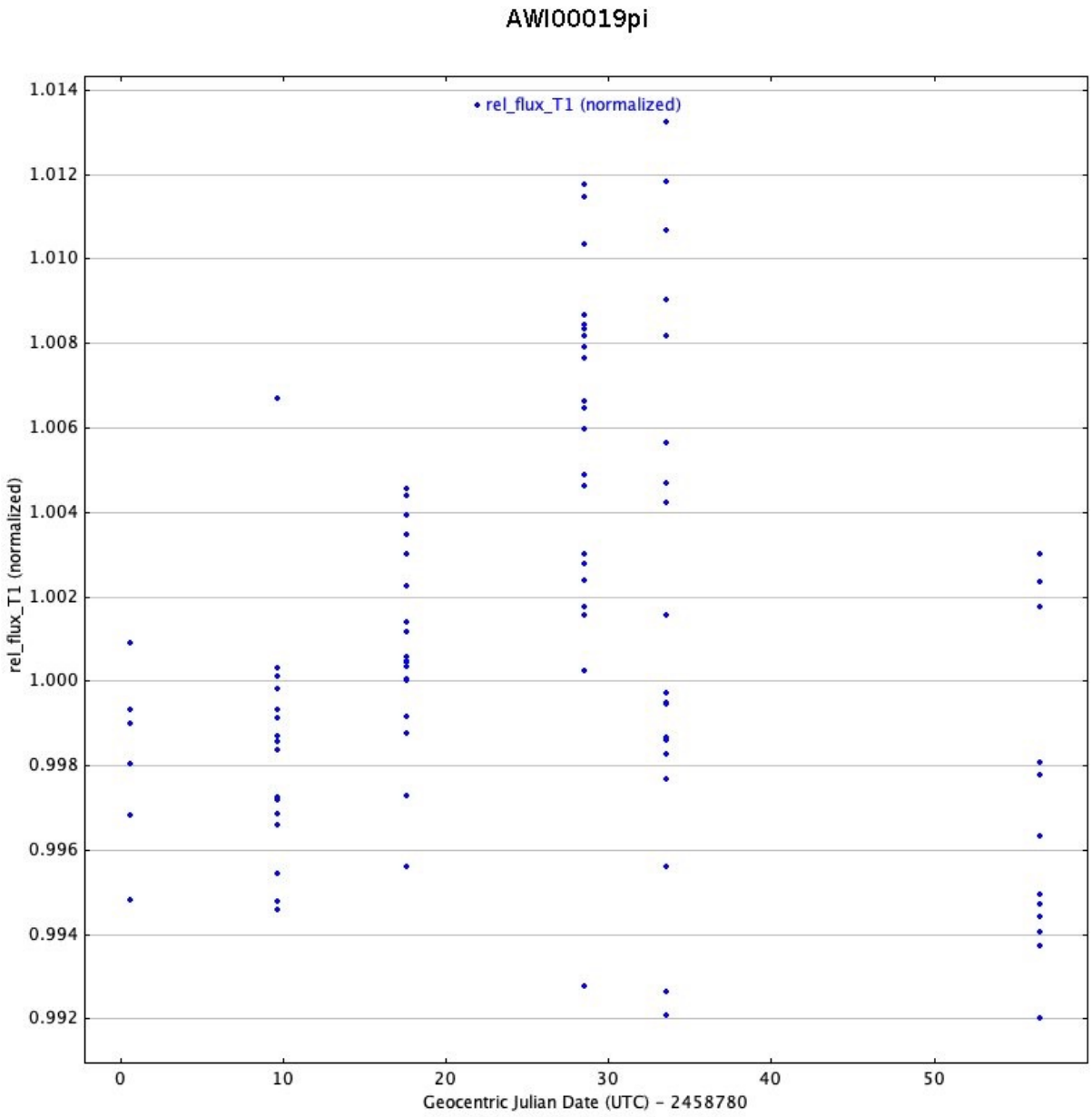
AWI00019pi
rel_flux_T1 (normalized)
rel_flux_T1 (normalized)
1.014
1.012
1.010
1.008
1.006
1.004
1.002
1.000
0.998
0.996
0.994
0.992
0
10
20
30
40
50
Geocentric Julian Date (UTC) - 2458780

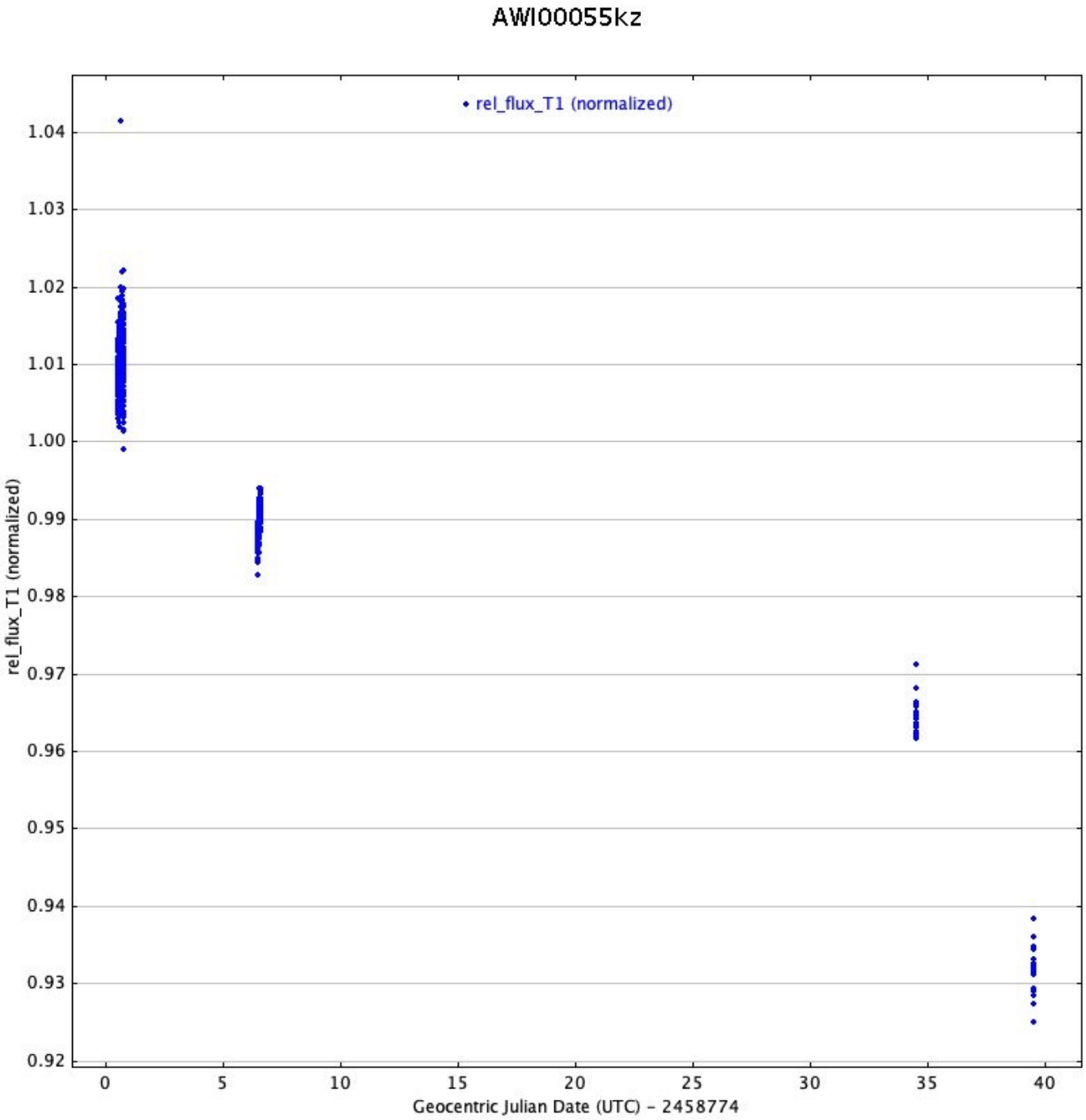
AWI00055kz
rel_flux_T1 (normalized)
rel_flux_T1 (normalized)
1.04
1.03
1.02
1.01
1.00
0.99
0.98
0.97
0.96
0.95
0.94
0.93
0.92
0
5
10
15
20
25
30
35
40
Geocentric Julian Date (UTC) - 2458774